Radiative Characteristics of Spherical Cavities Having Partially or Completely Specular Walls

by

Farshad Kowsary

Dissertation submitted to the Faculty of the
Virginia Polytechnic Institute and State University
in partial fulfillment of the requirements for the degree of
Doctor of Philosophy
in
Mechanical Engineering

APPROVED:

Dr. J. R. Mahan, Chairman

Dr. J. R. Thomas

Dr. B. Vick

Dr. J. B. Campbell

Dr. L. W. Johnson

November, 1989

Blacksburg, Virginia

Radiative Characteristics of Spherical Cavities Having Partially or Completely Specular Walls

by

Farshad Kowsary

Dr. J. R. Mahan, Chairman

Mechanical Engineering

(ABSTRACT)

The radiant exchange problem for an isothermal spherical cavity having diffuse-specular walls is solved and the distribution of the local heat transfer for various opening angles and surface emissivities is obtained. Subsequently, the overall emission from the cavity (i. e., the apparent emissivity of the cavity) is calculated for various opening angles and surface conditions. In addition, the overall absorption characteristics of spherical cavities having purely specular walls is investigated analytically for the case of collimated radiation entering the cavity. Various opening angles and surface conditions are considered. The Monte Carlo method is utilized to support the results obtained from the analytical calculations. Results show that in spherical cavities the apparent emissivity is not very sensitive to the degree of specularity of the cavity wall. Also, there are situations in which the diffuse cavity is a more efficient emitter than a specular cavity. Absorption characteristic results show that for cavities having purely specular walls the absorption of collimated radiation is highly dependent on the angle of incidence of radiation on the opening for small opening angles.

Acknowledgements

My sincere gratitude goes to my major advisor, Prof. J. R. Mahan, who patiently and without any hesitation guided me throughout this work and at trying moments came up with invaluable suggestions. I would also like to thank him for careful review of this dissertation. I would like to thank Dr. J. R. Thomas, Dr. B. Vick, Dr. L. W. Johnson, and Dr. J. B. Campbell for serving on my doctoral committee and reviewing this work. I would like to thank the Radiation Sciences Branch of the Atmospheric Sciences Division of NASA's Langley Research Center for their partial support of this work under NASA contracts NAS1—18471, Tasks 2 and 13, and NAS1—18106, Task12. A particular debt of gratitude is owed of the Radiation Sciences Branch.

Finally, I owe a great deal of appreciation to my parents,

, for their kindness and ever present support.

Table of Contents

List of Illustrations

List of Tables

Nomenclature

A, dA	Arbitrary area elements
A_o	Opening area of the spherical cavity
A'	Surface area of the spherical cavity
A_{nk} , dA_{nk}	The fictitious area defined in Section 3.2.2
A_s	Surface area of the sphere
B	Radiosity (W/m²)
E, dE	Exchange Factor (-)
F, dF	View Factor (-)
df_{nk}	factors defined in Eq. (3.17)
H	Irradiance (W/m²)
i_{max}	Total number of subareas in collections w or v
I_o	Flux of collimated radiation (W/m²)
q	Net heat flux to the surface (W/m²)
T	Temperature (K)
v	Collection of subareas defined in Section 3.3
w	Collection of subareas defined in Section 3.2.3

Greek

α	Absorptivity (-), Polar angle (rad)
α_a	Apparent absorptivity (-)
α^a, α^b	Polar angles defining the limits of the intersection of a longitudinal line with area A_2
ε	emissivity (-)
ε_a	Apparent emissivity (-)
γ	Angle of incidence of collimated radiation (deg)
θ	zenith angle of a spherical coordinate system (rad)
θ'	zenith angle of the source-oriented coordinate system defined in Fig. 13 (rad)
θ^a, θ^b	Zenith angles defining the limits of the intersection of a longitudinal line with area A_2 (rad)
ρ	Reflectivity (-)
ρ^s	Specular component of the reflectivity (-)
ρ^d	Diffuse component of the reflectivity (-)
σ	Stefan-Boltzmann constant (5.667×10^{-8} W/m^2-K^4)
ϕ	Azimuthal angle of spherical coordinate system (rad)
ϕ'	Azimuthal angle of the source-oriented coordinate system defined in Fig.13 (rad)
ϕ^a, ϕ^b	Azimuthal angles which define area A_2 (rad)
ψ	Opening angle of the spherical cavity (deg)
ψ^a, ψ^b	Polar angles defining the limits of the intersection of a longitudinal line with the opening of the cavity (rad)

Subscripts

i	Refers to an area element in collections w or v
k	Sequence of reflections
n	Number of reflections
1	Source element
2	Receiving element

Superscripts

L	Refers to the lower limit of the polar or zenith angles for an area in collections v or w
U	Refers to the upper limit of the polar or zenith angle for an area in collections v or w

1.0 Introduction

When thermal radiation enters a cavity, it has a better chance of being absorbed than when it strikes a flat surface having the same area as the cavity opening. This is, of course, because of the possibility of multiple reflections within the cavity walls. In the same manner, radiation leaving the opening of an isothermal cavity is greater than radiation emitted by a flat surface of the same material as the cavity walls, and having the same area as the cavity opening. This behavior of cavities is commonly referred to as the *cavity effect.* This effect makes cavities attractive devices for construction of laboratory blackbodies, which are used extensively in pyrometry, thermometry, and radiometry. It also suggests that the absorptivity and emissivity of a surface can be increased by drilling, stamping, etching, or otherwise deforming the surface.

The performance of a cavity as compared to that of a blackbody is described by its *apparent* radiative properties. For example, the apparent emissivity is defined as the ratio of the energy emitted through the opening of an isothermal cavity to the energy emitted by an imaginary black surface stretched across the cavity opening and which is at the same temperature as the cavity wall. Similarly, the apparent absorptivity of a cavity is defined as the ratio of the energy absorbed by the cavity to that which enters

the cavity. Since cavities are used as standards in radiometric measurements, it is of interest to obtain their apparent radiative properties by precise analytical means.

The aim of this work is to investigate the radiative behavior of spherical cavities whose walls are completely or partially specular. Spherical cavities have been suggested as field of view limiting baffles in Earth Radiation Budget Experiment (ERBE) instrumentation applications. Specifically, this work addresses the following questions with regard to spherical cavities:

1. What distribution of wall heat flux is required to maintain the cavity isothermal?

2. What is the cavity's apparent emissivity?

3. What is the apparent absorptivity of the cavity as a function of angle of incidence of collimated radiation incident to the cavity?

Answers to the first two questions are given for completely and partially specular cavities, while the answer to the third question is given only for purely specular cavities. The answer to the third question provides a basis for designing surfaces which are directionally selective. That is, for example, a surface can be designed so that its absorptivity is relatively strong in a desired direction and relatively weak in all other directions. Such a surface can be used to control the heat transfer to or from the surface.

For simple cavity configurations, such as cylindrical, conical, rectangular-groove, V-groove, and circular-groove cavities, answers to most of the above questions are given in the literature. Radiative behavior of diffuse spherical cavities has also been investigated previously. These results were obtained during the 1960's. According to Sparrow and Cess [1], the case of diffuse-specular spherical cavities is one of the remaining unsolved problems in radiation heat transfer.

Chapter 2 is an overview of methods commonly used for obtaining radiative characteristics of cavities, and investigations on other cavity configurations are cited. The method for analyzing radiative characteristics of spherical cavities having partially or completely specular walls is developed in Chapter 3. In Chapter 4 the results are discussed and confidence in their validity is established by comparing them with results obtained by an independent method, namely the Monte Carlo technique. Finally, relevant conclusions and recommendations are made in Chapter 5.

2.0 Literature Review

Analysis of radiative behavior of cavities has received attention since as early as the 1920's. However, great advances in achieving solutions have been made only within the past thirty years during which digital computers have become widely available. This chapter introduces the most common methods that have been used to analyze the radiative behavior of cavities and to review previous investigations on various cavity configurations. The underlying principle in any formulation of the problem of cavity radiation is, naturally, the law of conservation of energy. Therefore, from this point of view, it is difficult to make a distinction between different approaches commonly taken by the investigators. The most common approach, and the one which yields the most accurate results, is the approach based on the radiant exchange among surface elements. This approach, which is discussed in Section 2.1, is more common among the investigators in the field of radiation heat transfer. In the applied optics literature, where the interest in cavities is from the practical point of view of designing and constructing laboratory blackbodies, several approximate methods can be cited which are based on multiple reflections inside the cavity. The two most common approaches which fall in this category are discussed in Section 2.2. In Section 2.3 a survey of the publications

describing analytical investigations of thermal radiative behavior of various cavity configurations is given.

2.1 Methods of Radiant Exchange

The need for precise heat transfer calculations for vehicles operating in outer space resulted in development of various formulations based on radiant exchange among surfaces. In outer space radiation is the most important (if not the only) means for transfer of heat. The intent of this section is merely to introduce the unfamiliar reader to various concepts and terminologies used in radiant exchange formulations. Readers interested in a more elaborate discussion may refer to texts by Sparrow and Cess [1] or Siegel and Howell [2].

One of the fundamental concepts in radiant exchange methods is that of an *enclosure*. An enclosure is defined as a volume in space enclosed by one or several surfaces. These surfaces usually correspond to the physical boundaries of the system being studied. An opening can be considered as a virtual surface whose reflectivity is zero. The analysis in the radiant exchange method involves taking into account the radiation leaving a given surface on the enclosure wall and going to all other surfaces, and radiation arriving from all other surfaces to the given surface. Although the concept involved is seemingly simple, difficulties may arise if the geometry of the system being analyzed is complex.

For nonblack surfaces in an enclosure, the energy leaving a given location consists of reflected and emitted radiation. Therefore, radiative properties of a surface; i. e., emissivity, reflectivity, and absorptivity; have important roles in calculations. For most real surfaces these properties depend on the wavelength, direction, and surface temper-

ature. Although it is possible to give a formulation which includes all these functional dependencies, actually solving the resulting equations, some of which will be tabulated, is extremely difficult if not impossible except for the case of very simple geometries. Furthermore, there is insufficient knowledge of the directional and spectral behavior of the radiative properties of surfaces to carry out the implied calculations. Therefore, most analyses are carried out under certain simplifying assumptions. For example, radiative properties are assumed to be independent of the wavelength; i. e., the *gray* assumption is invoked. The emission from the surface is assumed to be *diffusely* distributed; i. e., it obeys the Lambert cosine law, and there are three commonly used models for reflection: diffuse, specular (mirror-like), and diffuse-specular (see Fig.1). The diffuse model for reflection is an accurate representation of the real behavior when the surface is *optically rough* (i. e., when the average size of surface irregularities is large compared to the wavelength of the incident radiation). On the other hand, when the surface is *optically smooth*, specular reflection is a good approximation for real surfaces. The diffuse-specular model is a mixture of specular and diffuse reflection and in many cases is a good approximation for the real behavior of surfaces. In this model the reflectivity ρ of the surface is postulated as having a diffuse, ρ^d, and a specular, ρ^s, component; that is,

$$\rho = \rho^s + \rho^d . \tag{2.1}$$

In radiant exchange formulations the *radiosity*, defined as the diffusely distributed energy leaving the surface, and the temperature are assumed to be uniform throughout a given surface. Surfaces may be subdivided further into smaller sections to improve the validity of this assumption. This higher accuracy is obtained at the expense of increasing the computational time and effort. For a generalized formulation, surfaces can be sub-

divided into infinitesimal elements. In analyses of the radiative behavior of cavities this latter approach is made preferable by the required accuracies.

Radiant exchange formulations require use of certain dimensionless *transfer coefficients*. These transfer coefficients are used to relate the *irradiance* of a given surface on the enclosure to the radiosities of other surfaces making up the enclosure. Irradiance is defined as the flux of radiative energy arriving at the surface. When surfaces of the enclosure are diffuse (i. e., the reflected radiation from the surfaces is diffusely distributed), the analysis is carried out with the use of the *view factor*. The view factor from one surface to another is defined as the fraction of the diffusely distributed radiation leaving the one surface which arrives at the other surface. The view factor is the only transfer coefficient that depends only on the geometry. Its derivation is relatively simple, and various methods for obtaining the view factor between two surfaces exist (see Reference 2).

When the surfaces in the enclosure are specular or diffuse-specular, the formulation requires knowledge of the *exchange factor* between surfaces. The exchange factor is defined as the sum of the fractions of the diffusely distributed energy leaving one surface which arrives at a second surface, both as a result of direct radiation and as a result of all possible specular reflections. Derivation of the exchange factor is considerably more difficult than that for the view factor because it involves taking into account all possible specular paths between the two surfaces, and it depends on the reflectivities of the intervening surfaces. For these reasons, efforts aimed at obtaining the exchange factor between surfaces in an enclosure have not been as successful as those for obtaining the view factor. For a more elaborate discussion on the view factor and the exchange factor see Sections 3.1.2 and 3.1.3, respectively.

The most difficult task in radiant exchange analysis is the derivation of the transfer coefficients. Once these have been determined, the problem becomes one of obtaining

the solution of a system of linear algebraic equations in which the unknowns are the radiosities (or irradiances) of the surfaces. The formulation based on infinitesimal surface elements yields a system of linear integral equations in which the unknowns are the functions giving the distribution of the radiosity (or irradiance). Numerical methods for solving the integral equations are discussed in Reference 1. What follows is a brief presentation of the historical development of radiant exchange formulations.

Prior to the 1960's, calculations of radiant exchange were carried out under the assumption of diffuse surfaces in the enclosure. Systematic procedures for calculating radiant exchange for enclosures with diffuse surfaces were developed and presented by Eckert and Drake [3], Hottel [4], Oppenheim [5], and Gebhart [6] . These formulations were based on the assumption of uniform radiosity along a finite surface and they yielded systems of linear algebraic equations. The generalized formulation based on radiant exchange between infinitesimal surfaces which yields a system of linear integral equations was presented by Jakob [7], and by Sparrow, et al. [8].

Eckert and Sparrow [9] were the first to develop a procedure, based on the method of images, for the calculation of radiant exchange in an enclosure with specularly reflecting walls. Later Sparrow, et al. [10] extended this procedure to enclosures consisting of some diffuse and some specular surfaces. In the discussion of the paper by Sparrow, et al. [10] , Seban suggested the diffuse-specular model. This model was later adopted by Lin [11] for calculation of radiant exchange in conical and cylindrical cavities having diffuse-specular walls. The diffuse-specular model was also suggested, apparently independently, by Sarofim and Hottel in Reference 12, where they used this model to develop a procedure for radiant exchange calculations in enclosures made of diffuse-specular surfaces.

The exchange factor was formally introduced by Lin and Sparrow [13] in developing a formulation for computations of radiant exchange between ring elements in curved

axisymmetric enclosures with specularly reflecting surfaces. A more general procedure for obtaining the exchange factor between curved specularly reflecting surfaces was suggested by Plamondon and Horton [14]. Their formulation is an extension of the method of images developed by Eckert and Sparrow [9] to enclosures containing specular surfaces of arbitrary "topography".

A method which is generally best suited for radiative passages has been introduced by Rabl [15]. This method is an approximate method and is based on the concept of the average number of reflections needed for rays to get from one element to the other. Rabl applied this method to several passages, including cylindrical passages, and V-groove and compound parabolic concentrators. His results for cylindrical passages were within three percent of the exact results obtained by Lin and Sparrow [13].

An exact analytical method was formulated by Mahan, et al. [16] for computation of the radiation exchange in concave axisymmetric enclosures whose surfaces are diffuse-specular. This method "synthesizes" the necessary exchange factors by evaluating a series of so-called *partial exchange factors*. Mahan, et al. [16] used this method, which also allows axial variation of surface properties, to evaluate the temperature distribution in parabolic reflectors.

A general formulation for calculation of the radiant exchange between curved surfaces has been developed by Masuda [17] . Unlike most other formulations which are based on the radiosity, this formulation is derived in terms of radiation intensity with the aid of the diffuse-specular reflection model.

There are some general formulations in the literature which take into consideration the dependency of surface properties on wavelength. One example is the formulation developed by Bobco [18], which extends the formulation of Sparrow, et al. [10] to include interreflection phenomena with *semigray* surfaces. These surfaces are postulated to emit energy in one spectral region and absorb energy in a different spectral region.

An even more general formulation by Bevens and Edwards [19] considers the directional characteristics of all surface properties in addition to the spectral variation of surface properties.

When difficulties arise in the analysis of a given radiant exchange problem as a result of the complex geometry or directional and/or spectral dependency of surface properties, the Monte Carlo method provides an effective alternative to the analytical methods. What follows is a brief introduction to the use of the Monte Carlo method in radiation heat transfer.

2.1.1 The Monte Carlo Method

The Monte Carlo method is a statistical method based on the Markov chain theory, which can be used to simulate a physical process. The Monte Carlo method was first developed for application in the field of neutron transport theory by the scientists working on the creation of early atomic bombs (see Reference 20 page 8). The use of the Monte Carlo method in heat radiation was first accomplished by Howel and Perlmutter [21] in computation of the radiant exchange in an enclosure in the presence of a participating medium. The utilization of the Monte Carlo technique in radiant heat exchange problems in the absence of a participating medium was accomplished by Corlett [22]. Ever since these initial successful attempts, the use of the Monte Carlo technique has been standard practice in complex radiant heat transfer problems. An example of a recent application is the use of the Monte Carlo technique as part of a comprehensive model, developed by Mahan, et al. [23] , to simulate the performance of the active cavity radiometer used by NASA in the Earth Radiation Budget Experiment (ERBE).

Although the analysis of a radiation problem by the Monte Carlo method cannot be described in general since it depends on the type of problem and the ability of the analyst to propose an efficient procedure, most analyses have the following steps in common. To simulate the radiant exchange process by the Monte Carlo method, the energy emitted by a surface is divided into a number of equal energy parts called *energy bundles.* Simulation involves emitting an energy bundle from a surface in a randomly chosen direction that is weighted according to the directional characteristics for the emission of the surface; e.g., cosine distribution for diffuse emission. The probable path of the energy bundle is then followed until it is either absorbed by or escapes from the enclosure. Upon contact with a surface the direction of the bundle is altered according to the type of reflection that occurs. Whether absorption occurs is determined by selecting a random number and comparing it with the absorptivity of the surface. When absorption occurs, the history of the bundle is terminated and the same procedure is repeated for another energy bundle. When a large number of energy bundles (in the order of 10,000 to 50,000) is followed and their paths are appropriately averaged, the fraction of the emitted energy that has been absorbed by each surface or has escaped from the system through an opening can be determined. The results obtained by the Monte Carlo method in different trials form a distribution function that peaks somewhere near the vicinity of the true answer. The uncertainty of the results, which depends on the efficiency of the program and the number of bundles, can be obtained from standard statistical techniques. More details about various statistical aspects of the Monte Carlo technique can be obtained from the text by Hammersley and Handscomb [20]. Applications to heat radiation problems are discussed in Reference 2.

Monte Carlo simulation of radiant exchange can be implemented with the use of a transfer coefficient known as the *distribution factor* introduced and exploited by Mahan and Eskin [24,25]. The distribution factor is defined as the fraction of the energy emitted

diffusely from one surface element which is absorbed by a second surface element due to direct emission as well as to all possible diffuse and specular reflections. The distribution factor is similar to the *absorption factor* defined by Gebhart [6], which considers only diffuse reflections. The *extended absorption factor* defined by Toor and Vistanka [26] considers the possibility of directional emission and bidirectional reflection. This latter, however, has a limited use because current data bases are inadequate for describing the directional behavior of the radiative surface properties. The use of the Monte Carlo method for the derivation of the necessary distribution factors in radiative exchange analysis of diffuse-specular spherical cavities is developed in Appendix A.

Recently, a stochastic model was proposed by Naraghi and Chung [27] that is based on the Markov chain theory and leads to some explicit matrix relationships for the absorption factor from which the heat transfer characteristics of the enclosure can be determined. This approach is similar to the Monte Carlo technique, but unlike the Monte Carlo technique, does not require a random number generator for determining the direction of the ray bundles.

2.2. Methods Based on Multiple Reflections Inside the Cavity

The two most well-known methods used by investigators in applied optics are introduced in this section. Unlike formulations based on radiant exchange, these methods require mathematical approximations to achieve solutions. Essential to both of these methods is Kirchoff's law which, in its most general form, states that the emissivity of a surface element in a given direction and at a given wavelength equals the fraction of any radiation at that wavelength, incident on the element from that direction, which is absorbed.

2.2.1 *Gouffé's Method*

The method developed by Gouffé [28] is the most simplified method for determination of the cavity emissivity. This method can be used for treatment of cavities having diffuse walls with a single opening. Consider a beam of radiation incident on element *dw* on the wall of the cavity shown in Fig. 2. Some fraction of this energy is reflected out of the cavity through the opening *do*. Assuming a diffuse reflection, this fraction is given by $(\rho/\pi)\,\Omega^{o}_{w}$, where Ω^{o}_{w} is the solid angle subtended by *do* at *dw*.

Gouffé made another assumption that the portion of the energy which remains inside the cavity after the first reflection, $1-(\rho/\pi)\,\Omega^{o}_{w}$, is distributed uniformly throughout the cavity. (This assumption is exactly true only in the case of spherical cavities.) Continuing on the same line of reasoning for subsequent reflections, he obtained a summation for the fractions of radiation which escape, and showed that the apparent emissivitiy of a cavity is given by

$$\varepsilon_o = \frac{\varepsilon[1+(1-\varepsilon)(do/w-\Omega^{o}_{w}/\pi)]}{\varepsilon(1-do/w)+do/w} \quad , \tag{2.2}$$

where do/w is the ratio of the surface area of the opening to that of the walls of the cavity including *do*. The quantity Ω^{o}_{w}/π is approximated by the ratio do/w', where w' is the surface area of a spherical cavity having the same depth as the cavity being analyzed.

2.2.2. *De Vos' Method*

The method developed by De Vos [29] allows treatment of cavities whose walls have directional-dependent reflectivities and cavities with multiple openings. This

method is based on evaluating the perturbation in blackbody radiant intensity caused by presence of a hole within the cavity surface. In a completely closed isothermal cavity the radiant intensity from an element within the cavity surface in a given direction is that of a blackbody, I_B, at the cavity temperature. This is true regardless of the properties of the cavity surface. When a hole is made within the cavity wall through which radiation can escape, the intensity of a surface element is reduced from that of a blackbody by an amount depending on the cavity surface properties, size of the opening, and the position of the element with respect to the hole.

Consider once again the cavity shown in Fig. 2. The intensity at *do* due to element *dw* (I_w^o in Fig. 2) has two components. One component results purely from the emission from *dw* itself, while the other component is the radiation from other elements reflected from *dw* in the direction of *do*. The emitted component can be determined easily since the wall temperature and the emissivity are known. Evaluation of the reflected component requires knowledge of the incident intensity I_n^w for all elements such as *n* and the *partial reflectivity*, ρ_{no}^w, at *dw* from the direction of *n* into the direction of *w* . The partial reflectivity ρ_{no}^w is defined as the fraction of energy contained in the solid angle Ω_w^n that is reflected by *dw* towards *do* per unit solid angle. As a first-order approximation it can be assumed that $I_n^w = I_B$, where I_B is the blackbody intensity. In the second-order approximation the intensity obtained from the first-order approximation can be used, and the third-order approximation uses the intensity obtained by the second-order approximation, and so on. The power leaving the cavity and hence the apparent emissiviy can be obtained from the intensity evaluated in this way. Normally derivations are carried out up to the third order because of the complexities that arise when higher order approximations are used. Two major assumptions in De Vos' method are that the intensity I_n^w is uniform throughout the cavity , and that the partial reflectivity of *dw* does not vary

across the opening. These assumptions are reasonable when the cavity opening is small and/or when the wall emissivity is large.

2.3. Historical Developments in the Treatment of Cavity Radiation

Having introduced the most common methods for treatment of cavity radiation, a review of the published works on analytical treatment of various specific cavity configurations can now be presented. The focus of this review is mostly the published works on the treatment of *isothermal* cavities. Cylindrical, conical, and spherical cavities have drawn the most attention; therefore, a subsection is devoted to each of them. Figure 3 shows the type of cavities that have frequently been studied. In Section 2.2.4 the analytical works on grooves, which are cavities of constant cross-section which extend indefinitely along a given axis, are presented. The reader should be cautioned that the use of terminologies is not consistent throughout the literature on this subject. For example, in many cases the apparent emissivity is defined as the ratio of the radiosity to the blackbody emissive power (σT^4) at a given location on the cavity wall (i.e., it is defined as a local quantity rather than an overall quantity). In these cases, the quantity being called the apparent emissivity in the present work is referred to as the *hemispherical apparent emissivity* or the *effective emissivity*.

2.3.1. Cylindrical Cavities

One of the first reported works on cylindrical cavities is that of Buckley [30]. He first considered diffuse cylindrical cavities with both ends open (i.e., passages). He derived an integral equation by using the generalized radiant exchange formulation and obtained

an approximate solution in the form of a two-term exponential expression. He also predicted that the radiosity near the cavity mouth is proportional to $\varepsilon^{1/2}$, where ε is the emissivity of the wall. In later publications, he extended his treatment to cylindrical cavities closed at one end [31] and improved his solution by obtaining an expression which contained a single exponent term [32]. Gouffé [28] and De Vos [29] found approximate solutions for this problem using the procedures outlined in Section 2.1.2.

The first exact results were reported by Sparrow and Albers [33], who considered infinitely long diffuse cylindrical cavities and solved the resulting integral equation by iteration. They showed that the local radiosity at the cavity wall approaches that of a blackbody with increasing distance into the cavity. They also verified the conclusion reached by Buckley [30] that the radiosity is proportional to $\varepsilon^{1/2}$ near the cavity mouth. Sparrow, et al. [34] extended this work to diffuse cylindrical cavities of finite length. Solving the integral equation using an accurate numerical procedure, they found the distribution of local heat flux and radiosity along the surface. They also obtained the overall heat transfer characteristics (the apparent emissivity) of cylindrical cavities for various surface and geometric parameters. By making comparisons, they showed that Buckley's results tend to be inaccurate when the cavity is shallow or when the wall emissivity is low. Their results show a significant variation of the radiosity over the back wall for shallow cavities. This variation gets small as the cavity becomes longer. Their results also show a discontinuity for the distribution of local heat flux at the junction of the cavity base and the side wall of the cavity which required that an extrapolation technique be employed to obtain numerical solutions of integral equations near these discontinuities. Peavy [35] presented a method which avoided the need for employing such an extrapolation technique.

Quinn [36] made a comparison of the results obtained by Sparrow et. al. [34], Gouffé [28], Buckley [31], and his own results, which were obtained by improving the method

of De Vos, for the apparent emissivities of long cylindrical cavities. His comparison showed that while his own results compared well with the exact results of Sparrow, et al., the results obtained by Gouffé's method underestimate and those due to Buckley overestimate the exact results of Sparrow, et al. He also reported that the experimental results by several investigations, notably those by Vollmer [37], compared well with the results obtained by Sparrow, et al. and by Gouffé, and confirmed that Buckley's results are too high for long cylinders.

The case of cylindrical cavities whose walls reflect specularly was first investigated by Krishnan [38], who derived the apparent emissivity based on the method by Berman, Simon and Ziman [39] for both open-ended and closed-ended cylindrical cavities. An error occurred in his original formulation which he corrected in a later publication [40]. Based on his results, he indicated that, unlike the case of diffuse cavities, radiation emitted by specular cavities approaches that of a blackbody as the cavity becomes longer, and that the approach to blackbody radiation holds over the whole of the 2π solid angle. He also showed that the apparent emissivities of cavities with both ends open are closely related to those of the cavities with one open end and one closed end.

Making use of the exchange factor, Lin and Sparrow [13] applied the radiant exchange formulation to obtain the local and overall heat transfer characteristics of cylindrical cavities with specularly reflecting walls for a wide range of geometrical and radiative parameters. By adopting Seban's model, Sparrow and Lin [41] carried out similar calculations for cylindrical cavities with diffuse-specular walls. C. S. Williams [42], showed that Krishnan's formula [40] for the apparent emissivity of cylindrical cavities with specularly reflecting walls can be reduced to that of Lin and Sparrow [13] after some manipulations.

The overall heat transfer behavior of cylindrical cavities can be inferred from Fig. 4, obtained from Reference 1, which shows the apparent emissivity for various aspect ratios

and radiation properties. As can be seen the apparent emissivity is always greater than the emissivity of the cavity wall. This phenomenon is the *cavity effect* mentioned in the Introduction. As the cavity becomes shallow, the apparent emissivity approaches the wall emissivity. In general a specular cavity has a higher apparent emissivity than the corresponding diffuse cavity[1]. For any given value of wall emissivity, as the ratio of radius to length decreases, the apparent emissivity gets larger. In the limiting case where this ratio is zero, the apparent emissivity for specular cavities approaches unity, whereas in diffuse cavities it approaches a value less than unity.

Some consideration has been given to cylindrical cavities whose opening is partially obstructed by a baffle. This type of cavity behaves more efficiently as a blackbody than do unbaffled cavities. Approximate solutions for the apparent emissivities of baffled cylindrical cavities were obtained by Gouffé [28], Quinn [36], and Fussel [43]. By applying the integral equation method, Alfano [44] obtained the exact solution for the distribution of radiosity throughout the wall of a baffled cylindrical cavity. His results show that the radiosity increases and becomes more uniform as the aperture gets smaller. He also shows that the approximate results of Gouffé and Quinn compare well with the exact results for the cases he considered. Calculations on the overall heat transfer (apparent emissivity) of baffled cylindrical cavities were performed by Sparrow, et al. [45] using an efficient Monte Carlo method. In their investigation they considered two cases of cavities with emitting and nonemitting (low temperature) baffles and showed that emitting baffles produce a higher value of the apparent emissivity than the corresponding nonemitting baffles. Not surprisingly, they also found that as the aperture gets smaller the apparent emissivity gets larger and the effect of aperture is more pronounced for shallow cavities than for deep cavities.

---

1 Actually, the more complete tabulated results in Lin's dissertation [11] show that for very shallow cylinders the opposite of this behavior occurs.

Some studies have been directed towards the directional behavior of the radiative properties of cylindrical cavities. Vollmer [37] obtained the normal emittance (normal apparent emissivity) of diffuse cylindrical cavities for the case of an infinitesimal receiver. His solution, however, contained a number of approximations, and he considered only a limited number of cases. Sparrow and Heinisch [46], using the appropriate view factors, obtained the exact results for the same problem. Their results show that the normal emittance exceeds the apparent (hemispherical) emissivity for the cavity having a depth-to-radius ratio greater than unity. A similar analysis was carried out by Alfano and Sarno [47] for cylindrical cavities with and without baffles.

Lin and Sparrow [48] performed a radiant exchange analysis in a specularly reflecting cylindrical cavity that is irradiated by an obliquely inclined beam of parallel radiation passing through the cavity opening. They obtained results for overall energy absorption and for the surface distribution of locally absorbed energy. Their results for the overall absorption of the cavity show that this type of cavity absorbs more efficiently as the direction of the collimated radiation becomes parallel to the plane of the opening.

2.3.2 Conical Cavities

The radiative behavior of conical cavities was first treated by Gouffé [28] within the framework of his highly approximate theory. Using the method of radiant exchange, Sparrow and Jonsson [49] performed the first exact numerical calculations on the radiative behavior of diffuse conical cavities. They considered both cases of a prescribed (uniform) wall temperature and a prescribed (uniform) wall heat flux. In the former case, they obtained the distribution of the local radiosity along the wall of the cavity, while in the latter case they obtained the temperature distribution along the wall of the cavity. They also determined the apparent emissivity of diffuse conical cavities for a

wide range of cone opening angles and surface emissivities and, after comparisons, they indicated that Gouffé's calculations are in substantial error. Sparrow and Lin [41] extended this work to the general case of conical cavities having diffuse-specular walls by using the exchange factor. Approximate solutions for the integral equations obtained based on the radiant exchange formulation of diffuse conical cavities were considered by Shirely and Eberly [50]. Their approximation technique is very good for the interior portion of narrow cones where the local radiosity is close to the blackbody radiation.

Like the apparent emissivity results for cylindrical cavities, the corresponding results for the conical cavities have provided valuable insights to the radiative behavior of cavities in general. The apparent emissivity results for conical cavities for various cone angles and surface conditions, also obtained from Reference 1, are shown in Fig. 5. In all cases decreasing the size of the cone opening angle results in increasing the apparent emissivity. The behavior of conical cavities is similar to that of infinite cylindrical cavities as the cone opening angle approaches zero. In other words, the apparent emissivity for specular cavities approaches unity while that for diffuse cavities approaches a limit less than unity. The apparent emissivity approaches the wall emissivity at the other limiting case, which corresponds to the cone opening angle of 180 deg. The apparent emissivity increases with the degree of specularity. However, the curves corresponding to the case in which the cavity wall is half diffuse and half specular do not fall midway between the corresponding curves for totally diffuse and specular cases. The specularity of the cavity wall becomes unimportant in determining the value of the apparent emissivity when the cavity opening angle, ϕ, is greater than 40 deg.

The radiant emission characteristics of baffled conical cavities with diffusely reflecting walls were studied by Heinisch, et al. [51] using an inventive Monte Carlo procedure. They considered both cases of emitting and nonemitting walls and expressed their results in terms of the apparent emissivity. Their results show that the apparent emissivity in-

creases more and more as the size of the aperture decreases. They also show that the increase of apparent emissivity is greater when the baffle is emitting than when the baffle is nonemitting. Yoshika [52] developed an iterative procedure to determine the apparent emissivity of baffled and nonbaffled conical cavities having diffuse walls. He also obtained the overall reflectivity of the cavity from a series that involves powers of the reflectivity of the wall.

The Monte Carlo method was also applied by Polgar and Howell [53] to the problem of determining the apparent directional radiative reflectivity and absorptivity of a conical cavity with diffusely reflecting walls. They studied this problem for various cases of cone opening angle, surface absorptivity, and angle of incident radiation. Their results show that for small cone angles radiation has a strong tendency to be reflected into the direction of the incident radiation.

2.3.3. Spherical Cavities

Radiative characteristics of spherical cavities having diffusely reflecting walls were analyzed in great detail by Sparrow and Jonsson [54] using the radiant exchange formulation. Sparrow and Jonsson showed that the apparent absorptivity, the apparent emissivity, and the local distribution of the radiosity are given by simple closed-form formulas that are similar to each other in form. They also showed that the absorption of radiant energy by spherical cavities is independent of the direction from which radiation enters the cavity. In Chapter 3 the derivations of Sparrow and Jonsson are reproduced as a background to the radiant exchange analysis in spherical cavities having diffuse-specular walls. The radiative behavior of diffuse spherical cavities is discussed in some detail in Chapter 4, where comparisons are made with the radiative behavior of spherical cavities having diffuse-specular walls.

Prior to the work of Sparrow and Jonsson, Jensen [55] had analyzed radiative emission of a spherical cap in his formulation of net radiative heat transfer between two bodies. De Vos [29] and Gouffé [28] had also applied their approximate formulations to obtain the radiation leaving an isothermal spherical cavity having diffuse walls. It should be mentioned that, as was proven by Fectau [56], the approximate methods developed by Gouffé and De Vos become exact for the case of spherical cavities having diffuse walls.

Emission characteristics of spherical cavities having partially specular walls were first considered by De Vos [29]. In his calculations, De Vos considered three types of partially specular surfaces having distributions as shown in Fig. 6. Similar calculations were also carried out by Edwards [57]. Campanaro and Ricolfi [58] applied the method of De Vos, with some improvements, and obtained the apparent emissivity of spherical cavities for the three types of partially specular surfaces which were considered by De Vos. Their reported result, shown in Fig. 6, gives the apparent emissivity as a function of the aspect ratio (they defined the aspect ratio for a spherical cavity as the ratio of the diameter of the sphere to the radius of the imaginary circular disk stretched across the cavity opening) for the case in which the emissivity of the cavity wall is 0.4. An interesting observation that can be made by referring to Fig. 6 is that, at least for the case shown, the apparent emissivity of spherical cavities decreases as the cavity wall becomes more and more specular. This behavior is contrary to the behavior of conical and cylindrical cavities and other cavities which have been studied. Results obtained in this dissertation indicate that, in spherical cavities, whether apparent emissivity increases or decreases with the degree of specularity of the surface depends on the emissivity of the cavity wall.

Absorption characteristics of hemispherical cavities having diffuse-specular walls were analyzed by Safwatt [59] using the method of radiant exchange. He considered

both the case in which diffuse radiation enters through the cavity opening and the case in which collimated radiation enters the cavity in a direction normal to the plane of the opening. The exchange factor that he derived in his analysis is based on an incorrect assumption, as is shown in Section 3.2.1.; therefore, his results are invalid.

2.3.4. Grooves

Sparrow and Jonsson [60] calculated the amount of energy absorbed when a stream of external radiation enters a rectangular-groove cavity having purely diffuse and purely specular walls. They considered the cases in which the incoming radiation is diffusely distributed across the opening and the case in which the energy enters the cavity as collimated radiation. They performed their calculations for a variety of surface conditions, cavity depths, and incident energy distributions. Their results show that for diffuse incoming radiation, a specular cavity absorbs more effectively than does a diffuse cavity. For the case of incident collimated radiation, comparison between a diffuse cavity and a specular cavity depends on the angle of incidence of the radiation. Comparison made in Reference 1 between the curves characterizing the overall emission from a cylindrical cavity and a rectangular-groove cavity show that the two cavities behave very similarly.

Sparrow and Jonsson [61] performed a similar analysis for the absorption characteristics of V-groove cavities as that of Sparrow and Jonsson [60] for rectangular-groove cavities. Their results indicate that when the angle between the two surfaces making the cavity is small, the energy-absorbing capability of a specular cavity is much greater than a diffuse cavity, and as this angle gets larger, the relative advantage of the specular cavity diminishes. For large angles there were some cases in which the diffuse cavity was superior in absorbing radiation. Interestingly, as is discussed in Reference 1, the radiative behavior of V-groove cavities is very similar to conical cavities.

Sparrow [62] analyzed absorption characteristics of circular-groove cavities having purely diffuse or purely specular walls. His analysis considered only the case of energy entering the cavity as a collimated radiation. He showed that when the cavity walls are diffuse, the direction of incident radiation plays no part in the absorption of radiation by the cavity. On the other hand, when the cavity walls are specular, the absorption depends greatly on the direction of incoming radiation. The relative advantage of a specular cavity over a diffuse cavity for absorption of radiant energy depends on the size of the opening and the direction of the incoming rays. Results obtained for spherical cavities in this dissertation suggest a similar type of behavior, which is unlike that of most other cavities.

In an attempt to investigate the role of surface irregularities in the directional characteristics of surface emissivities and reflectivities, Howell and Perlmutter [63] analyzed the apparent directional emissivity and reflectivity of specular groove cavities having a right-triangular cross-section. They developed a method for the analysis on the basis of the images of surfaces. Based on their results, they concluded that the directional radiant properties of a given surface strongly depend on the local macroscopic surface structure, which is considered to be large compared to the wavelength of radiant energy. Kanayama [64] took this problem a bit further and assumed that the roughness of a surface is composed of identical V-groove or circular-groove cavities. He performed a theoretical calculation for the apparent directional emittance of simplified rough surfaces as a two-dimensional problem. He also measured the directional emissivity of an aluminum specimen and obtained satisfactory agreement with the calculated values.

In a continuation of their work in Reference 63, Perlmutter and Howell [65] considered the possibility of designing surfaces which have a high emissivity (and absorptivitiy) in a desired direction and low emissivity (and absorptivity) in other directions, so that these surfaces can be used to control transfer of heat in a desired direction. Their design

consisted of a surface with a large number of V-groove cavities. These cavities had a black base located at an arbitrary distance from the apex of the groove, and the other two surfaces making the cavity were highly specular with a reflectivity close to unity. This type of surface emits very strongly and uniformly in directions close to the surface normal and very weekly in directions close to parallel with surface. The transition occurs very sharply at an angle which depends on the geometry of the cavity. Black and Schoenhals [66] performed a more general analysis for this type of cavity, which included the possibility of side surfaces having reflectivities of less than unity and calculation of the distribution of radiositiy along the side surfaces. They found that for a fixed geometry, as the reflectivity of the sides goes up, the apparent emissivity of the cavity becomes more directional. In a later study Black [67] compared the directional characteristics of the energy emitted by a V-groove and a rectangular-groove cavity. He concluded that the energy emitted by rectangular-groove cavities is focused in the direction parallel to the cavity opening as opposed to V-groove cavities that focus the emitted radiation in the normal direction.

The distribution of apparent emissivity across the narrow slit of a circular-groove cavity having specular walls was calculated by Kholopov [68] based on the "negatively reflecting method". His analysis was motivated by consideration of these type of cavities for experimental evaluation of the emissivities of electrically conducting materials. The cavity is made of the material for which the emissivity is to be determined. The ratio of the radiation emitted by the wall to the radiation emitted by the cavity through the slit, which is considered to be absolutely black, gives the emissivity of the material. His calculations show that for low emissivities and very narrow slits, radiation emitted by the cavity varies greatly across the slit, and there are locations in front of the slit at which the energy emitted by the cavity approaches that of a blackbody.

3.0 Theoretical Development

This chapter is divided into three major sections. Section 3.1 shows how basic concepts of radiant exchange analysis are in general applied for predicting the distribution of heat flux and the apparent emissivity in an isothermal cavity. Instead of considering a general cavity configuration, the discussion considers the case of a diffuse spherical cavity, the solution of which already exists in the literature [54]. The general formulation of the problem for the situation in which the cavity wall becomes diffuse-specular is given in Section 3.1.2. The material in Section 3.1 is then used as a stepping stone into Section 3.2 where a method is developed for actually solving for the distribution of heat flux and subsequently the apparent emissivity of an isothermal spherical cavity having diffuse-specular walls. Finally, Section 3.3 deals with evaluating the absorptive characteristics of a spherical cavity which has perfectly specular walls and into which enters collimated radiation with a given angle of incidence to the opening.

3.1. Background Theory

The material in this section, while available in textbooks, is repeated here because of its logical relation to the new material developed later in the dissertation.

3.1.1. The Isothermal Spherical Cavity with Diffuse Walls

In radiation exchange among surfaces in a cavity or an enclosure, three types of problems are encountered: surface temperatures are prescribed while the heat transfer to the surfaces is unknown, or the heat transfer to the surfaces is prescribed while the temperatures are unknown, or at some locations the temperatures are specified and at other locations heat transfers are specified. Suppose a cavity, whose surface is at a known uniform temperature, is emitting radiative energy through its opening to a surroundings which is at a temperature of absolute zero. In this problem the unknown quantity is the local heat flux to the cavity surface (as a function of position) required to maintain the prescribed temperature. By knowing the local heat flux the heat transfer across the cavity opening and hence the apparent emissivity of the cavity ε_a can be computed as

$$\varepsilon_a = \frac{1}{\sigma A_o T^4} \int_{A'} q dA' \ . \tag{3.1}$$

In Eq. (3.1) A' is the surface area of the cavity walls and A_o is the surface of an imaginary black membrane stretched across the cavity opening.

A spherical cavity of arbitrary opening angle ψ is shown in Fig. 7. The temperature T as well as the emissivity ε is uniform across the cavity walls. Moreover, the cavity

walls are assumed to be gray ($\alpha = \varepsilon$). Radiation from outside is not considered, but since the problem is linear in heat flux, this can be computed independently and then added to the results.

The net heat flux, q, to a differential surface element on the cavity wall is given by

$$q = \varepsilon\sigma T^4 - \alpha H \ , \tag{3.2}$$

where the quantity H is the irradiance. The irradiance at the element under consideration is related to its radiosity, B, and that of all other elements on the cavity wall by

$$H(\theta_1) = \int_{A'} B \, dF_{dA_1 - dA'} \ , \tag{3.3}$$

where the radiosity is given by

$$B = \varepsilon\sigma T^4 + \rho^d H \ . \tag{3.4}$$

The quantity $dF_{dA_1 - dA'}$ in Eq. (3.3) is the view factor which was defined in Section 2.1 and is discussed further in Section 3.1.3. Due to symmetry, the irradiance in Eq. (3.3) is solely a function of the zenith angle, θ, as defined in Fig. 7. The differential surface element dA_1 is at a fixed location (i.e., θ_1), while the surface element dA' is at an arbitrary location on the cavity wall.

Generally, the solution to Eq. (3.3), which is an integral equation of the Fredholm type (when the right-hand side of Eq. (3.4) is substituted for B), must be obtained either by iteration or by some other numerical technique. However, for the case of the spherical geometry Eq. (3.3) yields a closed-form solution. The reason for this is that in a sphere the view factor $dF_{dA_1 - dA'}$ is given by

$$dF_{dA_1-dA'} = \frac{dA'}{A_s} \quad . \tag{3.5}$$

That is, the view factor between two differential elements in a sphere depends only on the size of the receiving element.[2] By substituting the expression given by Eq. (3.5) for the view factor $dF_{dA_1-dA'}$ in Eq. (3.3), the latter can be written

$$H = \frac{1}{A_s} \int_{A'} (\varepsilon\sigma T^4 + \rho^d H)\, dA' \quad . \tag{3.6}$$

Examination of Eq. (3.6) reveals that the irradiance is uniform throughout the cavity. This is because the integral in the right-hand side of Eq. (3.6) yields a number which is independent of position. Using this fact, and after some algebraic manipulations, the irradiance is found to be given by

$$H = \varepsilon\sigma T^4 \frac{0.5(1 + \cos\psi)}{1 - 0.5(1 - \alpha)(1 + \cos\psi)} \quad , \tag{3.7}$$

where ψ is the opening angle shown in Fig. 7. By substituting into Eq. (3.2) the expression given for H in Eq. (3.7), the local heat flux q is found to be given by

$$q = \varepsilon\sigma T^4 \frac{0.5 \sin^2\psi/(1 + \cos\psi)}{1 - 0.5(1 - \alpha)(1 + \cos\psi)} \quad . \tag{3.8}$$

Hence, by substituting for q from Eq. (3.8) into Eq. (3.1), the apparent emissivity ε_a of a spherical cavity whose walls are diffuse is found to be given by

---

[2] It can be shown easily, by using the additive properties of the view factor, that this also holds for any two finite area elements on the wall of the sphere.

$$\varepsilon_a = \frac{\varepsilon}{1 - 0.5(1 - \alpha)(1 + \cos\psi)} \quad . \tag{3.9}$$

The procedure outlined in this section can be followed to obtain the apparent emissivity of a diffuse cavity regardless of its configuration. For a cavity with partially or completely specular walls the procedure is basically the same. The only modification is that the view factor must be replaced with the exchange factor.

3.1.2. The Isothermal Spherical Cavity with Diffuse-Specular Walls

When the cavity wall is diffuse-specular, the radiation leaving the surface at a given location is not diffuse. The effects of the nondiffuse component of the radiation leaving the surface may be included in a transfer coefficient known as the exchange factor. The exchange factor is defined and its properties are discussed in Section 3.1.4. In radiant exchange computations of enclosures made of diffuse-specular walls, the exchange factor plays the same role as that played by the view factor in diffuse problems. Hence, the local irradiance in a diffuse-specular spherical cavity can be obtained by replacing the view factor $dF_{dA_1 - dA'}$ in Eq. (3.3) with the exchange factor $dE_{dA_1 - dA'}$; that is,

$$H(\theta_1) = \int_{A'} (\varepsilon\sigma T^4 + \rho^d H)\, dE_{dA_1 - dA'} \quad . \tag{3.10}$$

For a diffuse-specular cavity Eq. (3.10) must be solved iteratively. However, when the cavity surface is perfectly isothermal and perfectly specular; i.e., $\rho^d = 0$, the irradiance is given simply by

$$H(\theta_1) = \varepsilon\sigma T^4 E_{dA_1 - A'} \quad , \tag{3.11}$$

where $E_{dA_1 - A'}$ is a function of θ_1 . In this case there is no need to solve an integral equation.

The procedure for evaluation of the the integral on the right-hand side of Eq. (3.10) is discussed in Section 3.2.4, where it is shown that this integral is represented by a triple summation of double integrals whose limits are obtained from a tedious procedure involving set theory operations. Definition and execution of this procedure is the essence of this dissertation.

3.1.3. Definition and Properties of the View Factor

The view factor is thoroughly discussed in all basic heat transfer textbooks. It is introduced at this point mainly as a logical stepping stone to the discussion of the exchange factor, which is continued in the next section. The view factor is the essential geometric parameter for the computation of radiation exchange among diffuse surfaces. The view factor $F_{A_i - A_j}$ is defined as the fraction of the diffuse radiation leaving surface A_i which is intercepted by surface A_j. From first principles the view factor $dF_{dA_i - dA_j}$ between two differential areas dA_i and dA_j (see Fig. 8) can be expressed by

$$dF_{dA_i - dA_j} = \frac{\cos\beta_i \cos\beta_j \, dA_j}{\pi r^2} \quad , \tag{3.12}$$

where r is the distance between the differential areas dA_i and dA_j, and β_i and β_j are the angles that the line joining dA_i and dA_j make with respect to the surface normals of dA_i

and dA_j. Then using the same quantities the view factor between two finite areas, A_i and A_j can be written

$$F_{A_i-A_j}=\frac{1}{A_i}\int_{A_i}\int_{A_j}\frac{\cos\beta_i\,\cos\beta_j\,dA_i\,dA_j}{\pi r^2}\quad . \tag{3.13}$$

The view factor between many common surfaces has been derived analytically using Eq. (3.13); however, there are many situations in which closed-form evaluation of the integral in Eq. (3.13) is very difficult or even impossible. Fortunately, there are some basic rules concerning the view factor that in many cases eliminate the need for integration. One such rule, based on conservation of energy, states that the view factor from an arbitrary element A' located at an arbitrary location on the surface of an enclosure to the entire enclosure surface area A is unity; that is,

$$\int_A dF_{A'-dA}\;=\;1\quad . \tag{3.14}$$

Moreover, if A_i and A_j are two arbitrary surfaces, and if the infinitesimal surface elements dA_i and dA_j are, respectively, located at arbitrary locations within A_i and A_j, then we have the reciprocity relations

$$A_i\,F_{A_i-A_j}\;=\;A_j\,F_{A_j-A_i}\quad , \tag{3.15a}$$

$$dA_i\,F_{dA_i-A_j}\;=\;A_j\,dF_{A_j-dA_i}\quad , \tag{3.15b}$$

and

$$dA_i\, dF_{dA_i - dA_j} = dA_j\, dF_{dA_j - dA_i} \ . \tag{3.15c}$$

The view factor also exhibits the additive property,

$$F_{A_i - A_j} = \int_{A_j} dF_{A_i - dA_j} \ , \tag{3.16a}$$

and by combining Eq. (3.16a) with (3.15a) and (3.15b) there results

$$F_{A_i - A_j} = \frac{1}{A_i} \int_{A_i} F_{dA_i - A_j}\, dA_i \ . \tag{3.16b}$$

3.1.3. Definition and Properties of the Exchange Factor

The exchange factor $dE_{dA_1 - dA_2}$ between two infinitesimal surface elements dA_1 and dA_2 on the walls of an enclosure is defined as the sum of the fractions of the diffuse radiation leaving dA_1 which arrive at dA_2 both directly and by all possible specular reflections. The reader is cautioned that this definition is misstated or stated in a misleading way in some familiar references. For example, Reference 1 states that, "The exchange factor is the fraction of the diffuse radiation leaving a surface which arrives at a second surface both directly and by all possible intermediate specular reflections." Similarly, Reference 2 states that, "The fraction of [the diffusely distributed radiation leaving surface *i*] that arrives at a second surface *j* both directly and by all possible intervening specular reflections is called the exchange factor $E_{A_i - A_j}$." Both of these definitions neglect to state clearly that the exchange factor is a *sum of fractions* (rather than just a fraction). The insistence in References 1 and 2 on the exchange factor as a frac-

tion is misleading because it gives the false impression that it cannot exceed unity. Since in general the number of possible reflective paths from dA_1 to dA_2 is limitless, the mathematical expression for the exchange factor is an infinite sum. Each term in the summation is a quantity somewhat analogous to the view factor. That is, each term represents a fraction of diffuse radiation leaving dA_1 which arrives at dA_2. The difference between these various terms is the manner by which the diffuse radiation gets from dA_1 to dA_2. The first term of the summation is actually the view factor $dF_{dA_1-dA_2}$, which can also be considered as the fraction of the diffuse radiation leaving dA_1 which arrives at dA_2 after zero reflections. A typical term in the exchange factor sum is given by

$$dP_{nk} = df_{nk} \prod_{m=1}^{n} (\rho^s)_m \ . \tag{3.17}$$

In Eq. (3.17) the factor df_{nk} is the fraction of the diffuse radiation leaving dA_1 which arrives at dA_2 after n ideal ($\rho^r = 1$) specular reflections following a certain sequence k of reflections, and is thus a purely geometric quantity. Generally there may exist more than one possible sequence for diffuse radiation to get from dA_1 to dA_2 by n specular reflections; hence, there is a need for the subscript k in order to make a distinction among the various sequences. Every time a reflection occurs a certain fraction of the radiation is absorbed by the reflecting surface. Therefore, to obtain the actual portion which arrives at dA_2 the quantity df_{nk} must be multiplied by the product of the specular reflectivities of all the specularly reflecting surfaces encountered. The subscript m then denotes the m^{th} surface from which a reflection takes place.

Having explained a typical term in the expression for the exchange factor, the entire summation may now be given as

$$dE_{dA_1-dA_2} = df_0 + \sum_{n=1}^{\infty}\sum_{k=1}^{l(n)} dP_{nk}$$
$$= df_0 + \sum_{n=1}^{\infty}\sum_{k=1}^{l(n)}\prod_{m=1}^{n}(\rho^s)_m \; df_{nk} \; . \tag{3.18}$$

The first term on the right-hand side of Eq. (3.18), df_0 , is the view factor from dA_1 to dA_2. Clearly, the exchange factor reduces to the view factor when the enclosure contains no specularly reflecting surfaces. The outside summation is over all numbers of reflections, while the inside summation is over the possible sequences for a given number of reflections n. The function $l(n)$ gives the total number of possible sequences for a given n. In the case of a spherical enclosure the function $l(n)$ has a simple analytical form, as is shown in Section 3.2.1.

It should be noted, as suggested earlier, that the exchange factor, unlike the view factor, can exceed unity. This is because the same energy that has arrived at the second surface may get other chances, through continuing specular reflections, to arrive there. An obvious illustration of this fact is the exchange factor $E_{A'-A}$ between an arbitrary element A' inside an enclosure whose walls have uniform specular reflectivity, ρ^s, to the entire enclosure surface area A. This can be obtained directly from the definition of the exchange factor as,

$$E_{A'-A} = 1 + (\rho^s) + (\rho^s)^2 + \ldots = \frac{1}{1-\rho^s} \; . \tag{3.19}$$

Therefore, in this case the exchange factor is always greater than or equal to unity. When ρ^s is uniform across the wall of an enclosure, Eq. (3.19) suggests a conservation rule similar to that given by Eq. (3.14) for the view factor; that is,

$$\int_A dE_{A'-dA} = \frac{1}{1-\rho^s} \quad . \tag{3.20}$$

Other rules of the exchange factor are similar to those of the view factor. These rules, which can be derived from conservation of energy, can be used to reduce the analysis effort substantially. If A_i and A_j are finite surface elements on the wall of an enclosure, and dA_i and dA_j are, respectively, infinitesimal elements at arbitrary locations within A_i and A_j , then we have the reciprocity relations

$$A_i E_{A_i - A_j} = A_j E_{A_j - A_i} \quad , \tag{3.21a}$$

$$dA_i E_{dA_i - A_j} = A_j dE_{A_j - dA_i} \quad , \tag{3.21b}$$

and

$$dA_i dE_{dA_i - dA_j} = dA_j dE_{dA_j - dA_i} \quad . \tag{3.21c}$$

Also by the additive property,

$$E_{A_i - A_j} = \int_{A_j} dE_{A_i - dA_j} , \tag{3.22a}$$

and by combining Eq. (3.22a) with Eqs. (3.21a) and (3.21b),

$$E_{A_i - A_j} = \frac{1}{A_i} \int_{A_j} E_{dA_j - A_i} dA_i \quad . \tag{3.22b}$$

Development of Eqs. (3.21) and (3.22) may be found in standard radiation heat transfer text books, for example, Reference 1.

It is clear that in order to derive the exchange factor $dE_{dA_1 - dA_2}$ the quantities df_{nk} must be evaluated for all n and k in terms of the location and size of dA_1 and dA_2. The common approach is to locate the area on the surface of the enclosure from which the diffuse radiation travelling from dA_1 to dA_2 is first reflected. Lin and Sparrow [13] called such an area the *fictitious area.* In the current discussion the fictitious areas are identified by the symbol dA_{nk} corresponding to a certain number of reflections n forming the sequence k. The fictitious area for the case of two reflections is shown in Fig. 9. From the definition given above for the quantities df_{nk} it can be concluded that,

$$df_{nk} = dF_{dA_1 - dA_{nk}} \quad . \tag{3.23}$$

Thus, for all n and k the size and location of the fictitious area dA_{nk} must be determined in terms of the sizes and locations of dA_1 and dA_2 . Clearly, in order to determine the fictitious area one has to identify the location where the first reflection occurs for all reflections n. This requires knowledge of the details of how radiative energy suffers multiple specular reflections inside the enclosure.

3.2. Radiant Exchange Analysis in a Spherical Enclosure Having Diffuse-Specular Walls

We now make the transition from the realm of known diffuse-specular radiation analysis to the solution of an important problem that until now has defied analytical solution; that of the diffuse-specular behavior of a spherical cavity.

3.2.1. The Exchange Factor in a Spherical Enclosure

A useful concept in the analysis of radiation exchange within an enclosure is that of a *ray*, defined as an infinitely thin beam of parallel radiation which can be depicted as a single line. It can be demonstrated that *all specular reflections of an arbitrary ray from the walls of a spherical enclosure occur entirely in a single plane.* Four consecutive reflection points are shown in Fig. 10. The subscripts indicate the order of occurrence of reflections. One of the laws of specular reflection states that the incident ray, the reflected ray, and the local normal to the surface must be in the same plane. But the normal to the interior surface of a sphere is directed toward the center of the sphere. Therefore, the reflection points C_{n-1} , C_n, and C_{n+1} as well as the center of the sphere O all lie in the same plane, say P_n. Similarly C_n, C_{n+1} , C_{n+2}, and O all lie in the plane P_{n+1}. Now two consecutive reflections, the n^{th} and the $n+1^{st}$, occur both in planes P_n and P_{n+1} . However, these planes are identical because they have the three points, C_n, C_{n+1}, and O, in common. Then by induction it can be inferred that all the reflections of a ray inside a spherical enclosure occur within one and only one plane. Clearly this plane can be identified by any two distinct reflection points and the center of the sphere. (Note that there is a special case for which this is not true: that is, when the three points C_n, C_{n+1}, and O are colinear. In this case C_n and C_{n+1} are located at opposing poles of the sphere and the ray bounces back and forth between these two poles.)

A corollary to the above result is that all of the rays that travel by way of specular reflections from an arbitrary point S_1 to another such point S_2 must remain in the plane defined by the two points and the center of the sphere O. This is simply because, regardless of the number of reflections, all such rays start out from S_1 and end up at S_2. Therefore, all of them must have the points S_1 and S_2 as common reflection points. Hence, by the above argument all the rays that travel from S_1 to S_2 by specular re-

flections remain in the plane defined by the points S_1, S_2, and the center of the sphere O. The intersection of this plane with the sphere is clearly a great circle which is also the locus of all possible reflection points for the rays travelling between S_1 and S_2. In this discussion such a circle is termed for convenience *the circle of reflection.* All circles of reflection corresponding to a point such as S_1 intersect the diameter of the sphere that goes through S_1. When the points S_1, S_2, and O are not colinear, they define one and only one plane. (However when they are colinear, reflections can occur through infinitely many planes that have these three points in common. This does not lead to difficulties in computing the exchange factor because, for two differential area elements centered on opposite poles within a spherical enclosure only a vanishingly small point on each area element, and thus a vanishingly small amount of energy, is involved.)

The above result may be exploited to determine the locations of the first reflection points for the rays travelling from S_1 to S_2. These first reflection points must lie on the circle of reflection, which is a one-dimensional entity. Consider, as shown in Fig. 11, the circle of reflection corresponding to a point S_1 which passes through the point S_2. Suppose S_1 emits rays; i.e., is a *source point.* A point such as S_2 within this circle of reflection can be identified by the polar angles it makes with reference to the source point S_1. That is, the polar angles which represent S_2 are given by $\alpha_0 + 2\pi k$, where $k = 0,1,2,\ldots$. In this definition we have arbitrarily selected α_0 to have a value between 0 and 2π. The integer k in the above context indicates a specific cycle; however, it will be shown shortly that it also implies a specific sequence of reflections consistent with the notion of Section 3.1.4.

A second law of specular reflection states that the angles which the incident ray and the reflected ray make with the surface normal are equal. A consequence of this law is that, if the first reflection point of an arbitrary ray starting from S_1 is at a polar angle of α then the second reflection point is at 2α, the third one is at 3α, and so on. This

means that if a ray is to get from S_1 to S_2 by way of n reflections then the polar angle of the first reflection point can be obtained by dividing the polar angles corresponding to S_2 by $n+1$. That is, if α_{nk} is the polar angle of the first reflection point then,

$$\alpha_{nk} = \frac{\alpha_0 + 2\pi k}{n+1} \quad . \tag{3.24}$$

Equation (3.24) implies that for a given n there are an infinite number of sequences having n reflections, corresponding to $k = 0,1,2,3, \ldots$. However, examination of Eq. (3.24) reveals that α_{nk} and $\alpha_{n(k+n+1)}$ differ by 2π. This means they represent identical points on the circle of reflection. In other words for a given n , only the values of α_{nk} corresponding to the first $n+1$ values of k provide unique sequences (this number of unique sequences corresponds to $l(n) = n$ in Eq. (3.18)). By way of example the four possible unique ways by which a ray can get from S_1 to S_2 by way of three reflections are shown in Fig. 12.

The result indicated by Eq. (3.24) must be rewritten in terms of the global spherical coordinates (θ, ϕ) shown in Fig. 10 (the radial coordinate for all points of the spherical enclosure is the same and therefore is not a variable in the analysis). That is, the parametric equations of the circle of reflection in terms of the parameter α must be determined. In general, the parametric equations for θ and ϕ of the circle of reflection passing through two arbitrary points such as S_1 and S_2 are complicated functions. Instead of taking such a direct approach, we look for a coordinate system in which a simple correspondence exists between the polar angle α defined for the circle of reflection and the spherical coordinates defined for this coordinate system. One such coordinate system, shown in Fig. 13, is obtained when the z'- axis of the x', y', z'-coordinate system passes through the source point S_1. Such a coordinate system in this discussion is termed the *source-oriented* coordinate system. With respect to the spherical coordinates defined

for the source-oriented coordinate system, the source is always located at $\theta'_1 = 0$ (i.e., at the north pole). Then the circle of reflection for S_1 and S_2 in terms of the newly defined coordinate system is simply all the points on the sphere whose azimuthal angles are either ϕ'_2 or $2\pi - \phi'_2$. In mathematical notation the azimuthal angle ϕ' for the points on the circle of reflection in terms of the polar angle α ($0 \leq \alpha \leq 2\pi$) is given by

$$\phi'(\alpha) = \begin{cases} \phi'_2, & \alpha \leq \pi \\ 2\pi - \phi'_2, & \alpha > \pi \end{cases} . \tag{3.25}$$

Moreover, considering those polar angles α whose values are limited between 0 and 2π, the zenith angle of the new coordinate system θ' is related to the polar angle α by

$$\theta'(\alpha) = \begin{cases} \alpha, & \alpha \leq \pi \\ 2\pi - \alpha, & \alpha > \pi \end{cases} , \tag{3.26}$$

which can be written

$$\theta'(\alpha) = \pi - |\pi - \alpha| \quad . \tag{3.27}$$

Equation (3.24) can now be rewritten in terms of the source-oriented coordinate system, as given by Eq. (3.27); that is,

$$\theta'_{nk} = \pi - \left| \pi - \frac{2\pi k + \theta'_2}{n+1} \right| \quad . \tag{3.28}$$

In Eq. (3.28) θ'_{nk} is the zenith angle corresponding to the first reflection, and θ'_2 is the zenith angle of S_2, as shown in Fig. 13.

The intent of the following sections is to eventually obtain a procedure for evaluating the integral on the right-hand side of Eq. (3.10), $\int_{A'} (\varepsilon\sigma T^4 + \rho^d H)\, dE_{dA_1 - dA'}$. As was stated at the end of the Section 3.1.2 and will be shown in the next two sections, the evaluation

of this integral involves a tedious procedure. As a concession to notational simplicity, the radiosity, $\varepsilon\sigma T^4 + \rho^d H$, is not carried along during the development, and so there results a method for evaluating $\int_{A_2} dE_{dA_1 - dA_2}$, where A_2 is an arbitrary area. This latter integral is the same as the exchange factor $E_{dA_1 - A_2}$, according to Eq. (3.22a). The radiosity is then reintroduced when the development is complete.

3.2.2. Exchange Factor in a Spherical Enclosure Having No Opening

In this section we consider the derivation of $E_{dA_1 - A_2}$, where A_2 is an arbitrary surface element in the wall of a spherical enclosure. It is assumed that there is no opening on the wall of the enclosure. In the next section the discussion is taken further to include the possibility of an opening of arbitrary shape.

As was discussed in Section 3.1.1. the view factor between two arbitrary surface elements within the surface of a spherical cavity depends solely on the size of the second surface (see Eq. (3.5)). Consequently in determining the factors df_{nk} based on Eq. (3.23), it is sufficient to obtain only the size of the fictitious area dA_{nk}. Taking advantage of this simplification we derive the exchange factor $E_{dA_1 - A_2}$ between an infinitesimal element dA_1 and a finite area A_2, as illustrated in Fig. 14. We first derive the exchange factor from dA_1 to dA_2; this latter is an infinitesimal subdivision of A_2 centered on the longitudinal line ϕ' and enclosed between longitudes $\phi' - \frac{d\phi'}{2}$ and $\phi' + \frac{d\phi'}{2}$ (see Fig. 14). Safwatt [59] assumed that dA_{nk} is given by $\frac{1}{n^2}\, dA_2$. This assumption holds true when the surfaces in the enclosure are flat; however, as is shown below, it is invalid in the case of spherical cavities.

One restriction on the shape of the area A_2 is that when a given longitudinal line intersects it, the intersection is one continuous circular arc. This restriction does not sacrifice the generality of the problem; it merely eliminates the unnecessary compli-

cations of dealing with two or more differential areas on a given longitudinal line. In the θ'-direction dA_2 extends from θ^a to θ^b, as shown in Fig. 14. The zenith angles θ^a and θ^b are in general functions of ϕ' and their magnitude can be obtained by solving simultaneously the analytical expression for the boundary of A_2 and the longitudinal line ϕ'. When A_2 includes the source element dA_1, the lower limit of the area dA_2 in the θ'-direction, θ^a, has a value of zero for all ϕ'. Moreover, when the area A_2 includes the point whose θ'-coordinate has a value of π, the upper limit of dA_2 in the θ'-direction, θ^b, has the value of π also.

Recalling that all the rays travelling from a point S_1 to a second point S_2 by way of specular reflections remain in the circle of reflection passing through these points, it can then be concluded that the rays leaving S_1 which arrive at dA_2 must lie within the longitudinal band bounded by $\phi' - \frac{d\phi'}{2}$ and $\phi' + \frac{d\phi'}{2}$ as well as within the longitudinal band bounded by $2\pi - (\phi' - \frac{d\phi'}{2})$ and $2\pi - (\phi' + \frac{d\phi'}{2})$. Therefore, the fictitious area dA_{nk} must also be bounded by these longitudinal bands. That is, its extent in the ϕ'-direction must be $d\phi'$. The remaining parameter for determination of the size of dA_{nk} is its extent in the θ'-direction. This can be obtained simply by referring to the circle of reflection of S_2 at ϕ', as shown in Fig. 15.

By convention the circular arc extending from some polar angle α^x to some other polar angle α^y in the circle of reflection will be indicated by the symbol $[\alpha^x, \alpha^y]$. As shown in Fig. 15, in the circle of reflection the area dA_2 is represented by the arc $[\alpha^a, \alpha^b]$, where $\alpha^a = \theta^a$ and $\alpha^b = \theta^b$. Similarly, the circular arc which corresponds to the fictitious area dA_{nk} can be represented by $[\alpha^a_{nk}, \alpha^b_{nk}]$, where α^a_{nk} and α^b_{nk} are obtained from Eq. (3.24). From application of Eq. (3.24) it can be shown that the circular arc $[\alpha^a_{nk}, \alpha^b_{nk}]$ always either lies entirely within $[0, \pi]$ or lies entirely within $[\pi, 2\pi]$. This is because α^a and α^b are both less than or equal to π, and for a polar angle $\alpha_0 \leq \pi$, it can be shown by using Eq. (3.24) that for all $k \leq \frac{n}{2}$, $\alpha_{nk} \leq \pi$; and for all $k > \frac{n}{2}$, $\alpha_{nk} > \pi$.

Therefore, it is impossible for the fictitious area dA_{nk} extend from a point on the longitudinal line ϕ' to a point on the longitudinal line $2\pi - \phi'$. Hence, the size (per unit radius squared) of the fictitious area dA_{nk} is simply given by

$$dA_{nk} = \left| \int_{\theta^a_{nk}}^{\theta^b_{nk}} \sin\theta' \, d\theta' \right| d\phi' \quad , \tag{3.29}$$

where θ^a_{nk} and θ^b_{nk}, the limits of the fictitious area dA_{nk} in the θ' direction, are obtained by substituting their respective polar angles, α^a_{nk} and α^b_{nk}, into Eq. (3.27). The absolute value operation is necessary since, for the cases where $k > \frac{n}{2}$, the lower limit of the integral θ^a_{nk} becomes greater than the upper limit θ^b_{nk} , as may be shown by application of Eq. (3.28). Even though not shown notationally in Eq. (3.29), the limits of the integral, θ^a_{nk} and θ^b_{nk}, are functions of ϕ'. This is because they are functions of θ^a and θ^b, respectively, which in turn are functions of ϕ'.

The quantities df_{nk} in Eqs. (3.17) and (3.18) can be obtained using Eqs. (3.5), (3.23), and (3.29), yielding

$$df_{nk} = \frac{1}{4\pi} \left| \int_{\theta^a_{nk}}^{\theta^b_{nk}} \sin\theta' \, d\theta' \right| d\phi' \quad . \tag{3.30}$$

Therefore, for a spherical enclosure the exchange factor $dE_{dA_1 - dA_2}$ is given according to Eq. (3.18), by

$$dE_{dA_1 - dA_2} = \frac{1}{4\pi} \sum_{n=0}^{\infty} \sum_{k=0}^{n} (\rho^s)^n \left| \int_{\theta^a_{nk}}^{\theta^b_{nk}} \sin\theta' \, d\theta' \right| d\phi' \quad . \tag{3.31}$$

Using the property given by Eq. (3.22b) the exchange factor $E_{dA_1-A_2}$ can be expressed

$$E_{dA_1-A_2} = \int_{\phi^a}^{\phi^b} dE_{dA_1-dA_2}$$
$$= \frac{1}{4\pi} \int_{\phi^a}^{\phi^b} \sum_{n=0}^{\infty} \sum_{k=0}^{n} (\rho^s)^n \left| \int_{\theta_{nk}^a}^{\theta_{nk}^b} \sin\theta' \, d\theta' \right| d\phi' \ , \tag{3.32}$$

where ϕ^a and ϕ^b are the appropriate limits of A_2 in the ϕ'- direction, and $(\rho^s)^n$ corresponds to $\prod_{m=1}^{n}(\rho^s)_m$ in Eq. (3.18) when the specular reflectivity is uniform throughout the cavity. Moving the outside integral inside the summations and at the same time moving the absolute value operator outside both integrals yields

$$E_{dA_1-A_2} = \frac{1}{4\pi} \sum_{n=0}^{\infty} \sum_{k=0}^{n} (\rho^s)^n \left| \int_{\phi^a}^{\phi^b} \int_{\theta_{nk}^a}^{\theta_{nk}^b} \sin\theta' \, d\theta' d\phi' \right| \ . \tag{3.33}$$

The justification for moving the absolute value operator outside of both integrals is that the inside integral, which is a function of ϕ' , does not change sign when ϕ' ranges from ϕ^a to ϕ^b. In the form shown, the double integral in Eq. (3.33) represents a surface area within the enclosure surface whose boundaries can be recognized by the integration limits. This surface is actually the fictitious area obtained for the surface area A_2 for a given number of reflections n and a given k. Denoting such a surface by A_{nk}, the exchange factor $E_{dA_1-A_2}$ is given simply by

$$E_{dA_1-A_2} = \frac{1}{4\pi} \sum_{n=0}^{\infty} \sum_{k=0}^{n} (\rho^s)^n A_{nk} \ . \tag{3.33}$$

Of course, the inside integration in Eq. (3.32) can be evaluated in closed form, but it is more convenient to leave it in the form shown since later the radiosity will be included in the integral, as discussed at the end of Section 3.2.1.

3.2.3. The Exchange Factor in a Spherical Enclosure with a Single Opening

When there exists a single opening O on the wall of the enclosure, as shown in Fig. 16, the procedure for the derivation of the exchange factor $E_{dA_1-A_2}$ must be modified. The needed modifications are discussed in this section. As in the case of the area A_2, the only restriction on the shape of the opening area O is that when a given longitudinal line intersects it, the intersection is one continuous circular arc. If, unlike what is shown in Fig. 16, the longitudinal lines that define the receiving element dA_2 do not intersect the opening, then the opening would have no influence on $dE_{dA_1-dA_2}$. That is, the size of the fictitious area dA_{nk} would be as given by Eq. (3.29). When the longitudinal lines which define dA_2 intersect the opening, as is the case shown in Fig. 16, the fictitious area, instead of being one continuous area, consists of a collection of disjointed areas that lie between θ^a_{nk} and θ^b_{nk}. The reason for this behavior can be best explained by once again referring to the circle of reflection of S_1 which passes through dA_2, as shown in Fig. 17.

The discontinuity $[\psi^a, \psi^b]$ shown in the circle of reflection is the result of the circle of reflection at ϕ' intersecting the opening O. When there is no discontinuity in the circle of reflection, the necessary and sufficient condition for the rays from S_1 to arrive in $[\alpha^a, \alpha^b]$ by some number of reflections n is that they strike one of the arcs given by $[\alpha^a_{nk}, \alpha^b_{nk}]$, where $k = 0,1,2,...,n$, as described in the previous section. When there is a discontinuity, however, not all of the rays which strike the circle of reflection for the first time at the arc $[\alpha^a_{nk}, \alpha^b_{nk}]$ will get to the arc $[\alpha^a, \alpha^b]$. This is because it is possible that some or all of these rays at some point on their path will strike the discontinuity defined

by $[\psi^a, \psi^b]$ and escape through it. The arc given by $[\alpha^a_{nk}, \alpha^b_{nk}]$ may then be divided into two collections of arcs, one whose members secure a "safe passage" to the arc $[\alpha^a, \alpha^b]$, and one consisting of the arcs that do not. Only the former collection is relevant to the determination of the fictitious area dA_{nk}. This collection is denoted by the symbol w. To obtain the collection w, we must first identify the collection of all arcs within the circle of reflection upon which, when a ray leaving S_1 first strikes, the ray will inevitably escape through the opening before its n^{th} reflection. We will denote this collection of arcs by u. Clearly, points on $[\alpha^a_{nk}, \alpha^b_{nk}]$ which are also in the collection u cannot be in the collection w; that is,

$$w = [\alpha^a_{nk}, \alpha^b_{nk}] - u \quad , \tag{3.35}$$

where the minus operator (—) means the intersection of $[\alpha^a_{nk}, \alpha^b_{nk}]$ with all points in the circle of reflection except those of u.

We now proceed to obtain the collection of arcs symbolized by u. It is clear that the rays leaving S_1 and striking the circle of reflection for the first time at $[\psi^a, \psi^b]$ do not have the opportunity for even one reflection. Similarly rays that strike the collection of $[\psi^a, \psi^b]$, $[\psi^a_{11}, \psi^b_{11}]$, and $[\psi^a_{12}, \psi^b_{12}]$, where the subscripts are those defined by Eq. (3.24), do not have the opportunity to undergo more than one reflection. Continuing this line of reasoning, the collection u can be expressed symbolically by

$$u = \bigcup_{n'=0}^{n-1} \bigcup_{k'=0}^{n'} [\psi^a_{n'k'}, \psi^b_{n'k'}] \quad , \tag{3.36}$$

where the mathematical symbol $\bigcup_{j=1}^{l} [\alpha_j, \beta_j]$ means the union of all arcs $[\alpha_j, \beta_j]$ for which $j = 1,2,...,l$. The logical operations implied by the symbol $\bigcup$ and by the minus operator (—) in Eq. (3.35) may be implemented on a digital computer in a straightforward man-

ner. The collection w can be obtained by combining Eq. (3.34) with Eq. (3.33). Generally the collection w consists of a set of disjointed circular arcs $[\alpha_i^L, \alpha_i^U]$, where $i = 1,2, \ldots, i_{max}$, and i_{max} indicates the total number of such circular arcs. The zenith angles θ_i^L , θ_i^U, which correspond to the polar angles α_i^L , α_i^U, respectively, give the θ'-extents of each of the sub-areas which make up the fictitious area dA_{nk}. These zenith angles can be obtained from Eq. (3.27). Thus, the fictitious area dA_{nk} in this case is given by

$$dA_{nk} = \sum_{i=1}^{i_{max}} \left| \int_{\theta_i^L}^{\theta_i^U} \sin\theta' \, d\theta' \right| d\phi' \quad . \tag{3.37}$$

Following the procedure outlined by Eqs. (3.30) through (3.33), the exchange factor $E_{dA_1 - A_2}$ is found to be given by

$$E_{dA_1 - A_2} = \frac{1}{4\pi} \sum_{n=0}^{\infty} \sum_{k=0}^{n} (\rho^s)^n \sum_{i=1}^{i_{max}} \left| \int_{\phi^a}^{\phi^b} \int_{\theta_i^L}^{\theta_i^U} \sin\theta' \, d\theta' d\phi' \right| \quad . \tag{3.38}$$

Hence, when there exists an opening O on the enclosure surface area, the area corresponding to the fictitious area A_{nk} defined in the previous section is given by

$$A_{nk} = \sum_{i=1}^{i_{max}} \left| \int_{\phi^a}^{\phi^b} \int_{\theta_i^L}^{\theta_i^U} \sin\theta' \, d\theta' d\phi' \right| \quad . \tag{3.39}$$

3.2.4. *Isothermal Spherical Cavity with Diffuse-Specular Surface (Revisited)*

In this section the materials presented in two previous sections are applied to define a procedure for evaluating the local irradiance in specular and diffuse-specular cavities. The surface area of the cavity A' in Fig. 7 corresponds to the area A_2 in the two previous sections, and the opening O corresponds to a spherical cap bounded by the zenith angle ψ. In this situation the opening O and the cavity surface area A' share the same boundary. The source element dA_1 in Eq. (3.10) is located at zenith angle θ_1. Due to symmetry, the circumferential position of the element dA_1 is arbitrary for evaluation of H. Therefore, we have considered the area dA_1 to be located in the position shown in Fig. 18 (i.e., $\phi_1 = 3\frac{\pi}{2}$) since in this position the source-oriented coordinate system can be obtained by simply rotating the y,z-plane in the counterclockwise direction about the x-axis by the amount θ_1, as shown in Fig. 19. The relation between the (θ, ϕ) of the original coordinate system and (θ', ϕ') of the source-oriented coordinate system may be obtained by using the coordinate transformation matrix for this rotation,

$$\begin{bmatrix} 1 & 0 & 0 \\ 0 & \cos\theta_1 & \sin\theta_1 \\ 0 & -\sin\theta_1 & \cos\theta_1 \end{bmatrix} \begin{bmatrix} \sin\theta\cos\phi \\ \sin\theta\sin\phi \\ \cos\theta \end{bmatrix} = \begin{bmatrix} \sin\theta'\cos\phi' \\ \sin\theta'\sin\phi' \\ \cos\theta' \end{bmatrix} . \tag{3.40}$$

In order to follow the procedure defined in Sections 3.2.2 and 3.2.3, it is important to obtain a parametric equation for the boundary of the cavity in terms of the variables of the source-oriented coordinate system. By knowing this parametric equation, the angles corresponding to ψ^a and ψ^b can be obtained. Since the cavity opening and the cavity wall share the same boundary, the same parametric equation can be used to obtain the angles corresponding to θ^a and θ^b. This parametric equation can be obtained by first substituting the angle ψ, which defines the boundary of the cavity in the original

coordinate system, for θ in Eq. (3.40). After multiplying out the matrices on the left-hand side of Eq. (3.40) and some further algebraic manipulations, the boundary of the cavity in terms of the source-oriented coordinate system is expressed implicitly by

$$\cos\theta' + (\tan\theta_1 \ \sin\phi')\sin\theta' = \frac{\cos\psi}{\cos\theta_1} \quad . \tag{3.41}$$

Solutions of Eq. (3.41) for a given ϕ' can be used to obtain the angles corresponding to ϕ^a and ϕ^b, as well as θ^a and θ^b.

The equation for the distribution of the irradiance on the cavity wall, Eq. (3.10) may now be written

$$H(\theta_1) = \frac{1}{4\pi} \sum_{n=0}^{\infty} \sum_{k=0}^{n} (\rho^s)^n \sum_{i=1}^{i_{max}} \left| \int_0^{2\pi} \int_{\theta_i^L}^{\theta_i^U} (\varepsilon\sigma T^4 + \rho^d H) \sin\theta' \, d\theta' d\phi' \right| \quad . \tag{3.42}$$

Equation (3.42) is obtained by introducing the radiosity into Eq. (3.38) and setting the limits of integration over ϕ' (i. e., ϕ^a and ϕ^b) from 0 to 2π. However, due to symmetry, these limits can be assigned the values $\pi/2$ and $3\pi/2$, respectively, and the results then multiplied by two.

Solution of Eq. (3.42) for discrete points on the cavity wall can be obtained by an iterative procedure. The procedure is started by assigning guessed values for H at discrete points (i.e., θ's). Then, by using these values the integral on the right-hand side at all the points considered is evaluated to obtain improved values for H. This process is repeated until a convergence criterion is met. In order for the distribution of H to be continuous, it can be assumed to behave linearly as a function of θ between the considered points. Once the distribution of H on the cavity wall is obtained, the distribution

of the heat flux can be obtained by using Eq. (3.2). The apparent emissivity can then be evaluated by using Eq. (3.1). As was previously mentioned, when the cavity wall is purely specular, there is no need for iteration. The distribution of irradiance can be obtained by using Eq. (3.11) in which the exchange factor $E_{dA_1-A'}$ is obtained from Eq. (3.38).

The Computer program CVTY, listed in Appendix B, has been used to obtain the distribution of the local heat flux on the wall of a diffuse-specular cavity. The results obtained for various cavity opening angles and surface conditions are presented and discussed in Chapter 4. All the integrations were performed by using the Romberg method (sometimes known as the method of extrapolation to the limit) in conjunction with simple trapezoidal rule for integration. The subroutine which performed the integration was obtained from Reference 69. For the inside integration the tolerance for terminating the successive integrations was set at 10^{-3}, while for the outside integration it was set at 10^{-5} . These tolerances address the question of convergence rather than accuracy. The interested reader is referred to Reference 69 for a detailed interpretation of these tolerences.

The points considered for the evaluation of H were separated by about 3 deg. The initial guessed values for H at the mesh points were those obtained by assuming $\rho^d = 0$ in Eq. (3.42). The convergence criterion used to determine the number of iterations I was

$$\frac{1}{\sigma T^4} \sqrt{\sum_j (H_j^I - H_j^{I-1})^2} \leq 0.001 \ , \tag{3.43}$$

where H_j^I is the radiosity at the j^{th} mesh point evaluated at the I^{th} iteration. The number of reflections N considered for evaluation of the exchange factor was determined from the criterion

$$(\rho^s)^N = 0.001 \ . \tag{3.44}$$

This yielded N =3, 6, 10, 20, and 66 for ρ^s = 0.1, 0.3, 0.5, 0.7, and 0.9, respectively. Reducing the convergence criterion in the right-hand side of Eq. (3.43) by a factor of ten changed the results only at the fourth significant figure and beyond.

3.3. Absorption of Collimated Radiation Entering a Specular Spherical Cavity at a Specified Angle

For a diffuse spherical cavity the apparent absorptivity has been found in Reference 54 to be independent of the manner in which radiation enters the cavity. In the same reference the apparent absorptivity was shown to be given by the same expression as Eq. (3.9) except with the emissivity of the wall ε replaced by the wall absorptivity α. Thus, when the wall of the cavity is gray the apparent emissivity and the apparent absorptivity both are given by Eq. (3.9). In this section a method is developed to obtain the apparent absorptivity of a perfectly specular spherical cavity when parallel radiation enters its opening at a given angle. The development draws on some of the fundamental concepts used in the previous section.

Figure 20 shows a spherical cavity, whose wall is a perfectly specular reflector ($\rho = \rho^s$) , subject to a parallel radiation flux of I_0 (watts per unit normal area) to the opening at a given angle. The y,z-plane of the x,y,z- coordinate system shown in Fig. 20 is arbitrarily oriented parallel to the direction of the incoming radiation. The direction of the radiation can then be identified by the angle γ it makes with respect to the z-axis, as shown in Fig. 20. The radiation can be considered to be originating from a point source infinitely far from the cavity. Consistent with the approach taken in Sec-

tion 3.3. the y,z-plane is rotated by an amount γ so that the z-axis passes through the source, thus obtaining the source-oriented coordinate system shown in Fig. 21. With respect to the spherical coordinates of this coordinate system, the rays entering the cavity on a given longitudinal line ϕ' undergo specular reflections as a group within the circle of reflection at ϕ'. Hence, the total energy absorbed by the cavity can be obtained by finding the portion of the energy that enters the cavity through a longitudinal band $d\phi'$ at ϕ' that is absorbed, and then integrating over the appropriate limits of the cavity opening in the ϕ' -direction. The boundary of the cavity opening with respect to the spherical coordinates of the source-oriented coordinate system is given by Eq. (3.42) in which θ_1 is replaced by γ.

Figure 22 shows the circle of reflection at the azimuthal angle ϕ' . The rays, which in this arrangement are parallel to the z'-axis, enter the circle of reflection through the discontinuity shown by $[\psi^a, \psi^b]$ in the figure, and undergo multiple reflections within the circle of reflection. As a result, some of these rays may be reflected into the discontinuity and escape through it. We now proceed to determine the portion absorbed, during the n^{th} reflection, of that which enters the circle of reflection through the opening. Note that each ray that enters the circle of reflection can be completely identified by the polar angle of its point of entry on the circular arc $[\psi^a, \psi^b]$. For a given number of reflections n , it is possible to divide the circular arc $[\psi^a, \psi^b]$ into two collections of arcs. One collection identifies the rays that do not encounter the discontinuity during their first n reflections, while the other collection identifies the rays that do encounter the discontinuity during their first n reflections. The former collection is identified by the symbol v. By using collection v the fraction absorbed by the cavity during the n^{th} reflection of that portion of the energy which enters the cavity through the longitudinal band $d\phi'$ at ϕ' can be calculated. In order to obtain the collection v the reflection points of a given ray entering the circle of reflection must be determined. From Fig. 22 it can

be seen that the polar angle between two consecutive reflection points for a ray entering the circle of reflection at a polar angle α_0 is given by $\pi - 2\alpha_0$. Hence the polar angle of the n^{th} reflection point is given by

$$\alpha_n = n\pi - (2n-1)\alpha_0 \quad . \tag{3.45}$$

By using Eq. (3.45) the procedure for finding the collection v can be easily implemented on a digital computer. Clearly the circular arc where the first incidence occurs has no point in common with the discontinuity. Hence, the procedure for finding the collection v starts out by finding the circular arc where the second reflection occurs by substituting ψ^a and ψ^b into Eq. (3.45) for $n = 2$. Next we compare the circular arc thus obtained with the discontinuity. If there is a common region, then the rays that strike the common region escape through the discontinuity. We exclude the circular arc corresponding to those rays from $[\psi^a, \psi^b]$ and continue the procedure up to and including the n^{th} reflection.

The circular arcs which make up the collection v are identified by $[\psi_i^L, \psi_i^U]$, where $i = 1,2, \ldots, i_{max}$. Through each circular arc $[\psi_i^L, \psi_i^U]$ of width $d\phi'$ enters an amount of energy which can be identified by the symbol $dQ_{(\psi_i^L \to \psi_i^U)}$. The portion of this energy which is absorbed during the n^{th} reflection is given by $(1-\rho^s)(\rho^s)^n\, dQ_{(\psi_i^L \to \psi_i^U)}$. Hence, the total energy which is absorbed due to that which has entered the cavity through the longitudinal band $d\phi'$ at ϕ' is given by

$$dQ_n = (1-\rho^s)(\rho^s)^n \sum_{i=1}^{i_{max}} dQ_{(\psi_i^L \to \psi_i^U)} \quad . \tag{3.46}$$

The amount that is absorbed during all reflections is thus given by

$$dQ(\phi) = \sum_{n=0}^{\infty} dQ_n = (1-\rho^s) \sum_{n=0}^{\infty} (\rho^s)^{(n-1)} \sum_{i=1}^{i_{max}} dQ_{(\psi_i^L \rightarrow \psi_i^U)} \quad . \tag{3.47}$$

The quantity yet to be determined is $dQ_{(\psi_i^L \rightarrow \psi_i^U)}$. Also shown in Fig. 22 is the radiative energy which enters the circle of reflection through a differential polar angle of $d\alpha_0$ at α_0. The normal component of the differential area where the first reflection occurs is given by $\cos \alpha_0 \sin \alpha_0 \, d\alpha_0 \, d\phi$. Hence,

$$dQ_{(\psi_i^L \rightarrow \psi_i^U)} = I_0 \int_{\psi_i^L}^{\psi_i^U} \sin \alpha_0 \cos \alpha_0 \, d\alpha_0 d\phi = \frac{I_0}{2} (\sin^2 \psi_i^U - \sin^2 \psi_i^L) \quad . \tag{3.48}$$

By substituting the right hand-side of Eq. (3.48) for $dQ_{(\psi_i^L \rightarrow \psi_i^U)}$ into Eq.(3.47), the amount of energy which is absorbed due to that which enters the cavity through the longitudinal band $d\phi'$ at ϕ' can be calculated. The amount of the energy which is absorbed by the cavity can be obtained by integrating Eq. (3.47) from $\phi = \pi/2$ to $\phi = 3\pi/2$ and multiplying the results by two, as the case discussed in Section 3.2.4. Dividing the energy absorbed by the total energy which enters the cavity gives the apparent absorptivity α_a. The amount of energy which enters the cavity is given simply by

$$Q_e = \pi \sin^2 \psi \cos \gamma \, I_0 \quad . \tag{3.49}$$

The computer program PRYS, shown in Appendix B, has been used to obtain the apparent absorptivity of a spherical cavity having purely specular walls for incident parallel radiation. The results, obtained for a variety of surface and geometric conditions are presented and discussed in Section 4.2. The program involves a numerical integration over the ϕ' variable. This integration is performed by using the Romberg

method. The tolerance for terminating the successive integration was set at 10^{-6} (see Reference 69). The number of reflections considered for calculations was obtained according to Eq. (3.44).

4.0 Results and Discussion

The results presented in this chapter reveal the behavior of two important properties of a spherical cavity: the apparent emissivity and the directional apparent absorptivity. When the cavity walls are gray, the apparent emissivity and the apparent absorptivity are identical (see Reference 11, page 59). This same equivalence also exists for the apparent directional absorptivity and the apparent directional emissivity if the surfaces are gray (see Reference 63, page 18). In Section 4.3 the exact analytical results presented in this chapter are verified by comparing them with results obtained independently using the Monte Carlo technique.

4.1. Results for Cavity Emission

In this section initial consideration is given to presenting the results for the local heat transfer distribution within spherical cavities whose walls are diffuse emitters and both diffuse and specular reflectors of thermal radiation. These results help achieve a better understanding of the overall emission characteristics of the cavity.

4.1.1. Local Heat Transfer Results

The distribution of the heat transfer to the cavity surface is shown in dimensionless form, $q/\sigma T^4$, where T is the uniform cavity wall temperature, for cavity opening angles ranging from 105 deg to 15 deg in Figs. 23 through 46. The positive values of $q/\sigma T^4$ are consistent with the idea that heat is lost from the walls since no radiation enters from outside where $T = 0$ The position on the cavity wall in each graph is indicated in terms of the zenith angle θ. There are two sets of graphs shown: one set (Figs. 23, 25, 27, 29, 33, 37, and 41) shows the local heat transfer characteristics of purely specular cavities, while the other set (Figs. 24, 26, 28, 31, 35, 39, and 43) shows the local heat transfer characteristics of cavities having diffuse-specular walls with a *reflectivity ratio* of 0.5, where the reflectivity ratio is defined as the ratio of $\frac{\rho^s}{\rho^s + \rho^d}$. When the opening angle $\psi \leq 60$ deg, a three-dimensional graph also accompanies the results for each case (Figs. 30, 32, 34, 36, 38, 40, 42, and 44). The local heat transfer distributions are obtained for the wall emissivities of 0.1, 0.3, 0.5, 0.7, and 0.9. Corresponding to every specular or diffuse-specular local heat transfer characteristic curve there exists a horizontal straight line which represents the uniform heat transfer distribution for diffuse cavities. These latter results were obtained from Eq. (3.9).

When the cavity opening angle is greater than or equal to 90 deg (Figs. 23-26), the heat transfer for specular surfaces increases slightly with θ. When the cavity opening angle is less than 90 deg (Figs. 27-44), starting from the cavity mouth the nondimensional heat transfer decreases slowly with increasing θ and, after reaching a minimum, it increases slowly. After passing though an inflection point at $\theta_i = 180 - \psi$ it reaches a maximum at the bottom of the cavity. The value of the nondimensional heat transfer at a given location θ_1 is related to the size of the spherical sector which is defined by all circles of reflection that pass through a differential surface element dA_1 located at θ_1 and

which intersect the hole. This is because the circle of reflection is the only specular path for the transfer of radiant energy in a spherical cavity having specular walls. When $\theta_1 > \theta_l$ this sector, unlike when $\theta_1 < \theta_l$, is actually the entire sphere because all circles of reflection that pass through A_1 intersect the hole. This explains the greater magnitude of the heat transfer when $\theta > \theta_l$ than when $\theta < \theta_l$. We will refer to the region of the cavity for which $\theta < \theta_l$ as the *side-wall* of the cavity and the region for which $\theta > \theta_l$ as the *bottom-wall* of the cavity.

For any given surface condition, as the size of the opening angle decreases, the nondimensional heat transfer also decreases and the spacing between the curves becomes less. This is an expected trend since in the limiting case where there is no opening on the cavity surface, the net heat transfer at all locations within the surface of an isothermal cavity must be zero regardless of the surface properties of the cavity wall.

At the other extreme, as the cavity opening angle approached 180 deg, the nondimensional heat transfer must approach the value of the surface emissivity. This is because the cavity becomes a flat surface in the limit, and so there is no reflection of radiation onto the surface, and the local heat transfer is given simply by $\varepsilon\sigma T^4$. For diffuse cavities this can be verified by inspection of Eq. (3.8). Specular and diffuse-specular cavities must also show the same type of behavior because, as pointed out previously, for large opening angles the heat transfer distribution curves for all reflectivity ratios converge to the constant horizontal line corresponding to the diffuse emissivity.

In a cavity with diffuse walls, higher emissivity ε results in a larger heat transfer throughout the surface, but this is not the case as the cavity surface becomes specular. By referring to the three-dimentional graphs for the cases when the cavity opening angle is less than or equal to 60 deg (even numbered Figs. 30-44) it may be seen that the peak value of heat transfer at the bottom of the cavity occurs at a value of surface emissivity

somewhere between but never equal to zero and one. As the size of the opening angle decreases, the value of emissivity corresponding to the peak heat transfer gets smaller.

It is also interesting to look at the difference between the values of the local nondimensional heat transfer for a diffuse surface and a specular surface. This difference is largest when $\varepsilon = 0.5$ (see for example Fig. 37). At high emissivities this difference is small because as the value of ε approaches unity, the cavity becomes a blackbody, and the type of surface reflection becomes irrelevant. At low emissivities as emissivity gets small (reflectivity gets large) the difference between the heat transfer in a diffuse cavity and a specular cavity is reduced. This is because with low surface emissivities, the directional effects of the surface reflection become less significant due to the large number of reflections. For small opening angles, assuming a diffuse wall when the wall is purely specular can lead to large errors in calculation of the local heat transfer. For example when the cavity opening angle is 45 deg and the emissivity $\varepsilon = 0.5$, this error is about 50 percent on the bottom wall of the cavity, and it can get as high as 300 percent when the opening angle is 15 deg (see Figs. 33 and 41, respectively)

In Figs. 45 and 46 the reflectivity ratio $\frac{\rho^s}{\rho^s + \rho^d}$ is varied for a cavity opening angle of 60 deg and an emissivity of 0.5. The results shown are for the reflectivity ratios of zero (purely diffuse), 0.25, 0.5, 0.75, and unity (purely specular). On the bottom-wall of the cavity the heat transfer curves are separated by an approximately equal distance. In contrast the curves on the side-wall region are not spaced equally. Another observation that may be made by referring to Fig. 45 is that the heat transfer curve for a purely diffuse surface and that for a purely specular surface do not bound all the other curves near θ_i. This indicates that the purely specular and purely diffuse surfaces do not always represent the limiting cases.

4.1.2. Overall Emission

The apparent emissivities were obtained by integrating the (discrete) values obtained for the local heat transfers, using the trapezoid rule, over the cavity surface and applying Eq. (3.1). The numerical results obtained in this manner are tabulated in Table 1 and are plotted in Fig. 47.

As in all cavities previously studied, the apparent emissivity is always greater than the surface emissivity. The apparent emissivity approaches the emissivity of the surface as the cavity becomes wide open (i. e., becomes a flat plate). When the cavity opening angle approaches zero, the apparent emissivity in all cases approaches unity.

There is, however, one important difference between the apparent emissivity results of spherical cavities and those of cylindrical and conical cavities. In spherical cavities, for a given surface emissivity, the apparent emissivity is not always an increasing function of the degree of specularity. As mentioned in Section 2.2, this difference has also been noted by Campanaro and Ricolfi [58] based on their approximate results. Based on the results shown in Fig. 47, specular cavities have a higher apparent emissivity when the surface emissivity is 0.9. However, as the emissivity of the surface decreases, curves representing the specular cavities begin to shift downward relative to the curves for the diffuse cavities. Eventually, as the emissivity of the cavity surface approaches a value of 0.1, the apparent emissivity of the diffuse cavity becomes greater than that of the specular cavity. This is a disadvantage of specular cavities having low surface emissivities. As the wall emissivity ε is changed, the apparent emissivity curves for the diffuse-specular ($\rho^s/\rho = 0.5$) cavities deviate from those for the diffuse cavities in the same manner but at a slower pace than those for the specular cavities. Note, however, that for low emissivities diffuse cavity and the diffuse-specular cavity have essentially the

same apparent emissivities for all opening angles. This seems to suggest that for low emissivities the diffuse effect dominates the specular effect.

Another curious observation that can be made regarding the apparent emissivity results for the spherical cavities is that the apparent emissivity for a diffuse-specular cavity does not always fall between the apparent emissivities of the corresponding purely diffuse and purely specular cavities. This is another example where purely diffuse reflection and purely specular reflection do not always represent limiting cases in radiation exchange.

The dependence of results on the degree of specularity becomes practically insignificant when the cavity opening angle becomes greater than approximately 105 deg for high and midrange values of emissivity. However, for small emissivities this is true for even smaller cavity angles.

Finally, variation of the apparent emissivity in spherical cavities is a weaker function of the degree of specularity than in the case of the conical and cylindrical cavities as can be seen by comparing Fig. 47 with Figs. 4 and 5. In fact, referring to Fig. 48 which shows the cavity effect $\varepsilon_a/\varepsilon$ as a function of opening angle with surface emissivity as a parameter, it can be seen that for $\varepsilon \geq 0.5$ the curves representing the cavity effect for the diffuse, specular, and diffuse-specular cases are almost indistinguishable.

4.2. Absorption of Collimated Radiation (Directional Apparent Absorptivity)

The results for the directional apparent absorptivity are shown in polar graphs for cavity opening angles ranging from 150 deg to 15 deg in Figs. 49 through 58. Each figure shows the directional apparent absorptivity $\alpha_a(\gamma)$ as a function of the angle of incidence γ for various surface absorptivities α. Apparent absorptivity results for the cor-

responding diffuse cavities, which are independent of γ, are also plotted for comparison. Results for the diffuse case were obtained directly from Eq. (3.8).

As expected, for a given opening angle and incidence angle, as the absorptivity of the wall α increases, so does $\alpha_a(\gamma)$. Moreover, for a fixed wall absorptivity α as the cavity opening angle increases $\alpha_a(\gamma)$ decreases for all γ. The apparent absorptivity is normally greater than the absorptivity of the cavity surface. However, for large opening angles, it is possible that for some values of γ the radiation entering the cavity reflects out of the cavity after one reflection. In these cases $\alpha_a(\gamma) = \alpha$. (See the results for $\psi = 150$ deg in Fig. 49).

The nature of the directional apparent absorptivity changes radically as the cavity opening angle decreases. For this reason, it is not possible to express a general trend for $\alpha_a(\gamma)$ that is applicable for all opening angles except that as the opening angle becomes smaller the behavior becomes more complicated. However, it is roughly true that in cavities with opening angles of less than 90 deg, the directional apparent absorptivity has its largest values when the angle of incidence approaches 90 deg. This is not the case, however, for cavities with $\psi \geq 90$ deg.

An interesting feature of the directional apparent absorptivity curves when the cavity opening angle is less than 90 deg is that they all have a local peak when the angle of incidence is the same as the cavity opening angle. This behavior may, however, be fortuitous for the specific cavity opening angles considered in this study. Therefore, more cases must be studied in order to establish whether this behavior is general for all cavity opening angles less than 90 deg.

Generally the curves for the directional apparent absorptivity become smoother either as the opening angle or as the surface absorptivity increases. To help explain this phenomenon, $\alpha_a(\gamma)$ may be written as

$$\alpha_a(\gamma) = 1 - (\rho^s)f_1(\gamma) + (\rho^s)^2 f_2(\gamma) + (\rho^s)^3 f_3(\gamma) + \ldots \quad , \tag{4.1}$$

where the functions $f_n(\gamma)$ give the fraction of the energy entering the cavity which is reflected out after n ideal ($\rho^r = 1$) reflections. Consider as an example the variation of $f_1(\gamma)$ with γ when the cavity opening angle is small. Then for a value of γ near 90 deg, all the radiation which enters the cavity stays inside the cavity after the first reflection; therefore, $f_1 = 0$. As the angle of incidence γ decreases, the value of f_1 remains zero up to a certain angle of incident, say γ^*, where the radiation starts to be reflected out of the cavity. Clearly, from this point on f_1 has a different behavior; therefore, a sudden change of slope occurs at γ^* . A similar behavior occurs for all the other f_n 's in Eq. (4.1). Therefore, when a fewer number of terms can be used in Eq. (4.1) to accurately express $\alpha_a(\gamma)$, its behavior as a function of incidence angle will be smoother. This happens when either the surface absorptivity becomes high, or the opening angle becomes large. When absorptivity of the surface is high, ρ^r is small; therefore, the higher order terms become negligible in Eq. (4.1). On the other hand, when the cavity opening angle is large, most of the radiation is reflected out of the cavity after the first few reflections (i. e., the functions f_n become very small or zero for large n); therefore, higher order terms in Eq. (4.1) become negligible in this case also.

At this point it is interesting to make some comparisons between the values of the directional apparent absorptivity for cavities with diffuse walls and those for cavities with specular walls. Note that in cavities with sufficiently small opening angles when the surface absorptivity has a small value, such as 0.1 (or lower), the value of $\alpha_a(\gamma)$ for a cavity with a specular wall is smaller than the corresponding value for a cavity with a diffuse wall for all incident angles. This is because when a ray enters a cavity having specular walls, it remains in a circle of reflection which intersects the hole. Therefore, the ray has a good chance of being reflected out of the cavity with a significant portion

of its original energy after a reasonable number of reflections. However, when a ray enters a cavity whose walls are diffuse, it gets "lost" in the cavity because the cavity opening is small, and there is a relatively small probability that the ray will be reflected out of the cavity by diffuse reflection.

As the value of the absorptivity of the cavity wall gets larger, heat transfer is defined by a decreasing number of reflections. In this case, the energy contained in a ray entering a diffuse cavity has a better chance of being reflected out of the cavity than a ray entering a specular cavity. This is because the diffusely reflected ray is not restricted to travel within a circle of reflection which, in most cases, guarantees some minimum number of reflections before the specularly reflected ray is reflected out. Therefore, as α gets larger, the values of $\alpha_a(\gamma)$ for specular cavities get closer to those of the diffuse cavities, and for high values of surface absorptivity, the former exceeds the latter for a large range of incident angles.

For large cavity openings, diffuse and specular cavities have directional apparent absorptivities that are close to each other. This is because most of the rays that enter the cavity are reflected out after a small number of reflections regardless of whether the cavity surface is diffuse or specular. In the extreme case of when the cavity is wide open, the apparent directional absorptivities of both diffuse and specular cavities become equal and equal to the surface absorptivity.

Finally, it should be mentioned that the results obtained suggest that there exists a potential for using spherical cavities having specular walls in designing directionally selective surfaces. Depending on the desired directional selectivity, a cavity with a certain opening size may be used. For example when the cavity opening angle is 105 deg and the absorptivity α is 0.1, the ratio of $\alpha_a(0)/\alpha_a(90)$ is approximately two. On the other hand, this ratio when the opening angle is 45 deg is approximately 0.5 for the same value of α.

4.3. Comparison With Monte Carlo Results

In order to support the apparent emissivity and directional apparent absorptivity results reported above, they are compared with values obtained using the Monte Carlo method, which is a completely independent approach. Implementation of the Monte Carlo method is discussed in detail in Appendix A.

For the Monte Carlo calculations of the apparent emissivity, the surface of the cavity was subdivided as follows. The surface of a complete sphere was divided into four equal-area latitudinal bands, and the surface of a given cavity was divided according to the greatest integral number of the sub-divisions of the complete sphere covered by the cavity. This roughly assured that cavities having larger surface areas (smaller opening angles) would be divided into a larger number of equal area elements than the cavities with smaller surface areas. For all cases 40,000 energy bundles were emitted per element. This number of energy bundles gives results that are within approximately 0.1 percent of the apparent emissivity results for the diffuse cavity, for which the exact closed-form solution is known. Two types of tests were performed. In the first type (Table 2a) the wall emissivity ε was fixed at 0.5 and the opening angle ψ was varied, and in the second type (Table 2b) ψ was fixed at 60 deg while the wall emissivity was varied.

By referring to Table 2, it can be seen that the Monte Carlo results agree, except in a few cases, to within one percent of the exact analytical results. This good agreement verifies that the assumptions made in the formulation of the analytical model are correct and that the computations are free of error (other than the usual numerical errors inevitably associated with numerical integration). The 2-3 percent disagreement observed in cases when the cavity opening angle is small is known to be attributable to insufficient statistical sampling in the Monte Carlo method.

The CPU times required to obtain the results in Table 2 are shown in Table 3. In all cases, as the surface emissivity decreases the required CPU time increases. This is because when the reflectivity is high, a larger number of terms must be retained in the series representation of the apparent emissivity. The same trend is observed as the cavity opening angle decreases. The required CPU times for the diffuse-specular cases in the exact analytical method are considerably larger than those for the Monte Carlo calculations because of the iterative technique that was used. In these cases the Monte Carlo method can be used to obtain results with reasonable accuracies while using relatively little computing time. It should, however, be pointed out that the Monte Carlo method developed for the present study does not provide the heat transfer distribution on the cavity wall, but that this is obtained as a by-product of the exact analytical method. The work by Toor and Vistanka [26] showed that the Monte Carlo method is not an efficient method for evaluation of the local heat transfer on the wall of an enclosure.

The Monte Carlo method was also used to verify the validity of the results obtained for the directional apparent absorptivity. The comparison of the two results, as well as the comparison of the required CPU times, are shown in Table 4. This comparison was performed for the case when the cavity opening angle is 15 deg and the emissivity is 0.3 for various incidence angles γ. Experience with the model indicates that this case provides a good check of the analytical results because the emissivity is low and the opening angle is small, both of which lead to more reflections within the cavity. Therefore, higher order terms must be used for the analytical computations, and if there is any error in the analysis it would be likely to show up in these results. In this case 10,000 energy bundles were introduced into the cavity opening to obtain the Monte Carlo results. As can be seen, the agreement between the two methods is excellent. The required CPU times are also smaller than those for the apparent emissivity calculations because the calculations for the apparent directional absorptivity required only one numerical inte-

gration. At all angles the CPU time is an order of magnitude less for the analytical method than for the Monte Carlo method.

5.0 Conclusions and Recommendations

Based on the results obtained in this investigation the following conclusions may be drawn:

1. In isothermal spherical cavities having specularly reflecting walls, the heat transfer distribution necessary to maintain the cavity isothermal can be highly nonuniform. This nonuniform distribution becomes more evident as the cavity opening angle decreases. The local heat transfer is always greatest on the cavity wall opposite the opening. This behavior is unlike diffuse spherical cavities in which the local heat transfer is uniform throughout the cavity wall.

2. Similar to other cavity configurations previously reported in the literature, the cavity effect in spherical cavities is most pronounced at small opening angles and low emissivities. The cavity effect is, however, not as sensitive to the degree of specularity of the cavity wall as in the case of other types of cavities.

3. Unlike other cavity configurations, there are cases in which the apparent emissivity of a diffuse cavity exceeds that of a specular cavity. Moreover, in some cases the

apparent emissivity for a diffuse-specular cavity does not fall between the apparent emissivities of a purely diffuse and a purely specular cavity. That is, purely diffuse and purely specular walls do not appear to always be the limiting cases.

4. The directional apparent absorptivity of spherical cavities having specular walls is found to be increasingly dependent on the angle of incidence of radiation as the opening angle gets small and the absorptivity of the wall decreases. This behavior is more apparent for opening angles less than 90 deg.

5. Comparison between the directional apparent absorptivity of spherical cavities having diffuse walls and specular walls depends on all of the parameters: the angle of incidence, the cavity opening size, and the surface absorptivity. However, for cavities having a small opening angle and a low absorptivity, the diffuse cavity is a more efficient absorber than a specular cavity for a wide range of angles of incidence. This is in contrast to the behavior of other cavity configurations.

The following recommendations are made for further work in this area:

1. The problem of a prescribed uniform heat flux to the cavity surface, which has theoretical value, may be solved using the procedure developed in this work with some modifications. In this problem heat conduction may be neglected or can be considered by a coupled conduction equation.

2. An attempt should be made to study the relative advantages of alternative approaches, such as the variational or the finite difference methods, for solving the integral equation resulting from the radiant exchange formulation.

3. In the problem of absorption of parallel radiation a point source was considered to be located at a distance infinitely far from the cavity. A more general procedure can be easily developed for the case when the point source is at a finite distance away from the cavity mouth using the idea of orienting the z-axis such that it passes through the source. It would also be interesting to study the case of a finite size (rather than a point) source.

4. The absorption problem can be extended further to obtain the local distribution of the absorbed energy. Also, a procedure should be developed for obtaining the angular distribution of the radiation reflected out of the cavity mouth. This distribution may help in prediction of the reflective behavior of real surfaces.

5. Finally, a comprehensive heat transfer model should be developed in which absorption and emisson are considered together to describe the heat flux distribution on the cavity wall. This comprehensive model may be of practical importance in radiometry.

Table 1. Apparent emissivities of spherical cavities, calculated by the exact analytical method, for various surface properties and cavity opening angles.

	$\varepsilon = 0.9$			$\varepsilon = 0.7$		
ψ	$\frac{\rho^s}{\rho} = 0$	$\frac{\rho^s}{\rho} = 0.5$	$\frac{\rho^s}{\rho} = 1$	$\frac{\rho^s}{\rho} = 0$	$\frac{\rho^s}{\rho} = 0.5$	$\frac{\rho^s}{\rho} = 1$
0	1.0000	1.0000	1.0000	1.0000	1.0000	1.0000
15	0.9981	0.9982	0.9985	0.9927	0.9941	0.9915
30	0.9926	0.9944	0.9965	0.9721	0.9769	0.9773
45	0.9840	0.9882	0.9927	0.9409	0.9519	0.9581
60	0.9730	0.9798	0.9865	0.9032	0.9198	0.9315
75	0.9604	0.9686	0.9765	0.8629	0.8816	0.8963
90	0.9474	0.9534	0.9591	0.8235	0.8364	0.8473
105	0.9346	0.9360	0.9371	0.7876	0.7901	0.7916
120	0.9231	0.9225	0.9218	0.7568	0.7554	0.7535
135	0.9134	0.9125	0.9115	0.7322	0.7303	0.7281
150	0.9061	0.9055	0.9049	0.7144	0.7132	0.7119
165	0.9015	0.9014	0.9012	0.7036	0.7033	0.7029
180	0.9000	0.9000	0.9000	0.7000	0.7000	0.7000

	$\varepsilon = 0.5$			$\varepsilon = 0.3$		
ψ	$\frac{\rho^s}{\rho} = 0$	$\frac{\rho^s}{\rho} = 0.5$	$\frac{\rho^s}{\rho} = 1$	$\frac{\rho^s}{\rho} = 0$	$\frac{\rho^s}{\rho} = 0.5$	$\frac{\rho^s}{\rho} = 1$
0	1.0000	1.0000	1.0000	1.0000	1.0000	1.0000
15	0.9832	0.9860	0.9684	0.9618	0.9611	0.9034
30	0.9372	0.9425	0.9266	0.8648	0.8659	0.8004
45	0.8723	0.8851	0.8771	0.7453	0.7537	0.7057
60	0.8000	0.8189	0.8213	0.6316	0.6444	0.6228
75	0.7296	0.7499	0.7603	0.5363	0.5499	0.5480
90	0.6667	0.6799	0.6891	0.4615	0.4699	0.4735
105	0.6137	0.6159	0.6162	0.4051	0.4062	0.4051
120	0.5714	0.5700	0.5674	0.3636	0.3627	0.3605
135	0.5395	0.5377	0.5352	0.3343	0.3332	0.3315
150	0.5173	0.5163	0.5149	0.3148	0.3142	0.3133
165	0.5043	0.5040	0.5036	0.3036	0.3035	0.3032
180	0.5000	0.5000	0.5000	0.3000	0.3000	0.3000

	$\varepsilon = 0.1$		
ψ	$\frac{\rho^s}{\rho} = 0$	$\frac{\rho^s}{\rho} = 0.5$	$\frac{\rho^s}{\rho} = 1$
0	1.0000	1.0000	1.0000
15	0.8671	0.8629	0.6401
30	0.6239	0.6199	0.4476
45	0.4314	0.4320	0.3413
60	0.3077	0.3101	0.2736
75	0.2307	0.2334	0.2247
90	0.1818	0.1833	0.1832
105	0.1500	0.1502	0.1496
120	0.1290	0.1289	0.1283
135	0.1152	0.1150	0.1146
150	0.1064	0.1063	0.1061
165	0.1016	0.1015	0.1015
180	0.1000	0.1000	0.1000

Table 2. Comparison of the apparent emissivities calculated by the exact analytical method and the Monte Carlo method.

a) $\psi = 60$ deg

	$\frac{\rho'}{\rho} = 0$			$\frac{\rho'}{\rho} = 0.5$			$\frac{\rho'}{\rho} = 1$		
ε	Analytical	Monte Carlo	% Differ.	Analytical	Monte Carlo	% Differ.	Analytical	Monte Carlo	% Differ.
0.9	0.9730	0.9732	0.021	0.9798	0.9795	-0.031	0.9865	0.9813	-0.527
0.7	0.9032	0.9030	-0.022	0.9198	0.9154	-0.478	0.9315	0.9315	0.000
0.5	0.8000	0.7989	-0.138	0.8189	0.8138	-0.623	0.8213	0.8223	0.122
0.3	0.6316	0.6315	-0.016	0.6444	0.6423	-0.326	0.6228	0.6264	0.578
0.1	0.3077	0.3079	0.065	0.3101	0.3096	-0.161	0.2736	0.2770	1.243

b) $\varepsilon = 0.5$

	$\frac{\rho'}{\rho} = 0$			$\frac{\rho'}{\rho} = 0.5$			$\frac{\rho'}{\rho} = 1$		
ψ	Analytical	Monte Carlo	% Differ.	Analytical	Monte Carlo	% Differ.	Analytical	Monte Carlo	% Differ.
120	0.5714	0.5716	-0.035	0.5700	0.5694	0.105	0.5674	0.5663	0.194
105	0.6137	0.6128	0.147	0.6159	0.6169	-0.162	0.6162	0.6177	-0.243
90	0.6667	0.6647	0.300	0.6799	0.6746	0.780	0.6891	0.6810	1.175
75	0.7296	0.7307	-0.151	0.7499	0.7498	0.013	0.7603	0.7638	-0.460
60	0.8000	0.7989	0.138	0.8189	0.8138	0.623	0.8213	0.8223	-0.122
45	0.8723	0.8688	0.401	0.8851	0.8854	-0.034	0.8771	0.8810	-0.445
30	0.9372	0.9390	-0.192	0.9425	0.9476	-0.541	0.9266	0.9455	-2.040
15	0.9832	0.9912	-0.814	0.9860	1.0002	-1.440	0.9684	1.0011	-3.377

$$\% \text{ Differ.} = 100 \times \frac{(\text{Analytical} - \text{Monte Carlo})}{\text{Analytical}}$$

Table 3. Comparison of the CPU times (s) for the exact analytical method and the Monte Carlo method.

(The times correspond to the calculated values in Table 2.)

a) $\psi = 60$ deg

ε	$\frac{\rho^s}{\rho} = 0$		$\frac{\rho^s}{\rho} = 0.5$		$\frac{\rho^s}{\rho} = 1$	
	Analytical	Monte Carlo	Analytical	Monte Carlo	Analytical	Monte Carlo
0.9	0.00	9.52	21.98	9.62	0.71	9.87
0.7	0.00	10.72	43.87	11.04	1.63	11.39
0.5	0.00	12.53	60.51	13.12	4.17	13.76
0.3	0.00	15.35	108.46	16.46	15.32	18.03
0.1	0.00	20.70	185.02	22.86	78.93	31.32

b) $\varepsilon = 0.5$ deg

ψ	$\frac{\rho^s}{\rho} = 0$		$\frac{\rho^s}{\rho} = 0.5$		$\frac{\rho^s}{\rho} = 1$	
	Analytical	Monte Carlo	Analytical	Monte Carlo	Analytical	Monte Carlo
120	0.00	4.52	2.58	4.61	0.20	4.71
105	0.00	4.83	3.22	4.94	0.31	5.09
90	0.00	7.93	4.19	8.21	0.45	8.39
75	0.00	8.52	34.33	8.85	2.23	9.17
60	0.00	12.51	60.51	13.18	4.17	13.79
45	0.00	13.53	117.01	14.45	5.17	15.39
30	0.00	14.66	194.79	15.54	5.98	16.89
15	0.00	15.26	315.07	16.39	9.15	17.75

Table 4. Comparison of the results obtained by the exact analytical method and the Monte Carlo method for the directional apparent absorbtivity in a spherical cavity with specular walls.

($\psi = 15$ deg, and $\alpha = 0.3$)

a) $\alpha_a(\gamma)$

γ	Analytical	Monte Carlo	% Differ.
0	0.8732	0.8711	0.240
6	0.8683	0.8706	-0.265
18	0.9134	0.9132	0.022
30	0.8657	0.8655	0.023
42	0.8890	0.8881	0.101
54	0.8982	0.8987	-0.056
66	0.9378	0.9326	0.554
78	0.9748	0.9746	0.021
84	0.9857	0.9857	0.000
90	0.9899	0.9908	-0.091

b) CPU time (s)

γ	Analytical	Monte Carlo
0	0.04	2.71
6	0.16	2.90
18	0.39	3.27
30	0.36	3.05
42	0.34	3.14
54	0.38	3.04
66	0.40	3.12
78	0.31	3.74
84	0.10	3.88
90	0.01	3.90

$$\% \text{ Differ.} = 100 \times \frac{(\text{Analytical} - \text{Monte Carlo})}{\text{Analytical}}$$

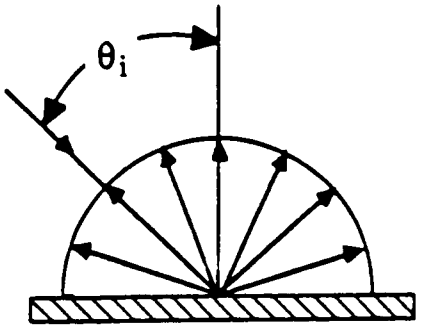

a) diffuse reflection

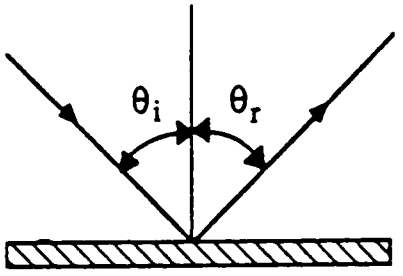

b) specular reflection

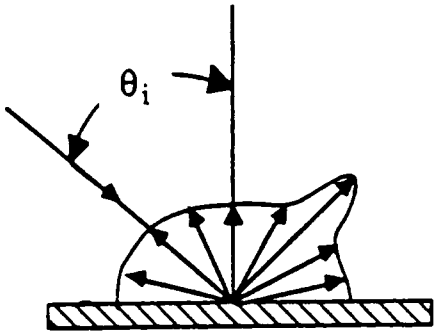

c) diffuse-specular reflection

Fig. 1. Reflection Models.

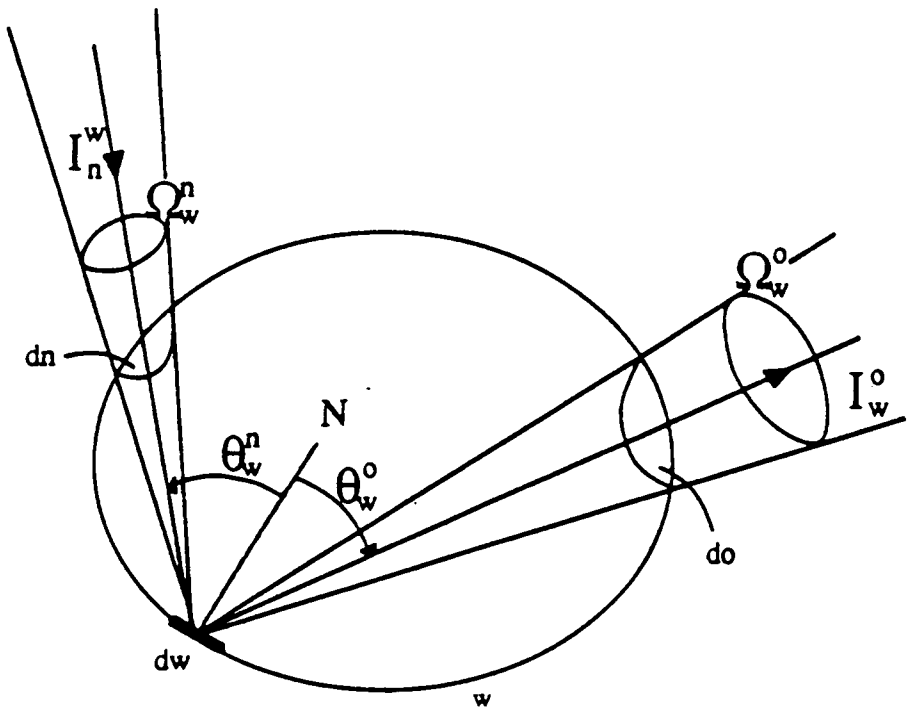

Fig. 2. Cavity Configuration for Gouffe's [28] and De Vos' [29] Methods.

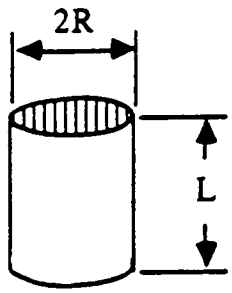

cylindrical cavity

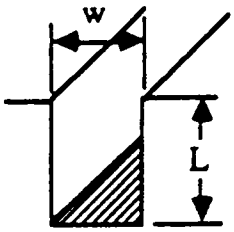

rectangular-groove cavity

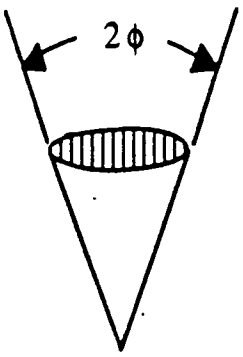

conical cavity

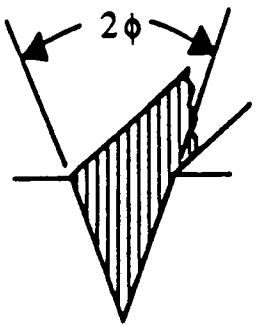

V-groove cavity

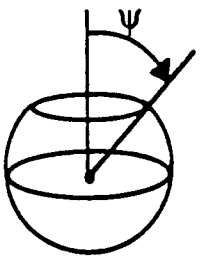

spherical cavity

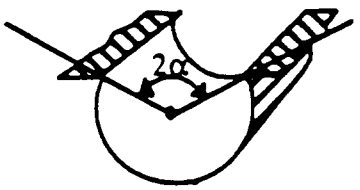

circular-groove cavity

Fig. 3. Various Cavity Configurations.

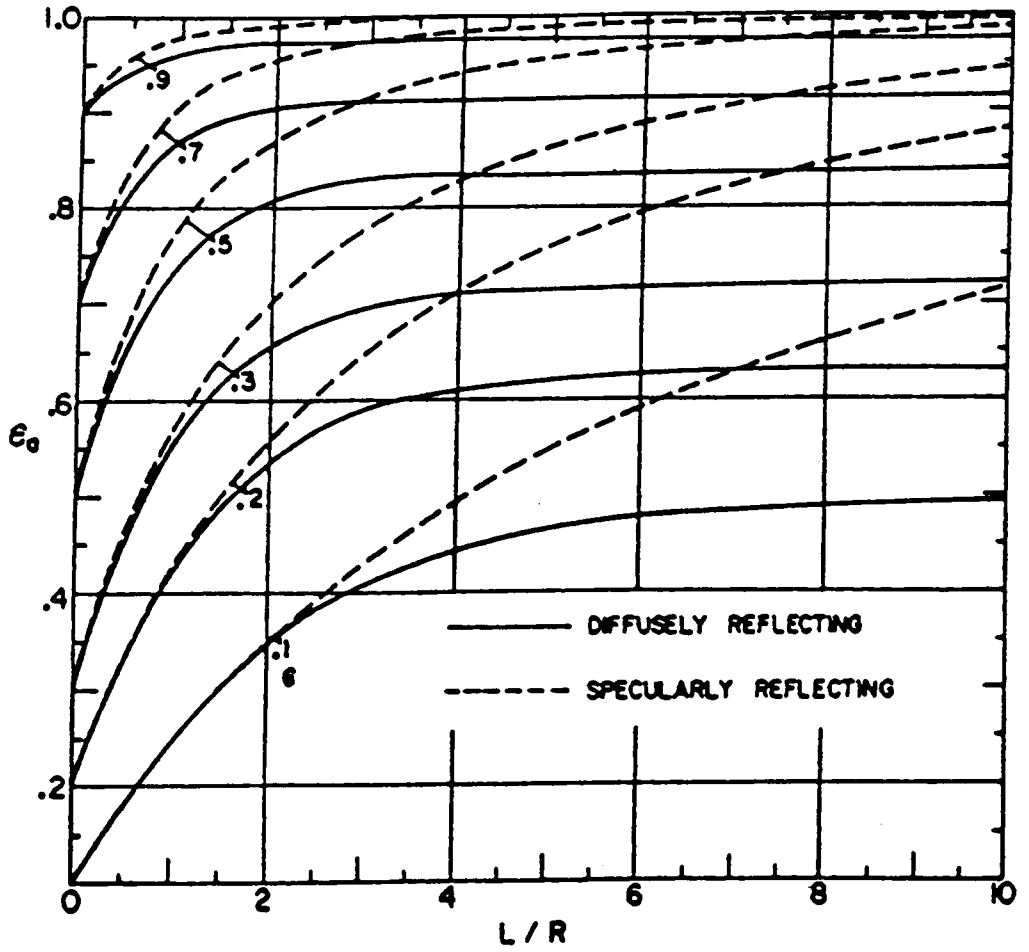

Fig. 4. Apparent Emissivity of Cylindrical Cavities for Various Geometries and Surface Conditions [1].

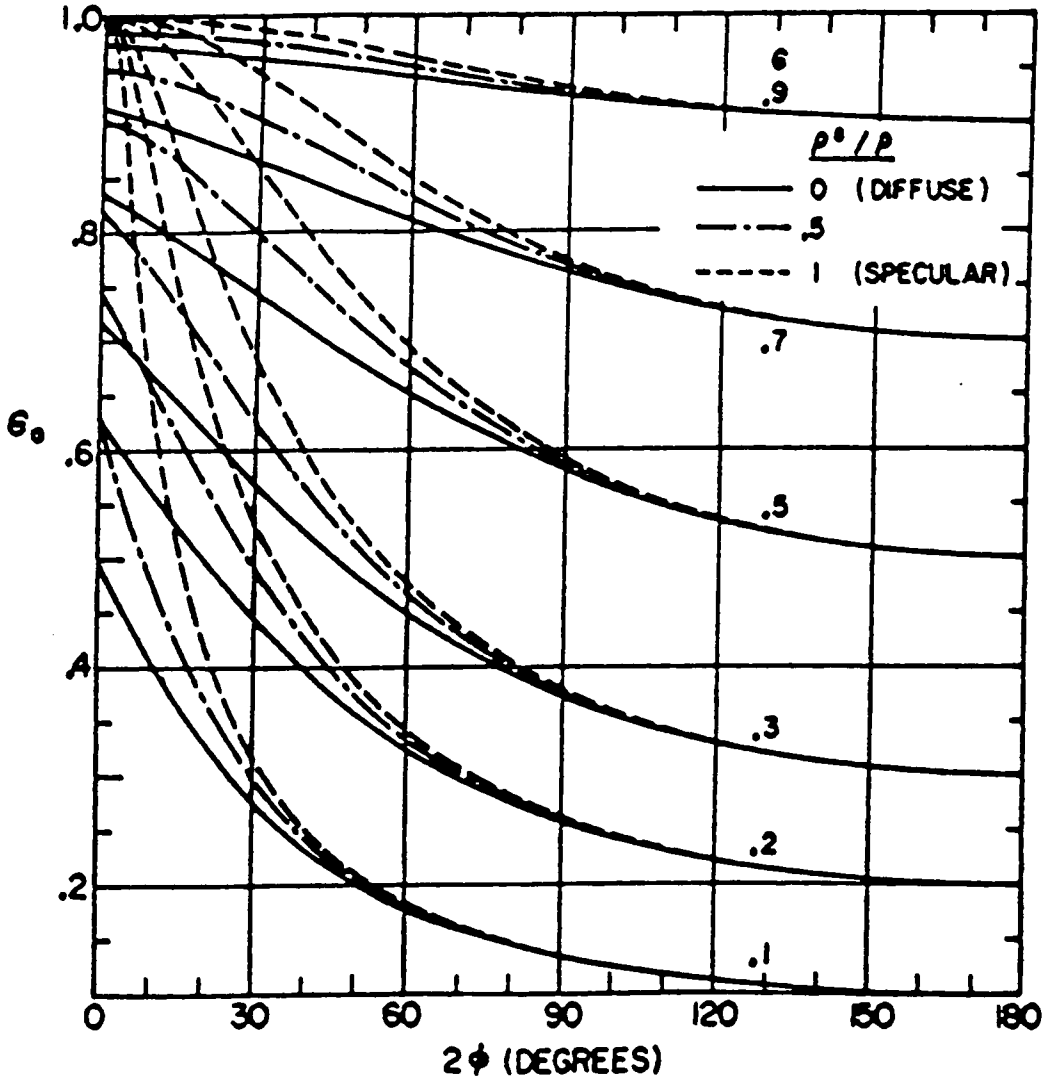

Fig. 5. Apparent Emissivity of Conical Cavities for Various Geometries and Surface Conditions [1].

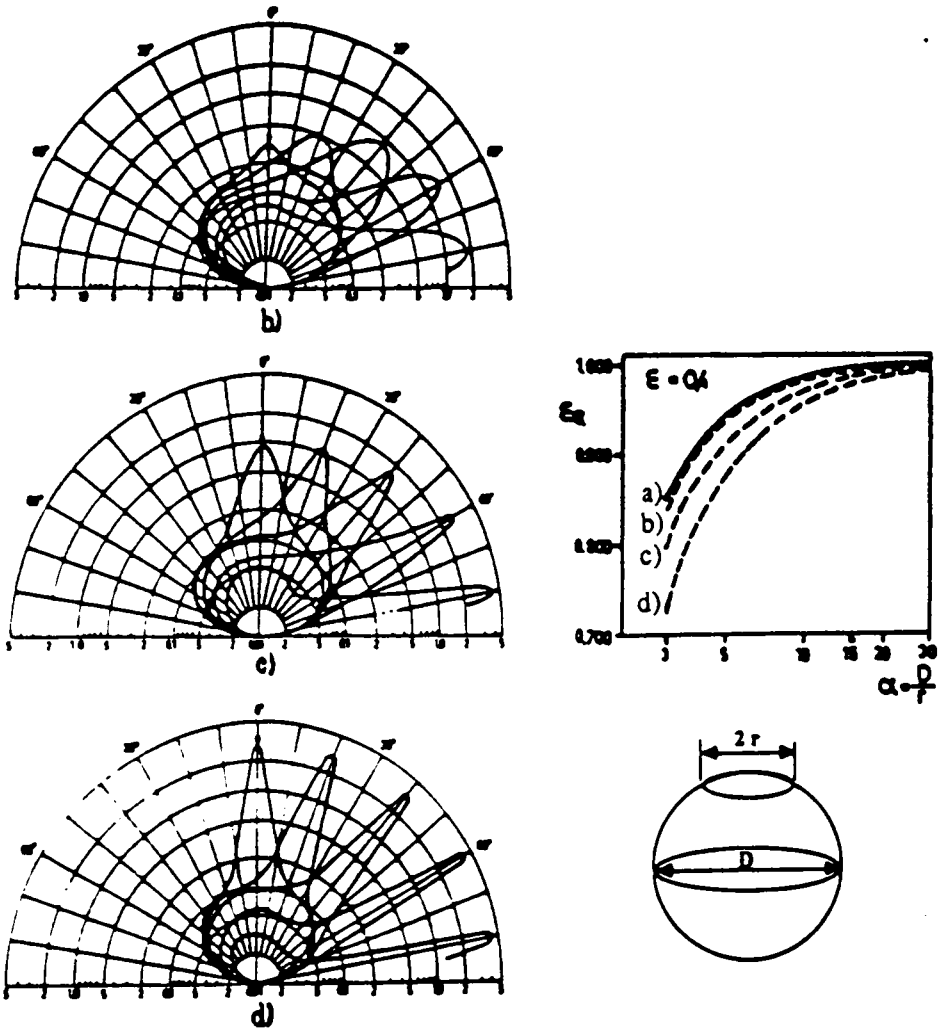

Fig. 6. **Apparent Emissivity Results for a Spherical Cavity obtained by Campanaro and Ricolfi [58].**

: In case a) the cavity walls are diffuse while in cases b-d) the cavity walls are partially diffuse and partially specular according to the distributions shown.

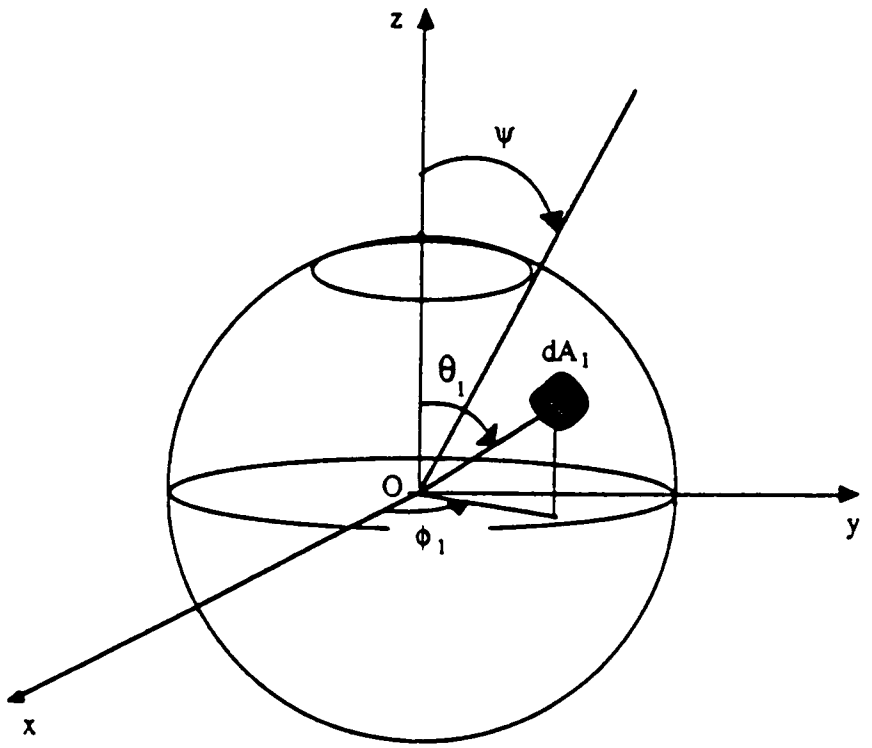

Fig. 7. Spherical Cavity Geometry.

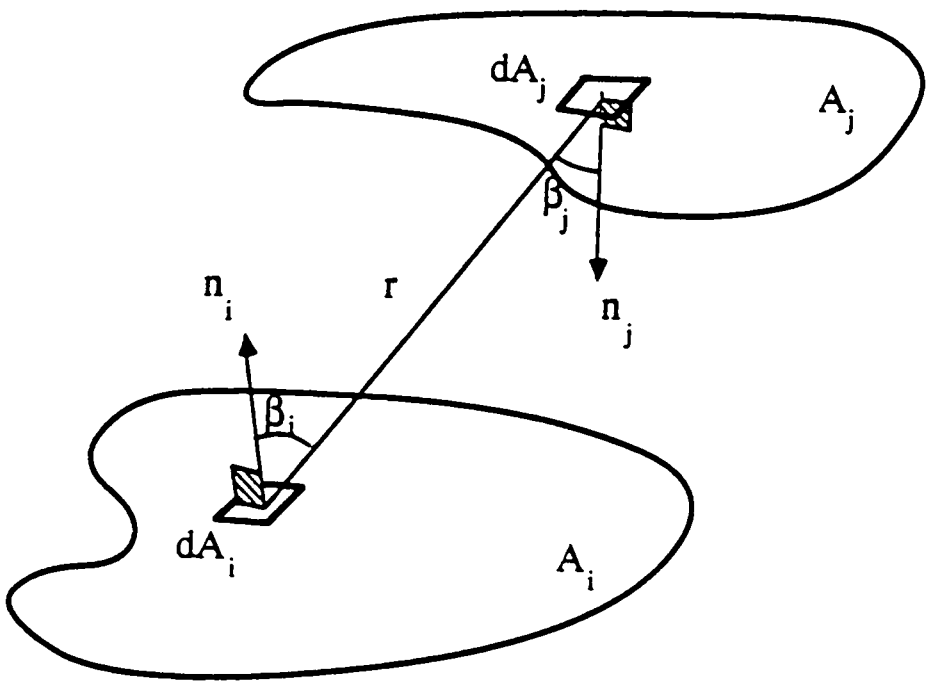

Fig. 8. Geometry for Defining the View Factor Between Surface Elements.

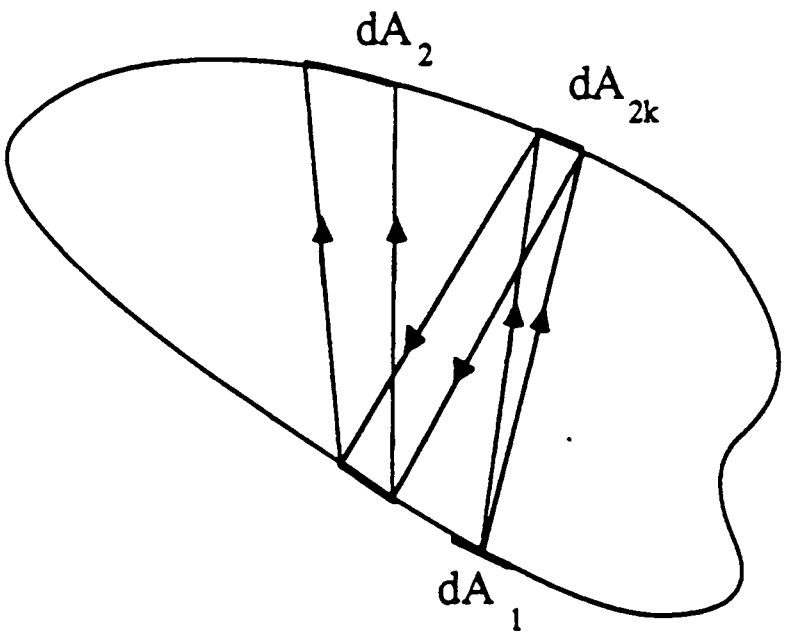

Fig. 9. Geometry for Defining the Exchange Factor Between Two Differential Surfaces.

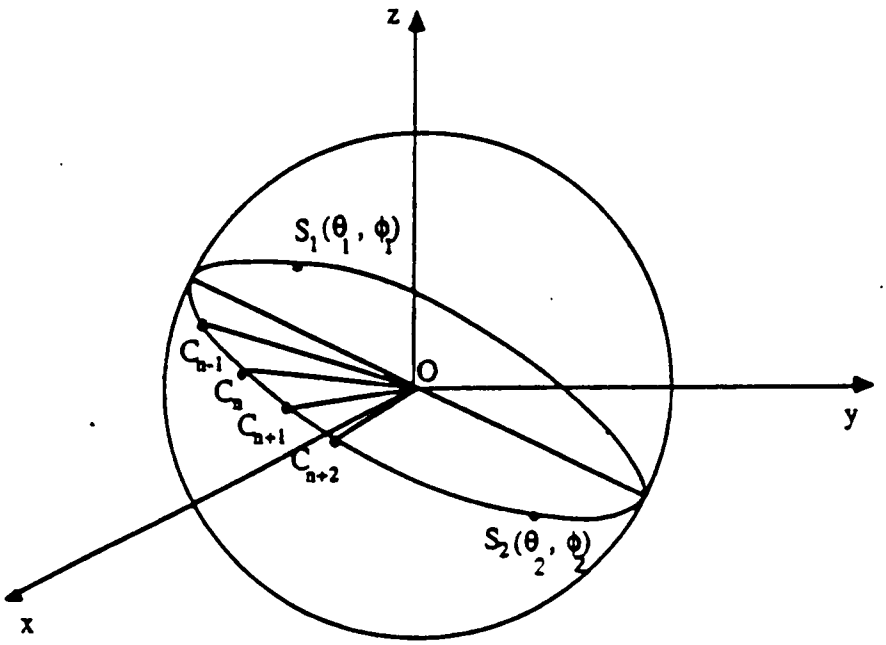

Fig. 10. Specular Reflection inside a Spherical Cavity.

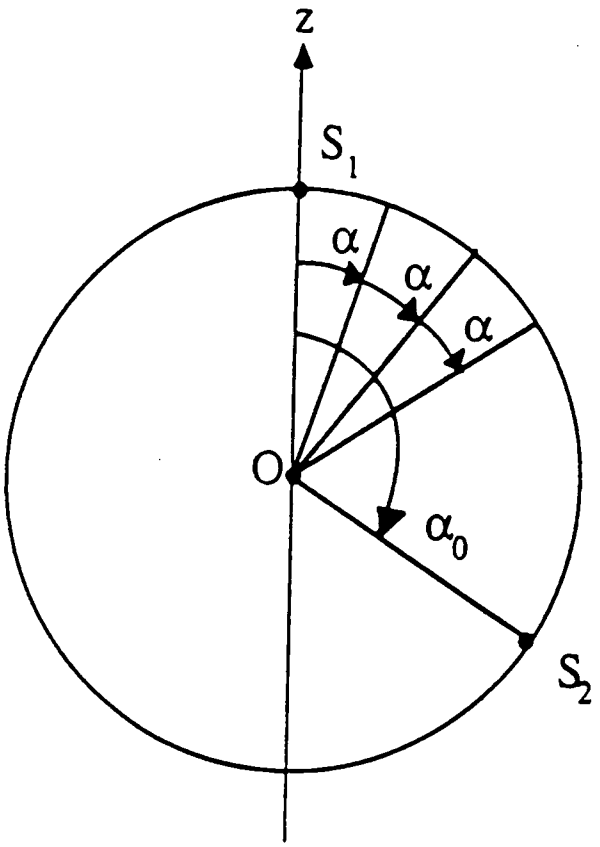

Fig. 11. The Circle of Reflection.

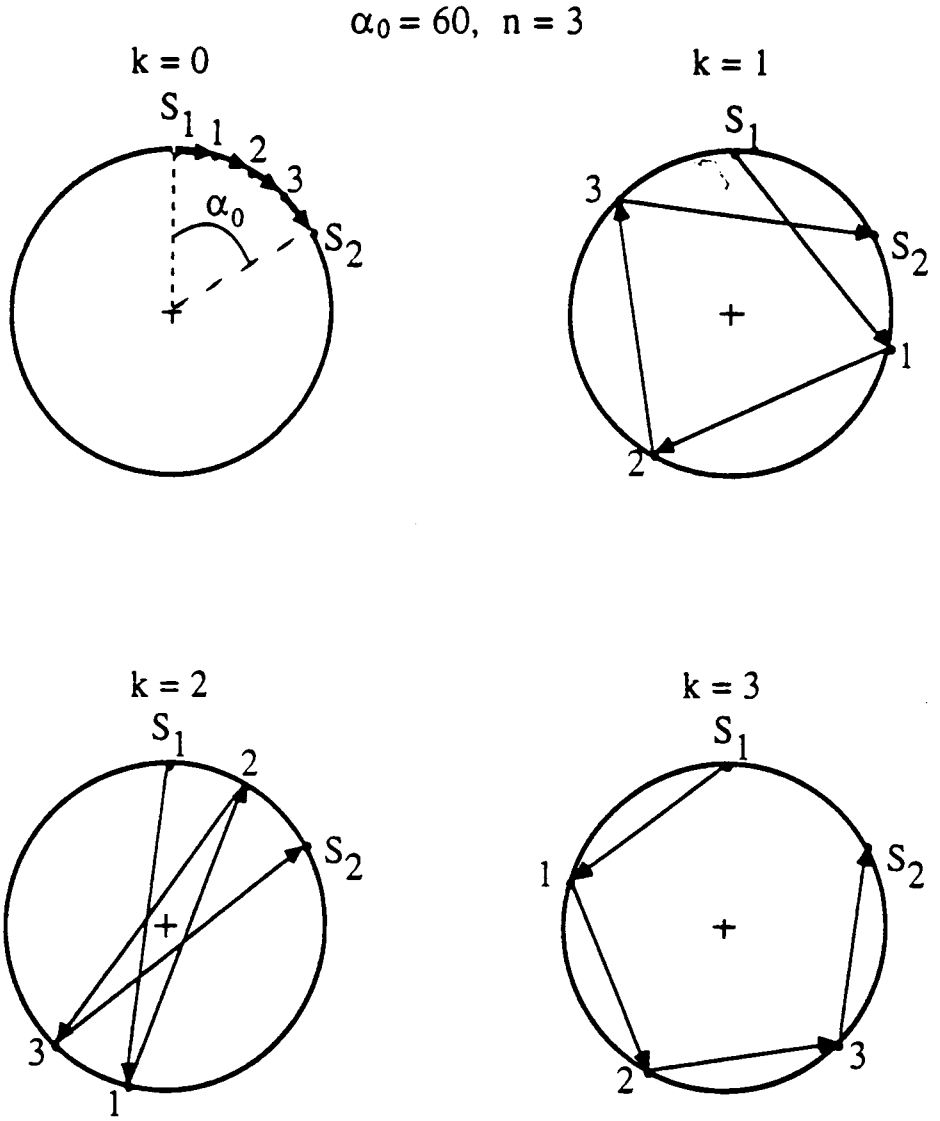

Fig. 12. The Four Possible Routes for a Ray to Go from S_1 to S_2 by Three Reflections.

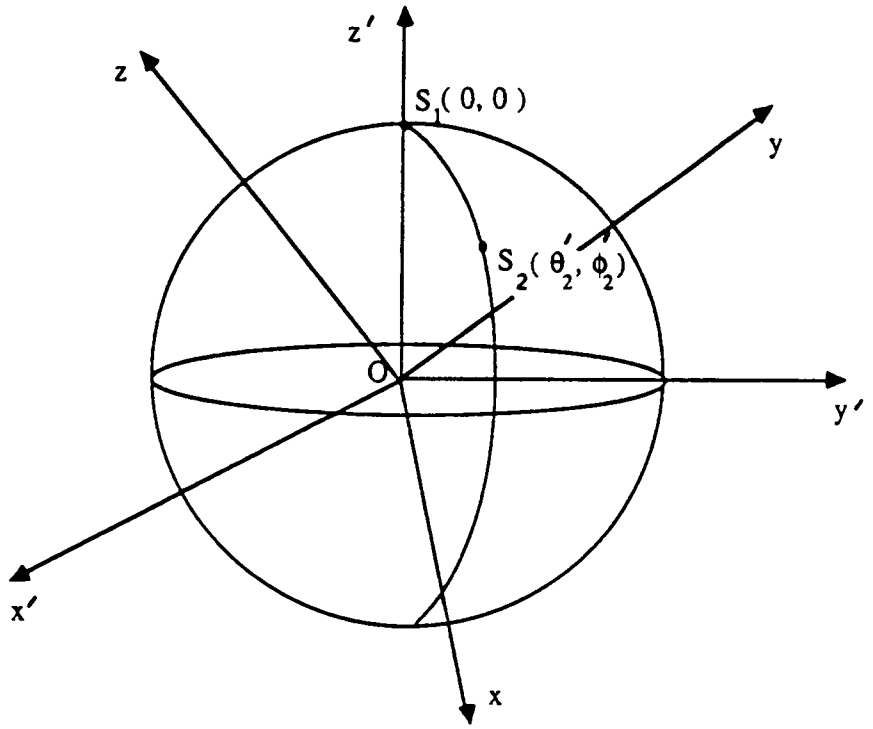

Fig. 13. The Source-Oriented Coordinate System.

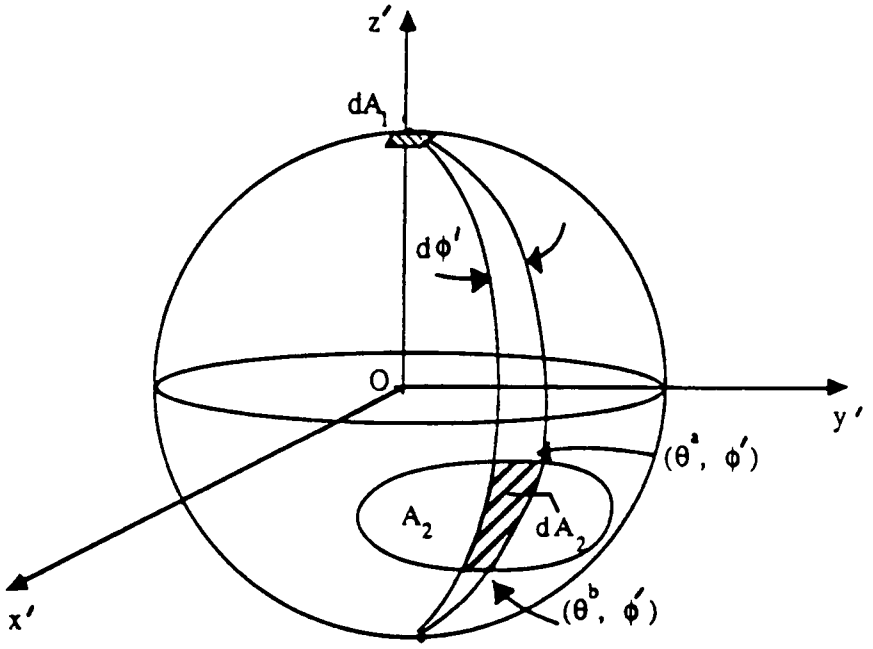

Fig. 14. Geometry for Defining the Exchange Factor in an Enclosure with no Opening.

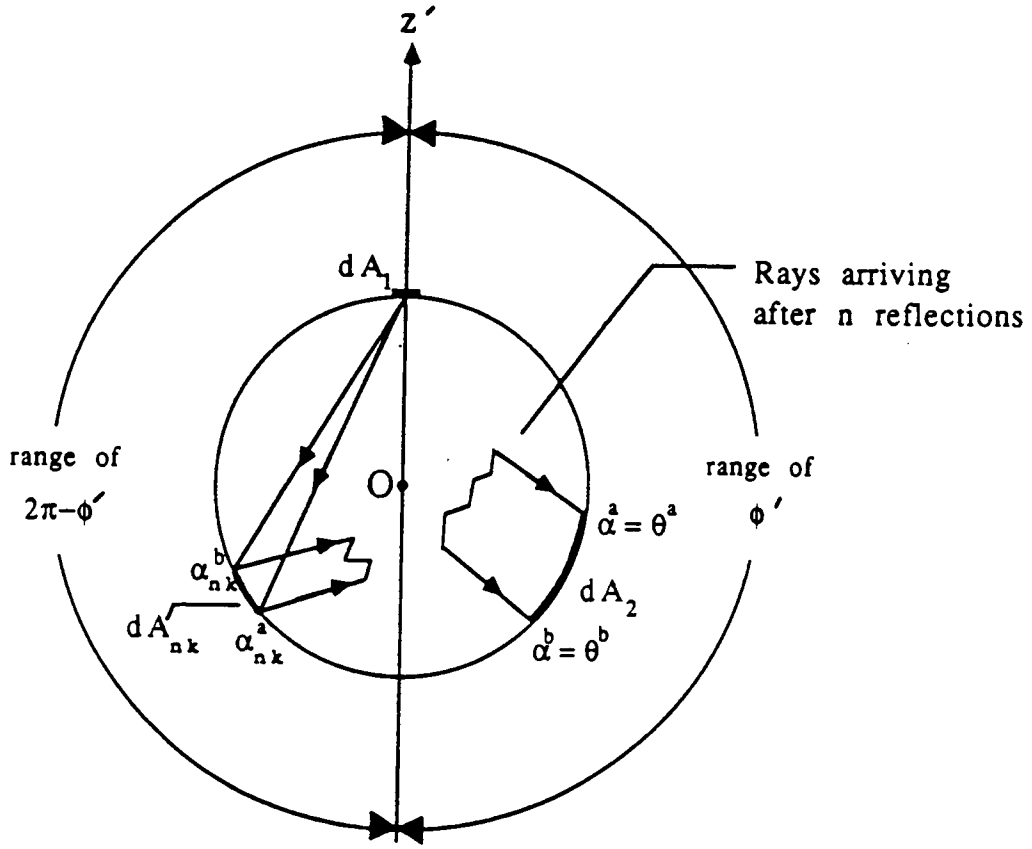

Fig. 15. Energy Exchange Corresponding to a Given Circle of Reflection (No Opening).

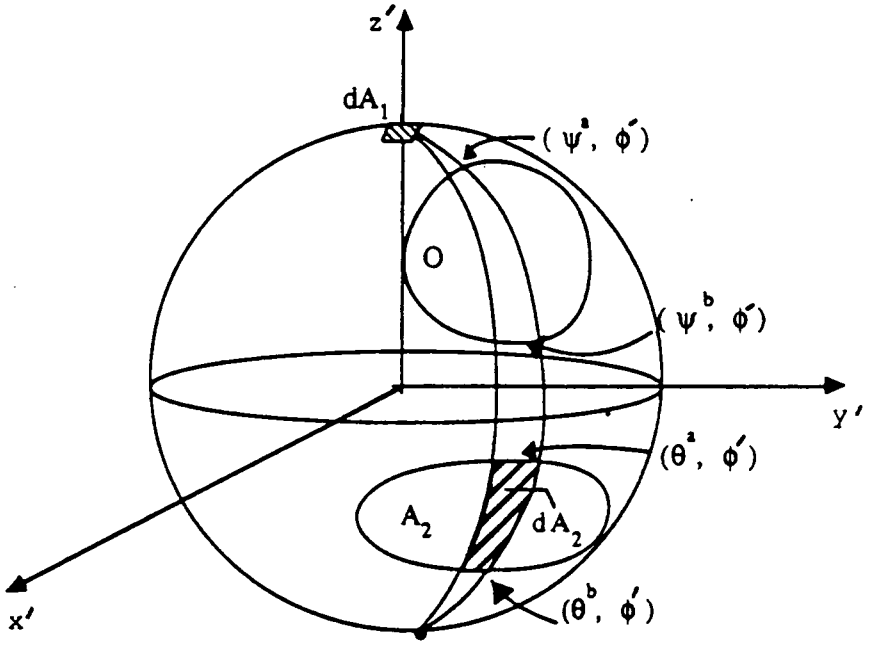

Fig. 16. Geometry for Defining the Exchange Factor in a Spherical Cavity with Opening.

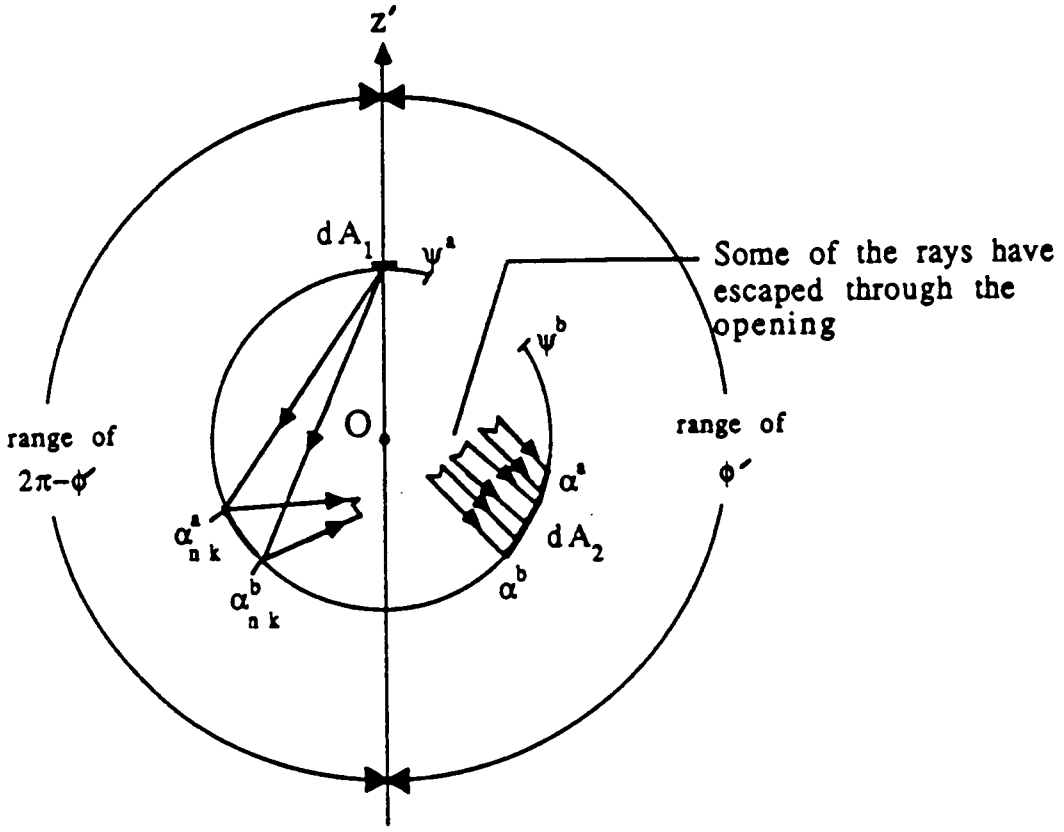

Fig. 17. Energy Exchange Corresponding to a Given Circle of Reflection with Opening.

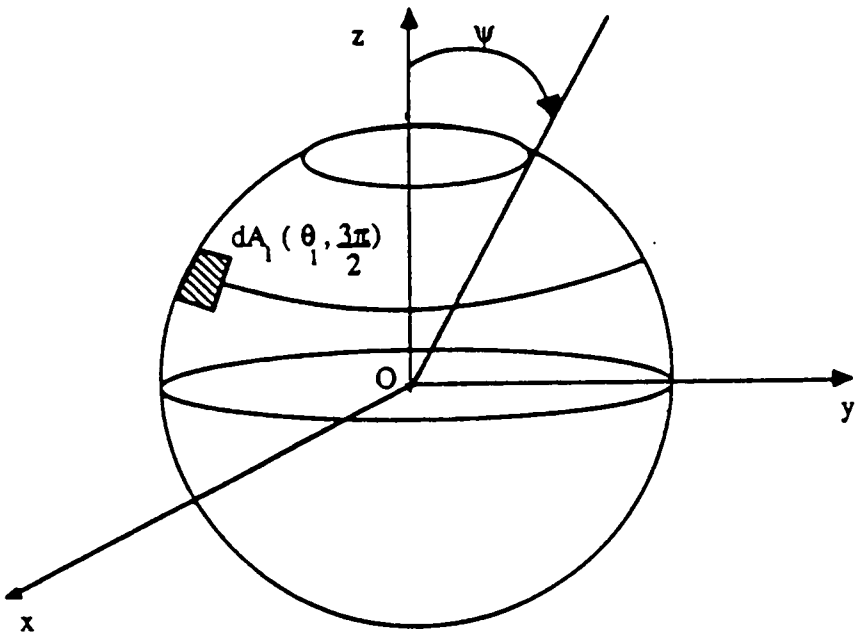

Fig. 18. Same as Fig. 7 with Source Element Moved to the Position Shown.

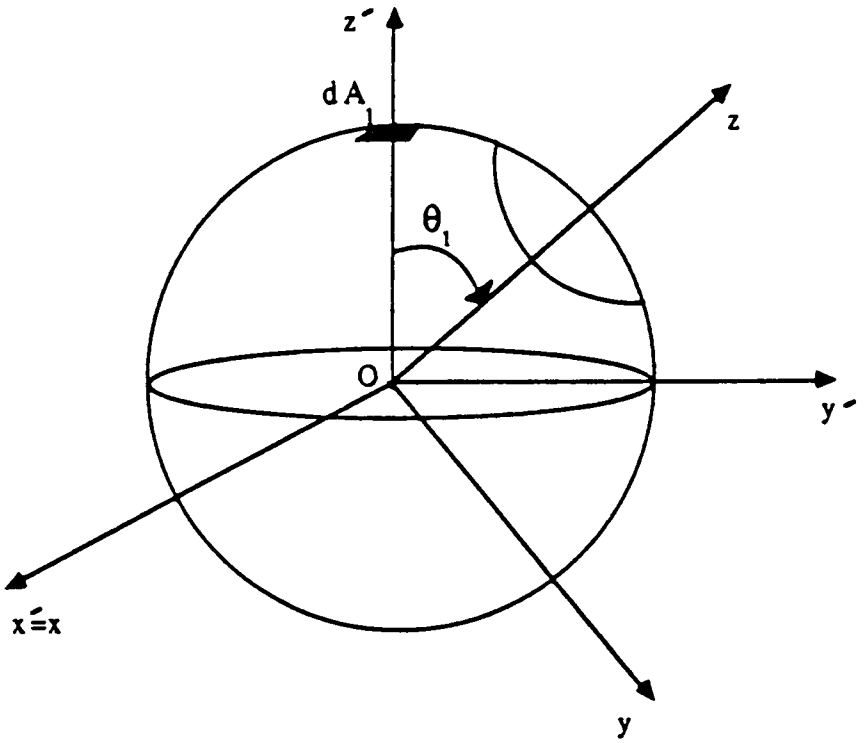

Fig. 19. Spherical Cavity as Seen by the Source Element in the Source-Oriented Coordinate System.

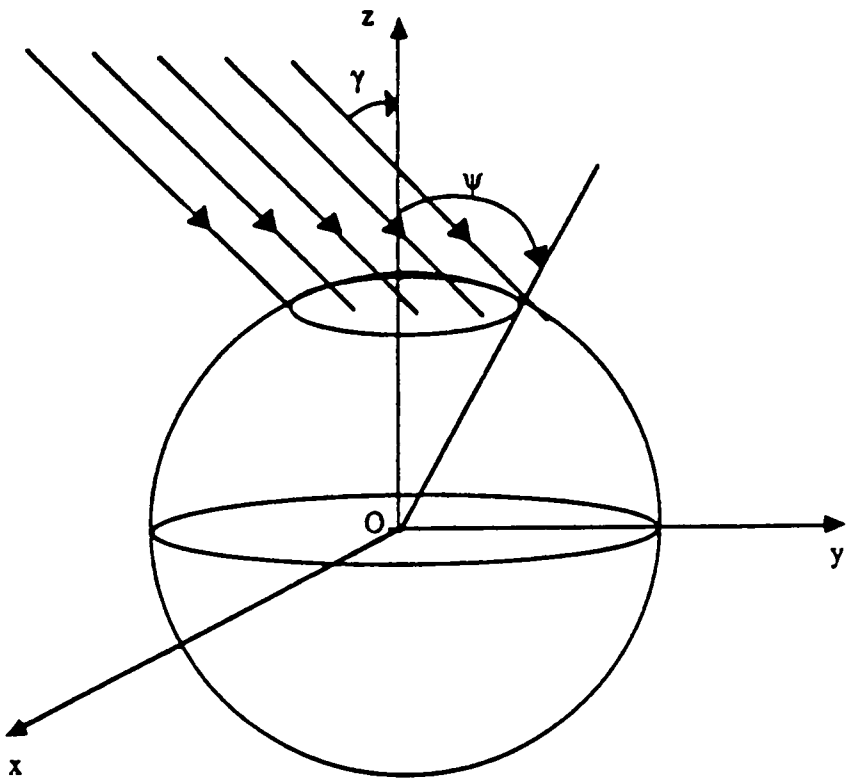

Fig. 20. Collimated Radiation Entering a Spherical Cavity.

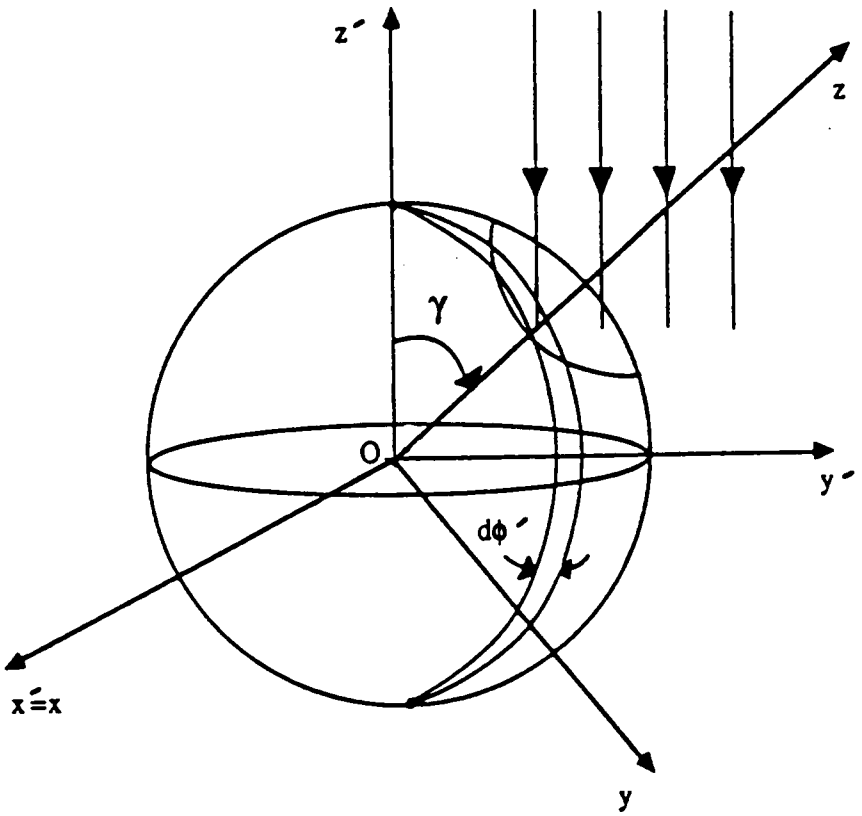

Fig. 21. Parallel Rays Entering the Cavity in the Source-Oriented Coordinate System

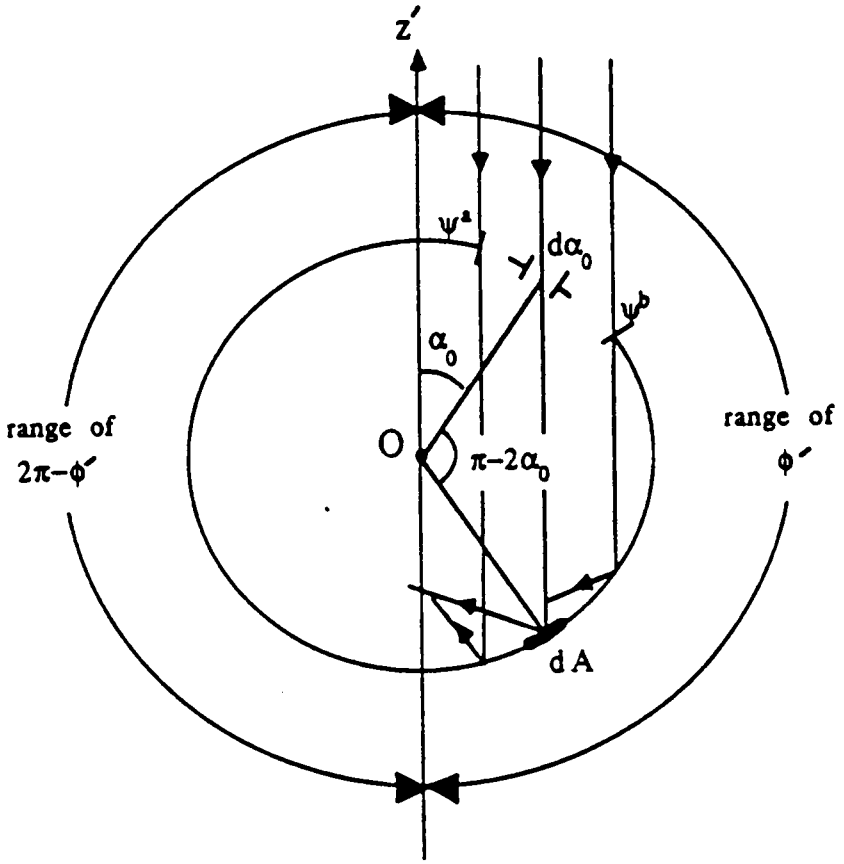

Fig. 22. Parallel Rays Entering the Circle of Reflection.

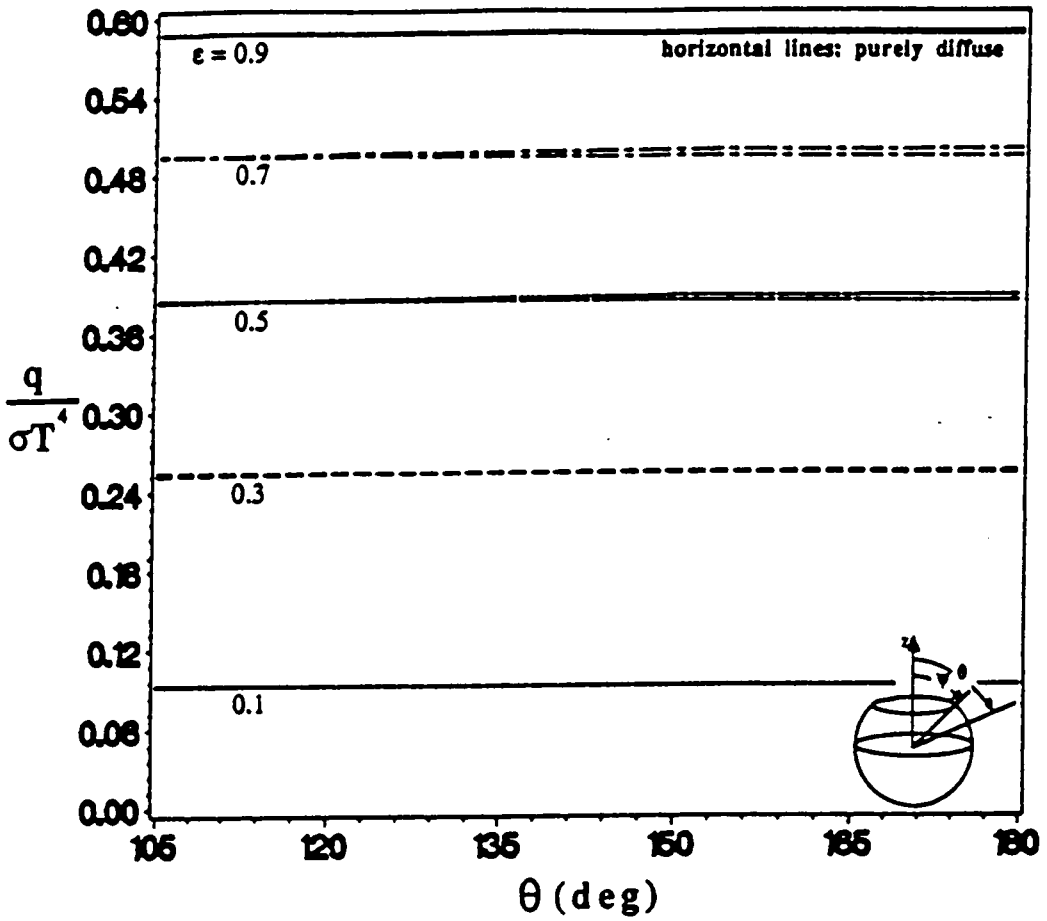

Fig. 23. Heat Transfer Distribution in a Spherical Cavity: Comparison of Purely Specular and Purely Diffuse Wall Cases; Opening Angle ψ = 105 deg.

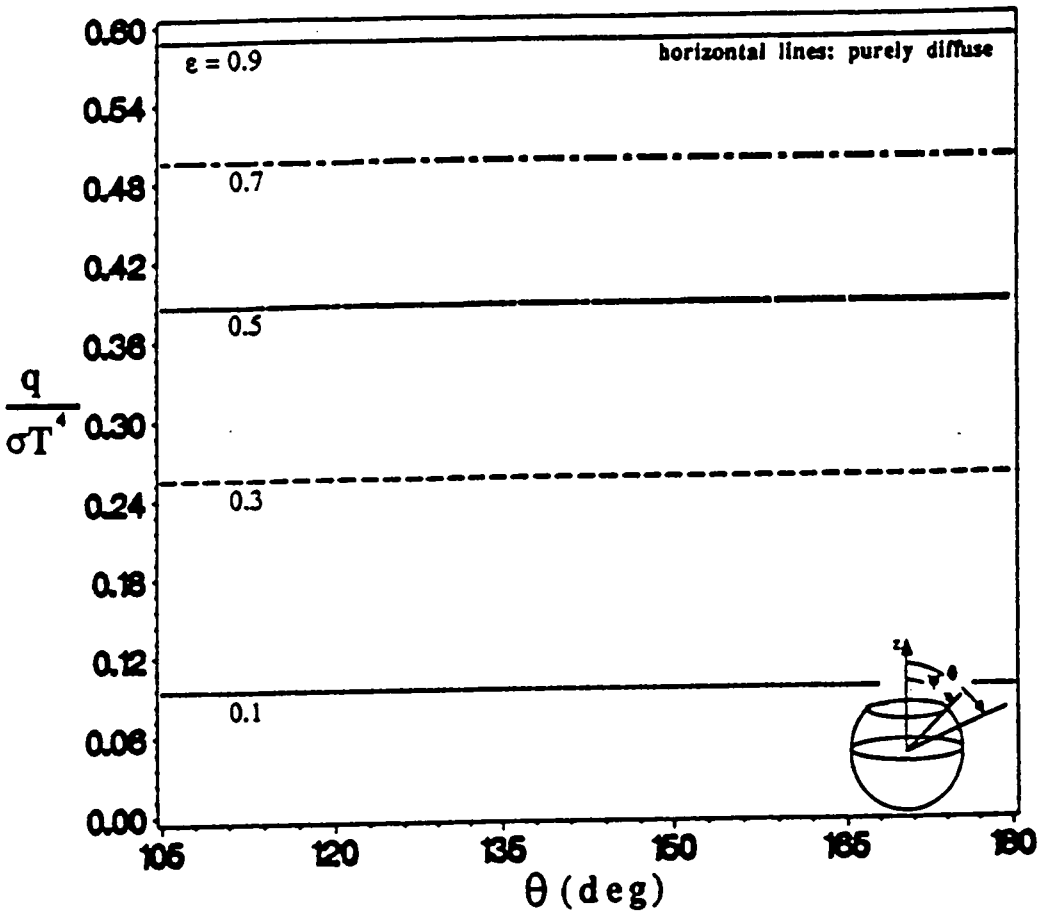

Fig. 24. Heat Transfer Distribution in a Spherical Cavity: Comparison of Diffuse-Specular and Purely Diffuse Wall Cases, Opening Angle ψ = 105 deg.

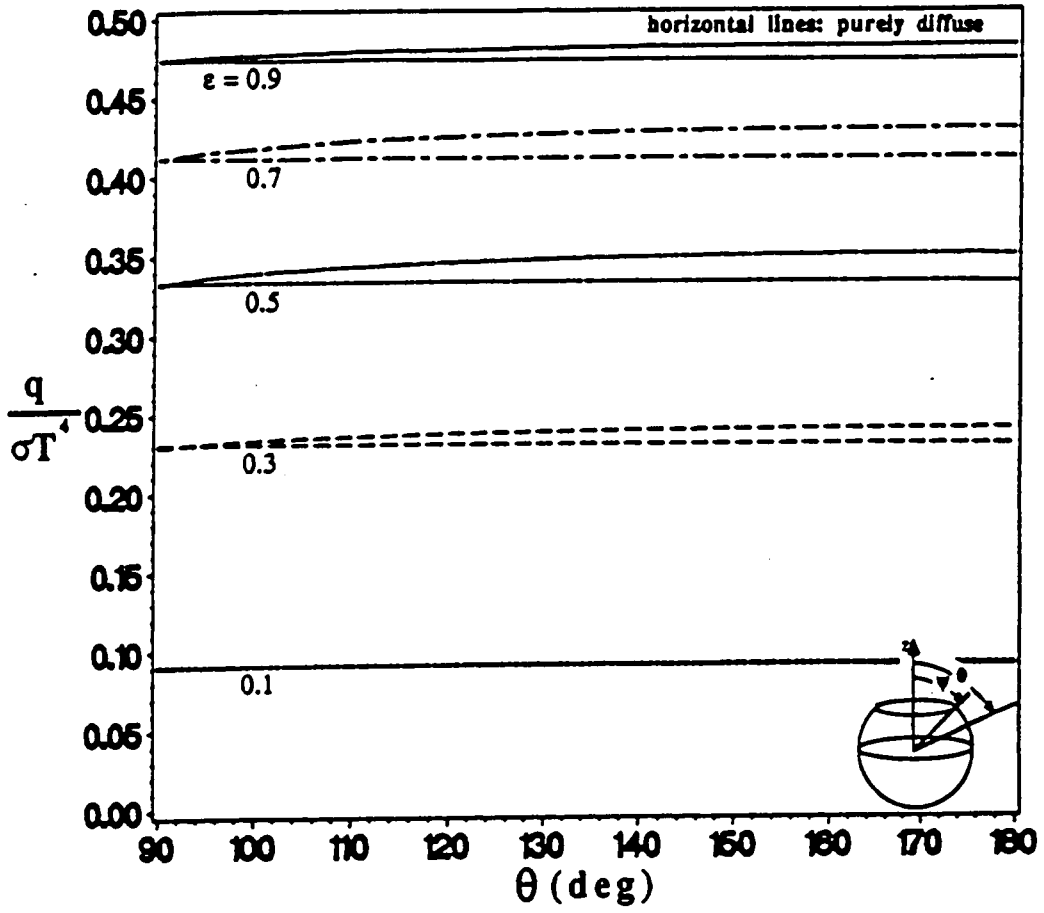

Fig. 25. Heat Transfer Distribution in a Spherical Cavity: Comparison of Purely Specular and Purely Diffuse Wall Cases; Opening Angle ψ = 90 deg.

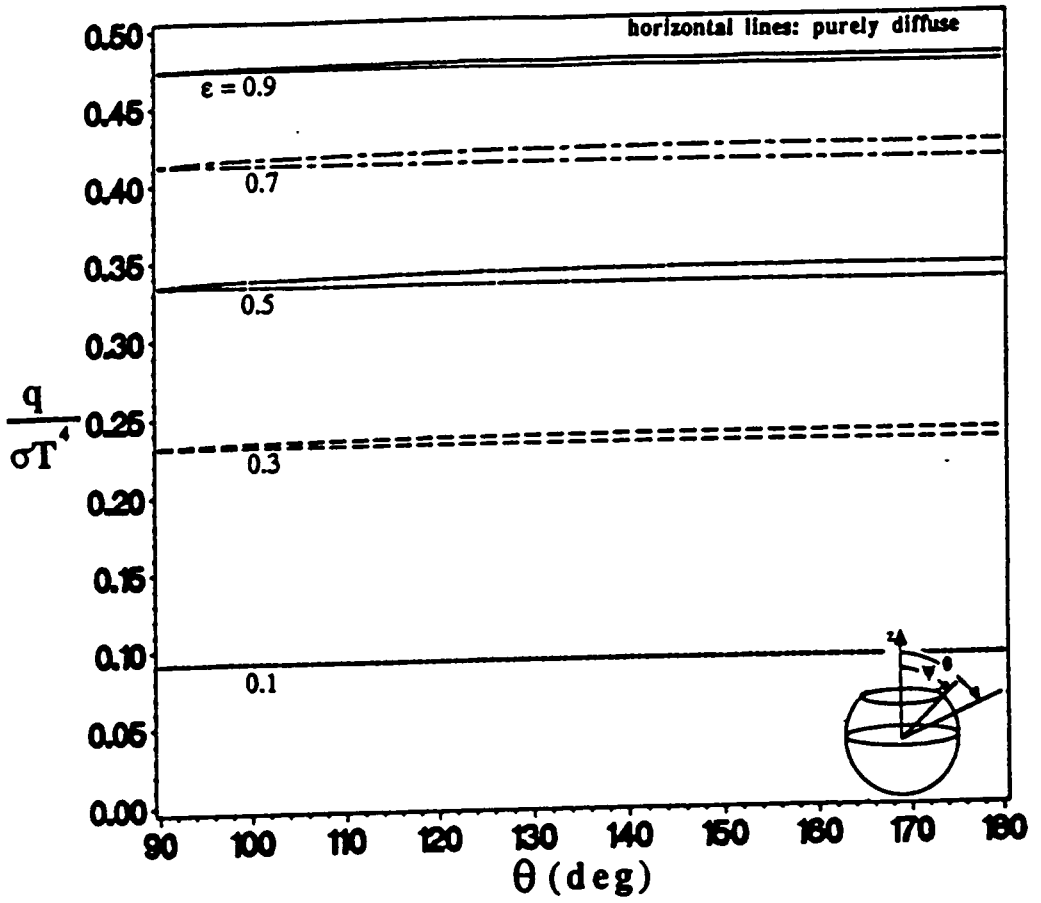

Fig. 26. Heat Transfer Distribution in a Spherical Cavity: Comparison of Diffuse-Specular and Purely Diffuse Wall Cases; Opening Angle ψ = 90 deg.

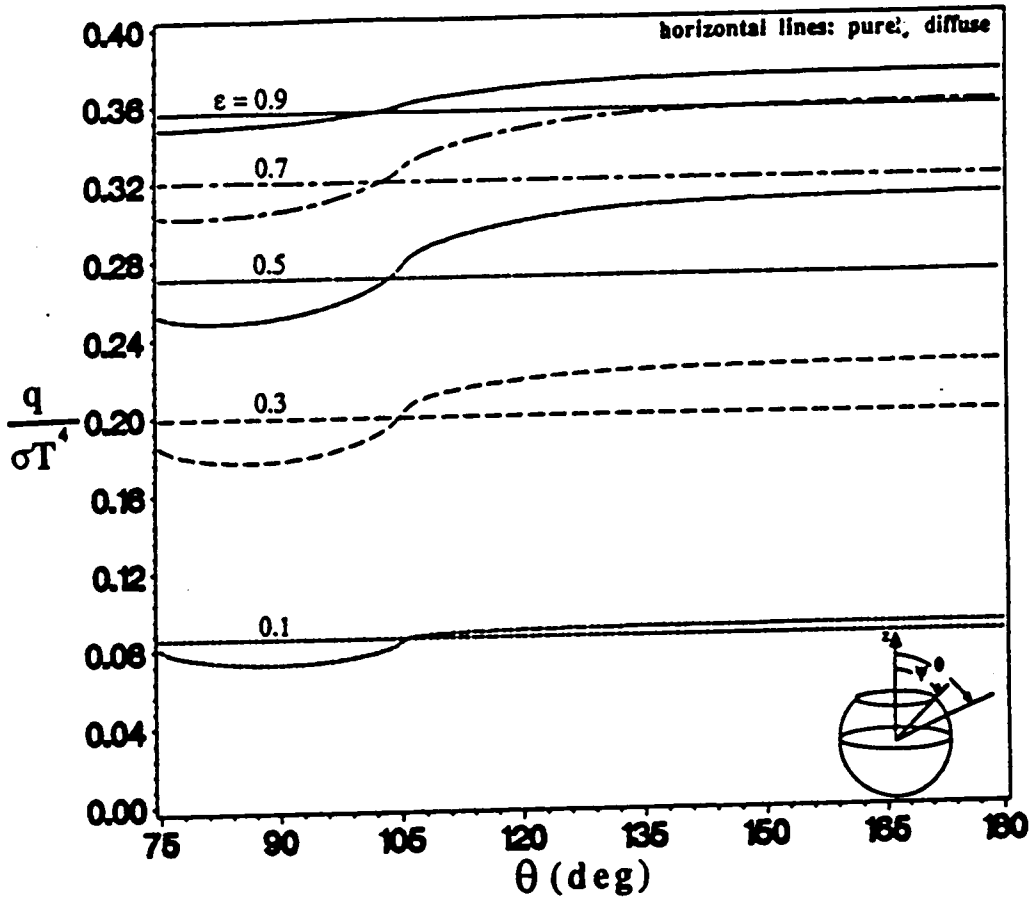

Fig. 27. Heat Transfer Distribution in a Spherical Cavity: Comparison of Purely Specular and Purely Diffuse Wall Cases; Opening Angle ψ = 75 deg.

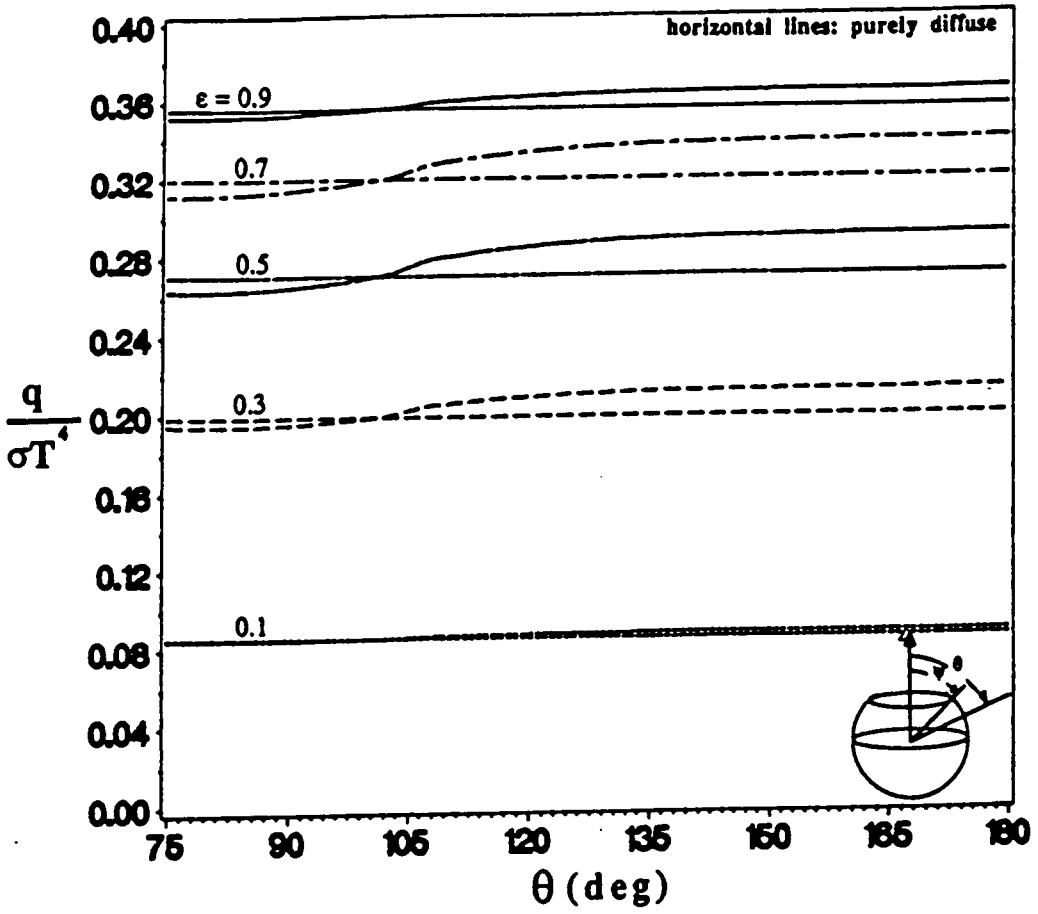

Fig. 28. Heat Transfer Distribution in a Spherical Cavity: Comparison of Diffuse-Specular and Purely Diffuse Wall Cases, Opening Angle ψ = 75 deg.

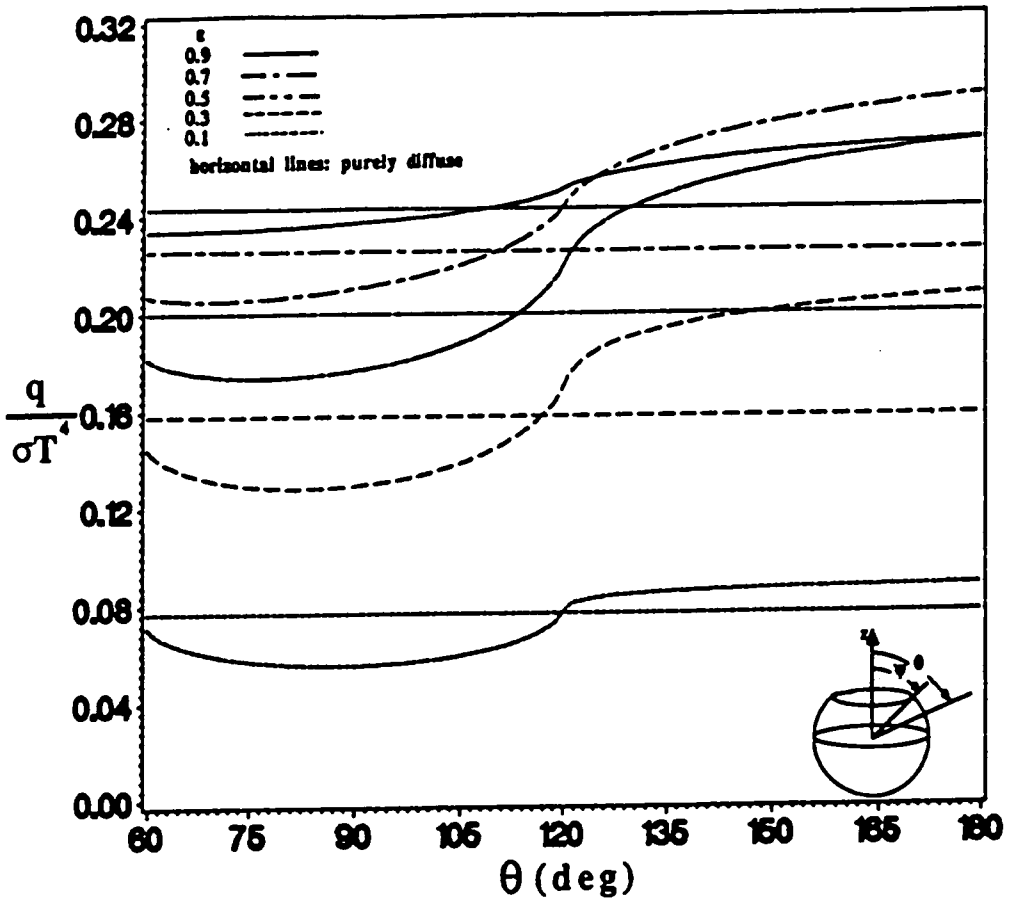

Fig. 29. Heat Transfer Distribution in a Spherical Cavity: Comparison of Purely Specular and Purely Diffuse Wall Cases; Opening Angle ψ = 60 deg.

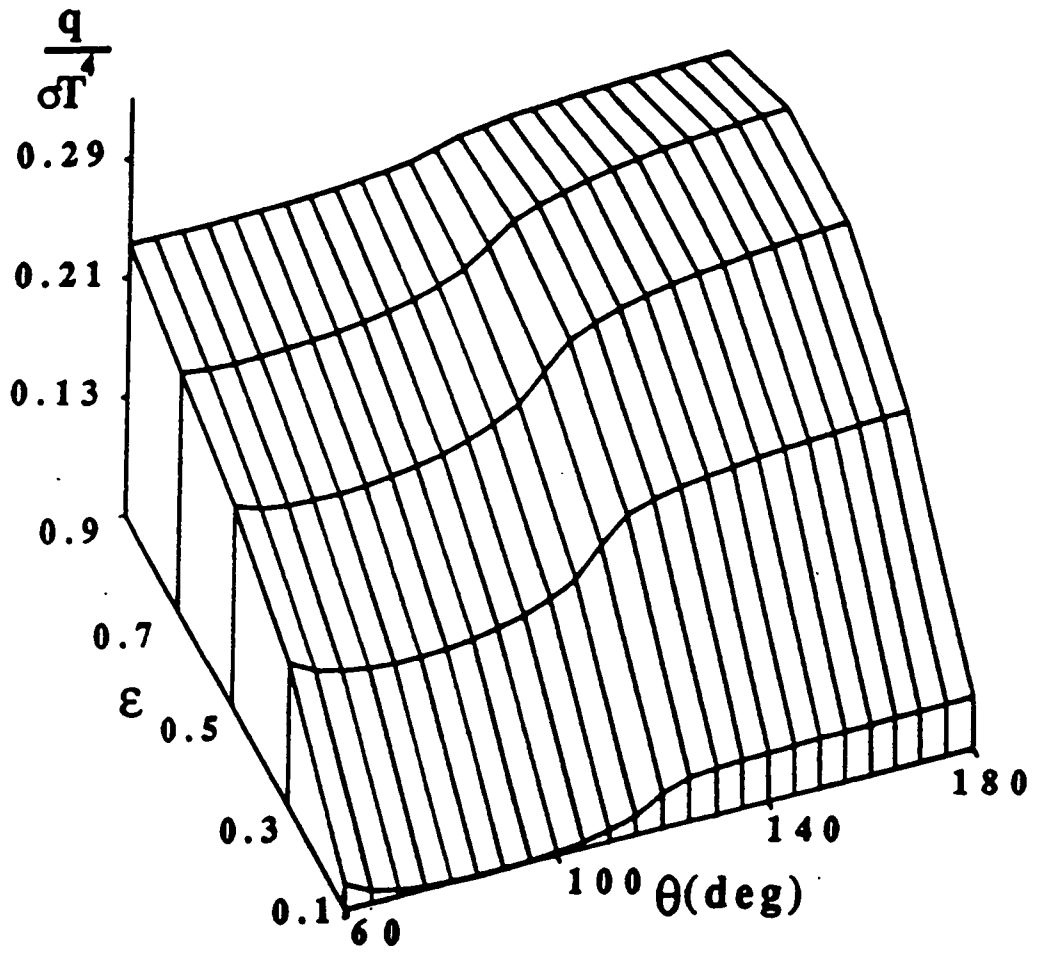

Fig. 30. Heat Transfer Distribution in a Spherical Cavity with Purely Specular Walls as a Function of the Surface Emissivity; Opening Angle ψ = 60 deg.

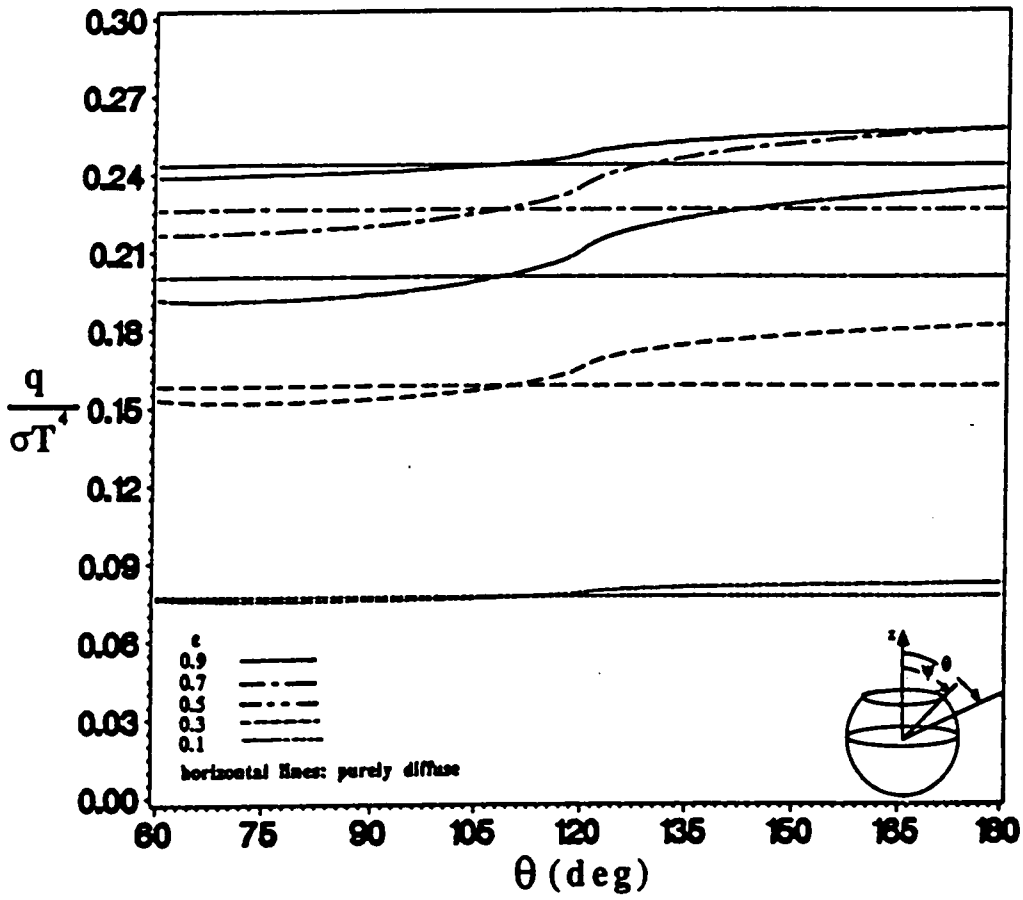

Fig. 31. Heat Transfer Distribution in a Spherical Cavity: Comparison of Diffuse-Specular and Purely Diffuse Wall Cases, Opening Angle ψ = 60 deg.

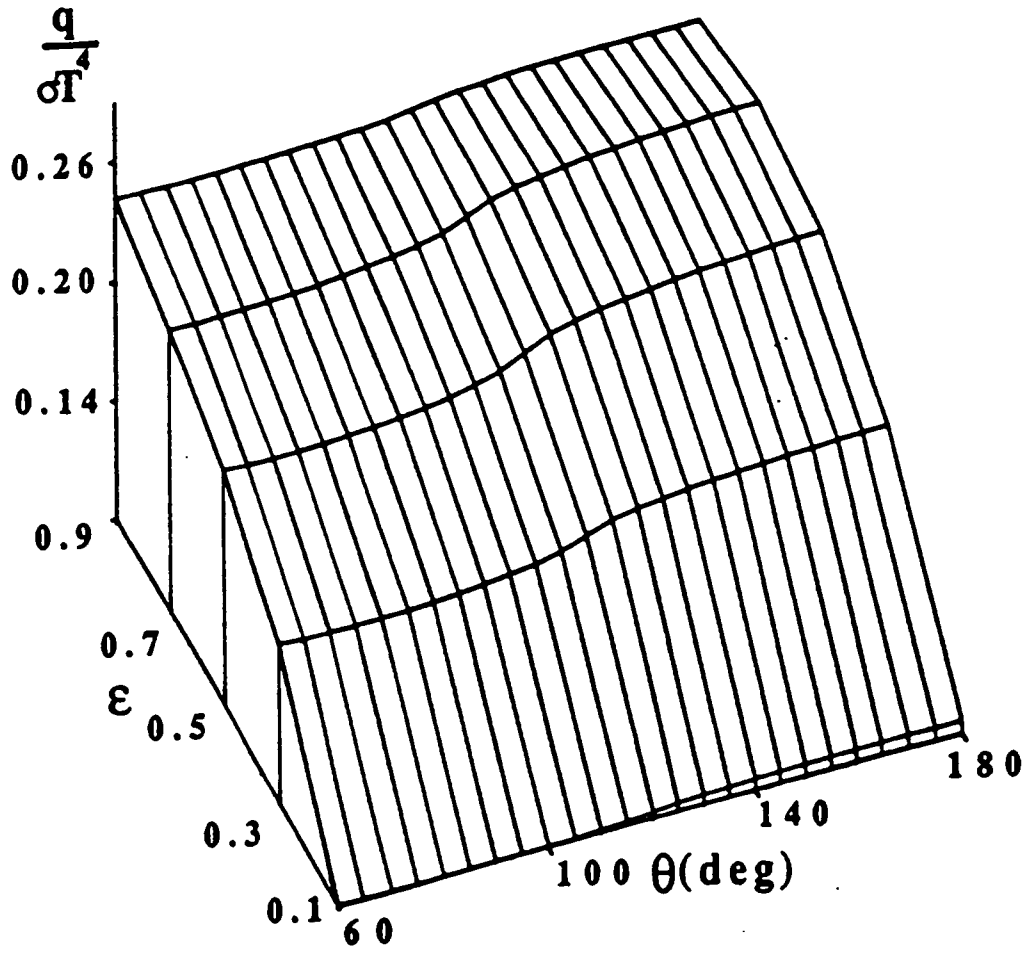

Fig. 32. Heat Transfer Distribution in a Spherical Cavity with Diffuse-Specular Walls as a Function of the Surface Emissivity; Opening Angle $\psi = 60$ deg.

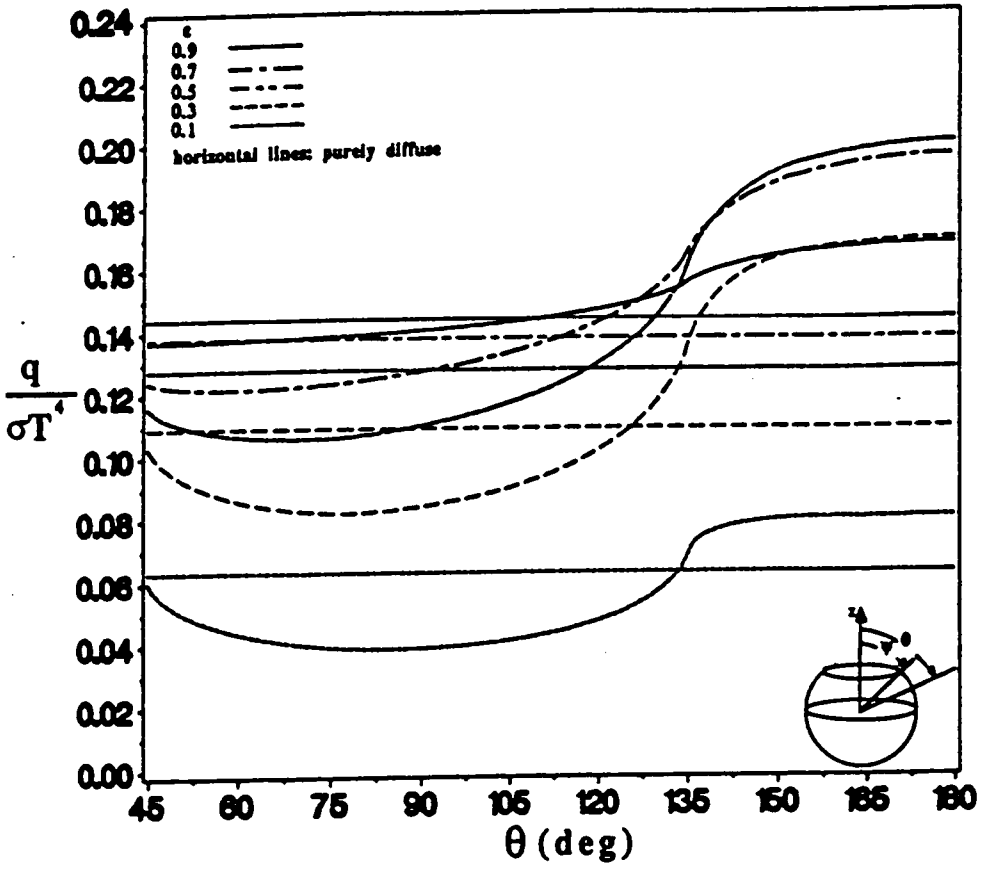

Fig. 33. Heat Transfer Distribution in a Spherical Cavity: Comparison of Purely Specular and Purely Diffuse Wall Cases; Opening Angle $\psi = 45$ deg.

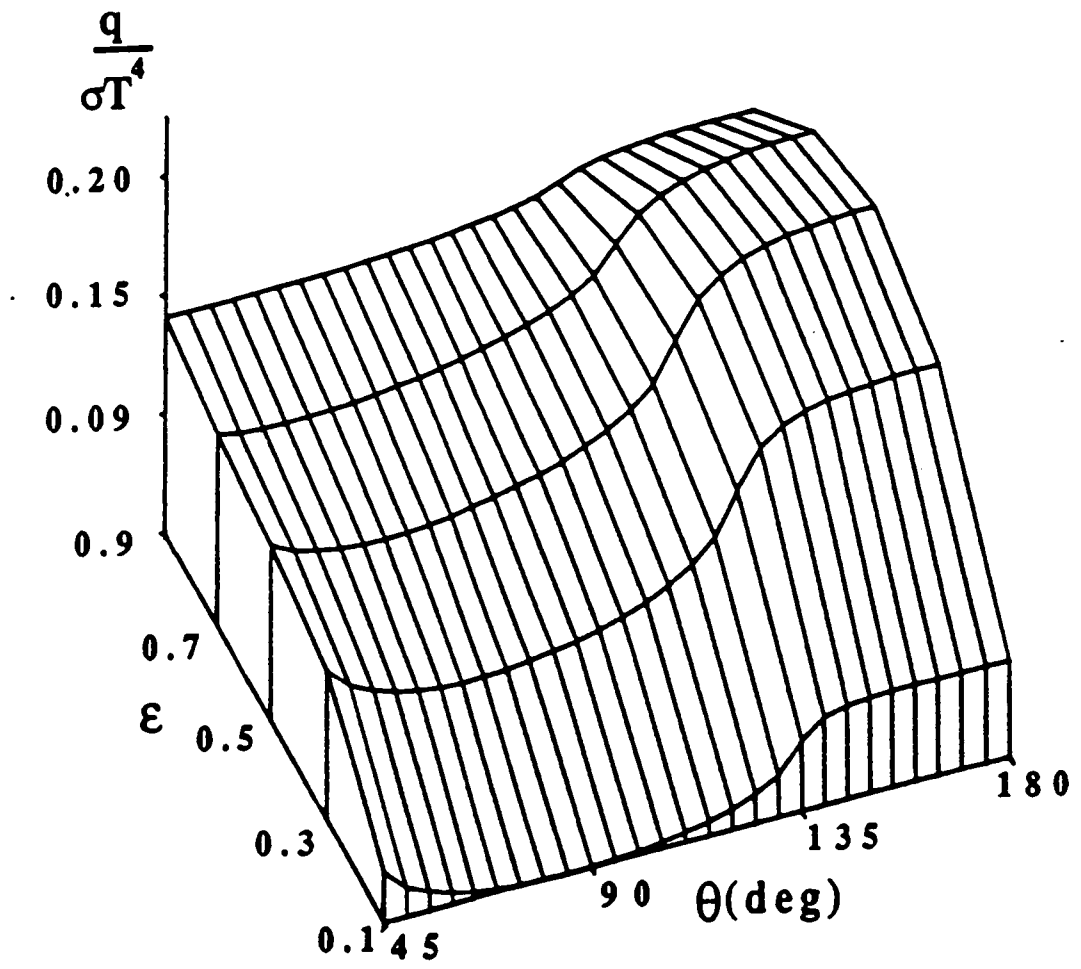

Fig. 34. Heat Transfer Distribution in a Spherical Cavity with Purely Specular Walls as a Function of the Surface Emissivity; Opening Angle ψ = 45 deg.

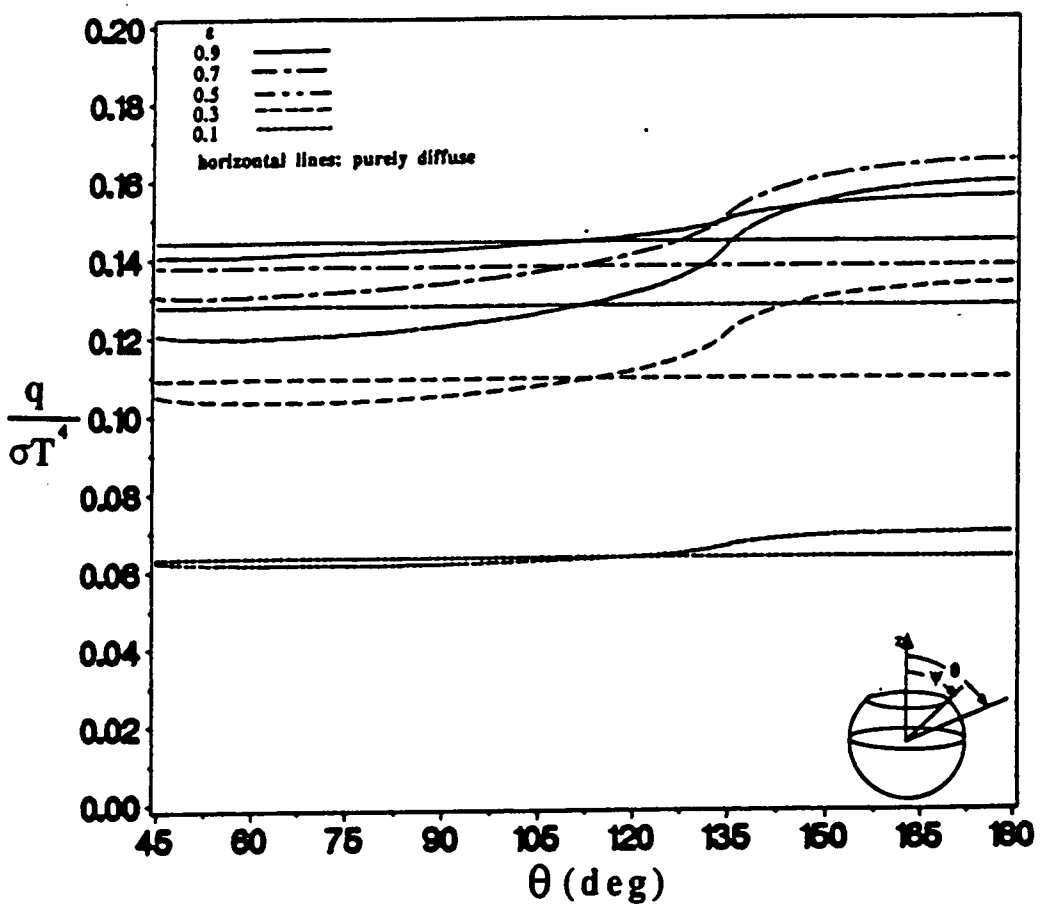

Fig. 35. Heat Transfer Distribution in a Spherical Cavity: Comparison of Diffuse-Specular and Purely Diffuse Wall Cases; Opening Angle ψ = 45 deg.

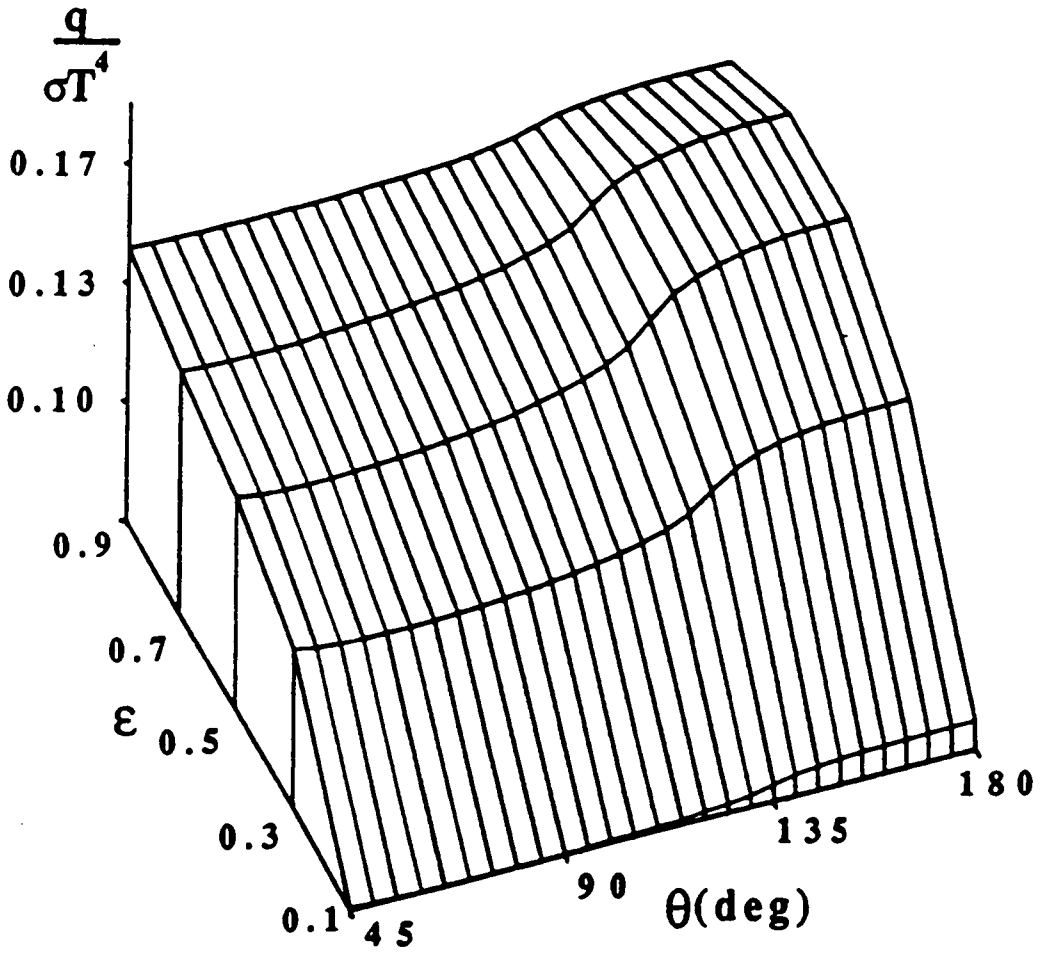

Fig. 36. Heat Transfer Distribution in a Spherical Cavity with Diffuse-Specular Walls as a Function of the Surface Emissivity; Opening Angle ψ = 45 deg.

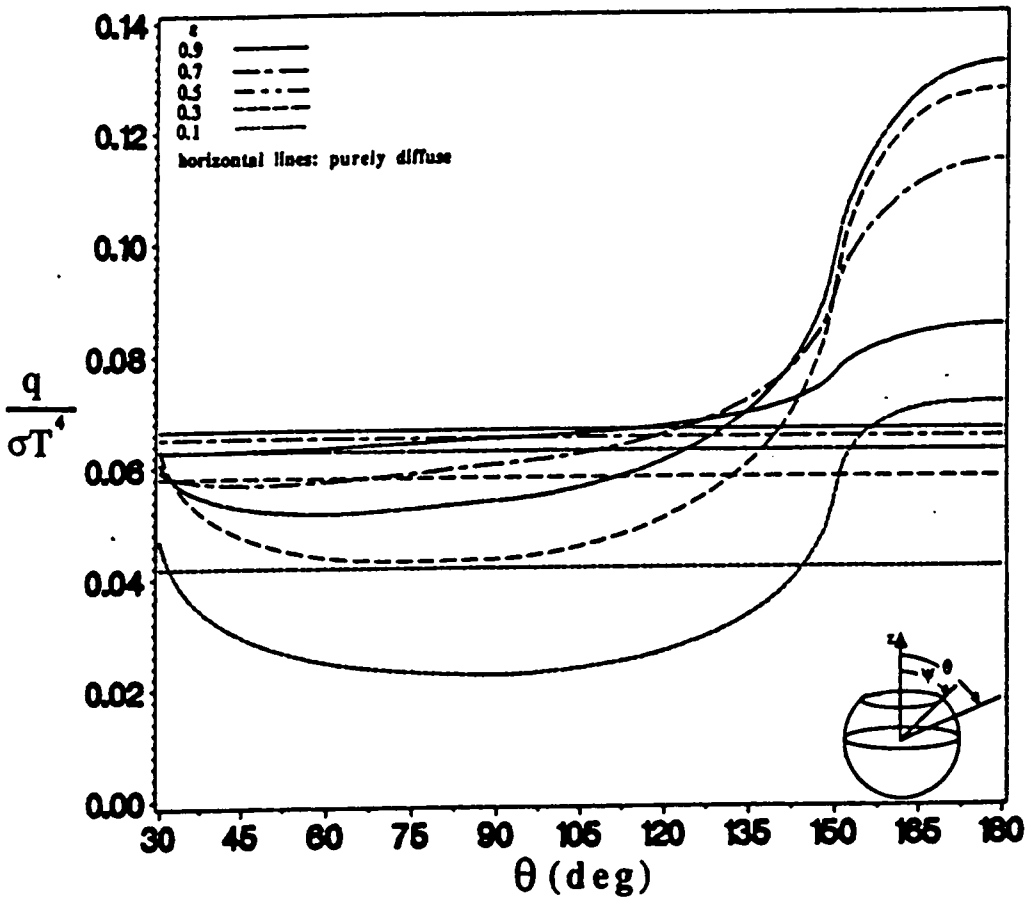

Fig. 37. Heat Transfer Distribution in a Spherical Cavity: Comparison of Purely Specular and Purely Diffuse Wall Cases; Opening Angle ψ = 30 deg.

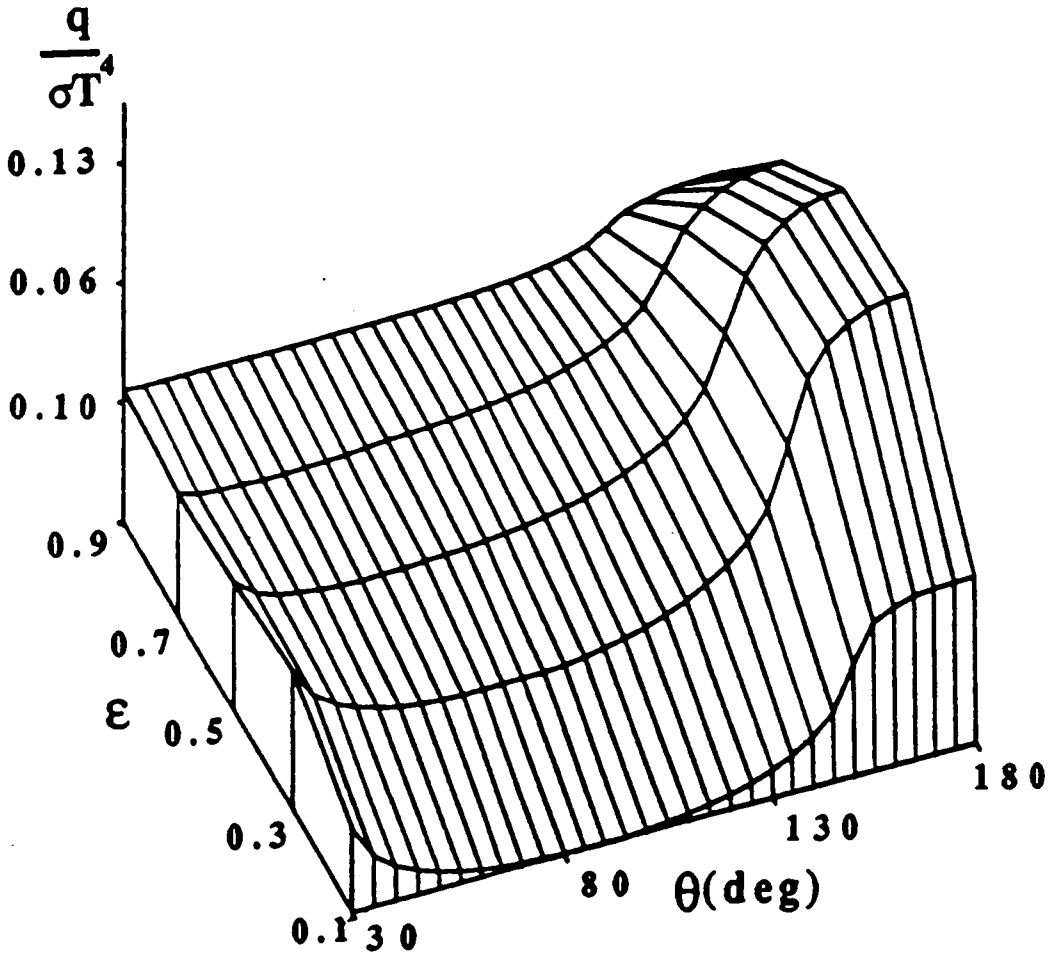

Fig. 38. Heat Transfer Distribution in a Spherical Cavity with Purely Specular Walls as a Function of the Surface Emissivity; Opening Angle $\psi = 30$ deg.

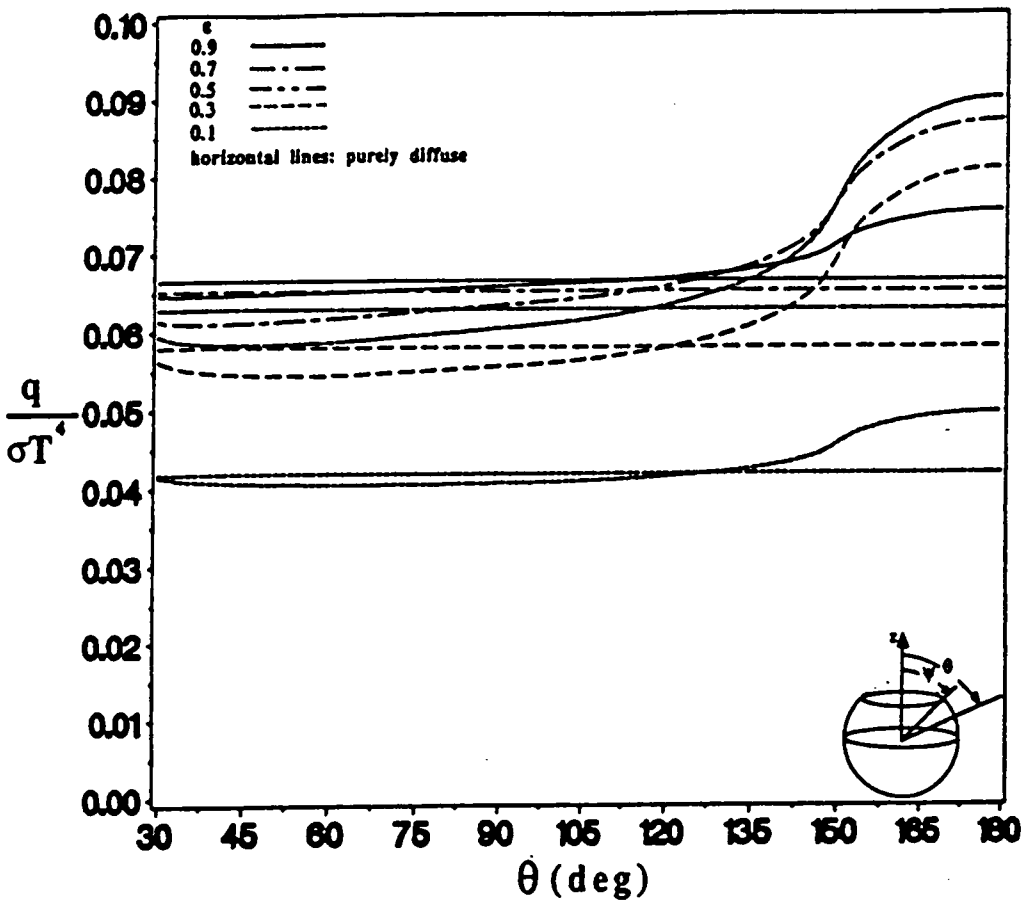

Fig. 39. Heat Transfer Distribution in a Spherical Cavity: Comparison of Diffuse-Specular and Purely Diffuse Wall Cases; Opening Angle ψ = 30 deg.

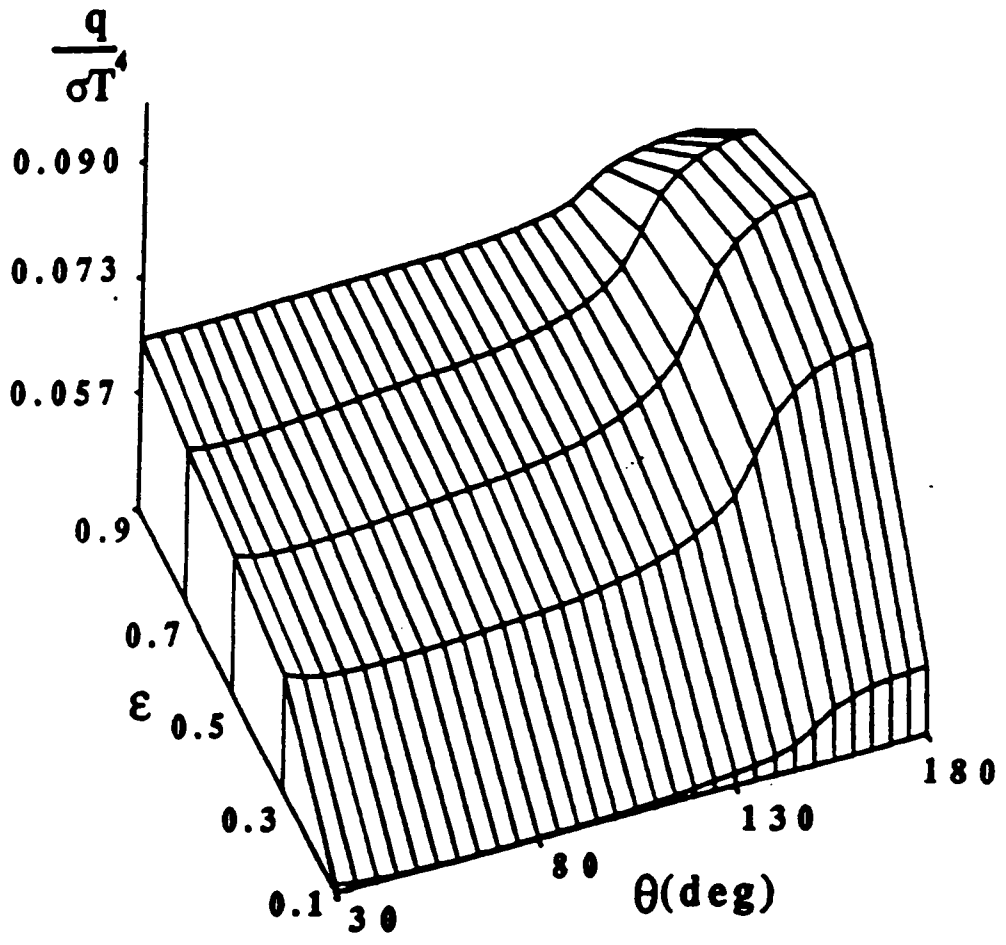

Fig. 40. Heat Transfer Distribution in a Spherical Cavity with Diffuse-Specular Walls as a Function of the Surface Emissivity; Opening Angle ψ = 30 deg.

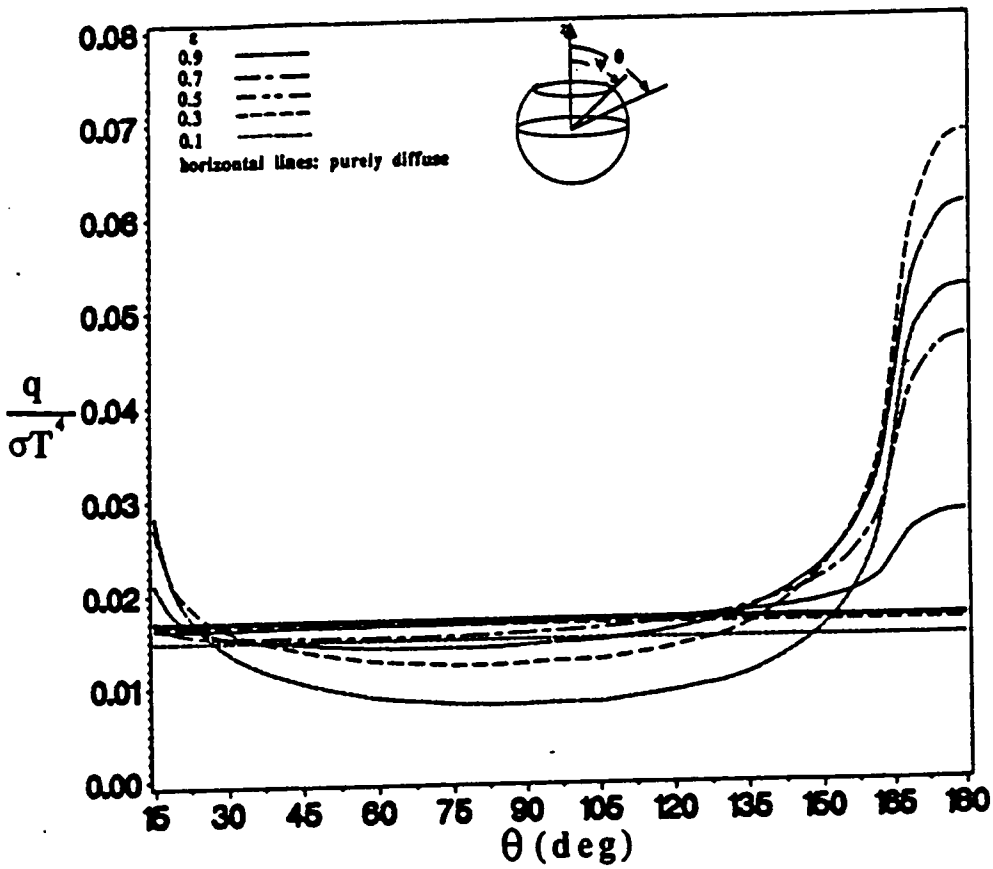

Fig. 41. Heat Transfer Distribution in a Spherical Cavity: Comparison of Purely Specular and Purely Diffuse Wall Cases; Opening Angle ψ = 15 deg.

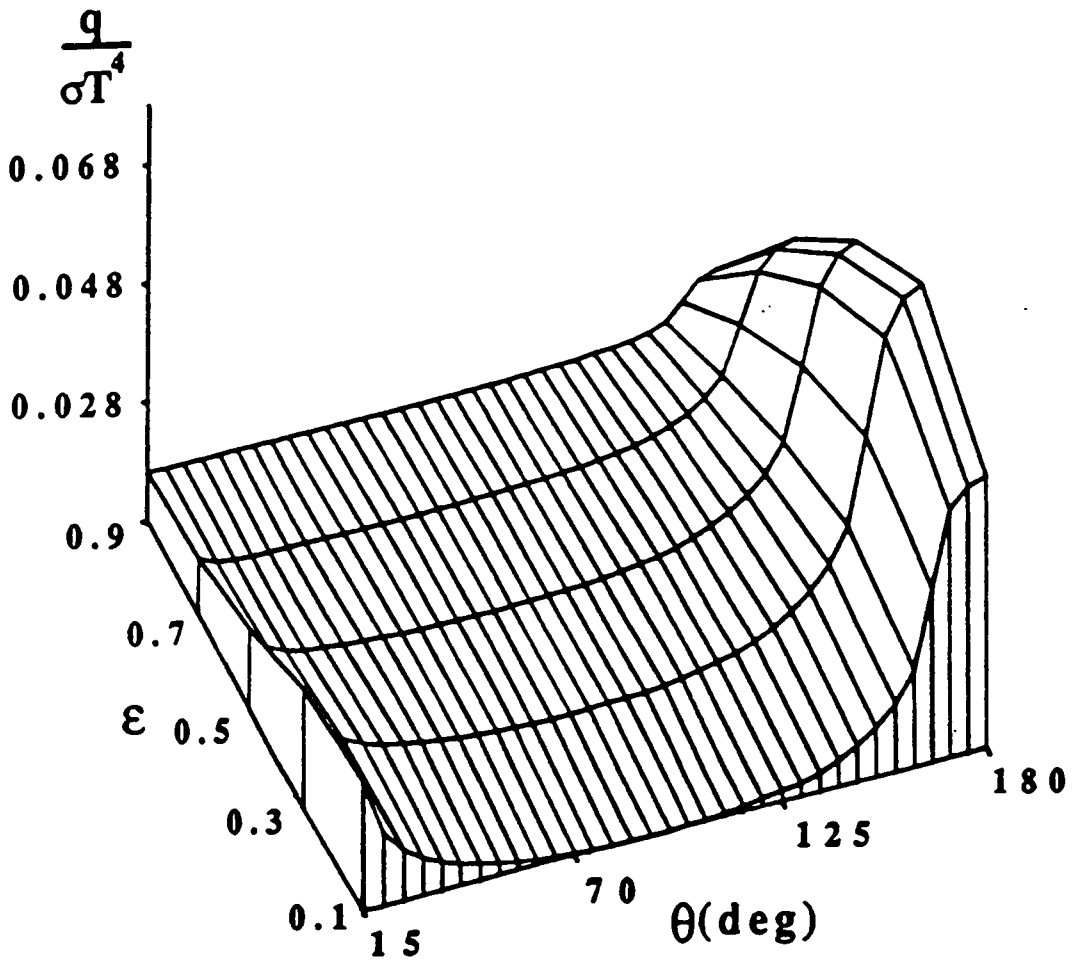

Fig. 42. Heat Transfer Distribution in a Spherical Cavity with Purely Specular Walls as a Function of the Surface Emissivity; Opening Angle ψ = 15 deg.

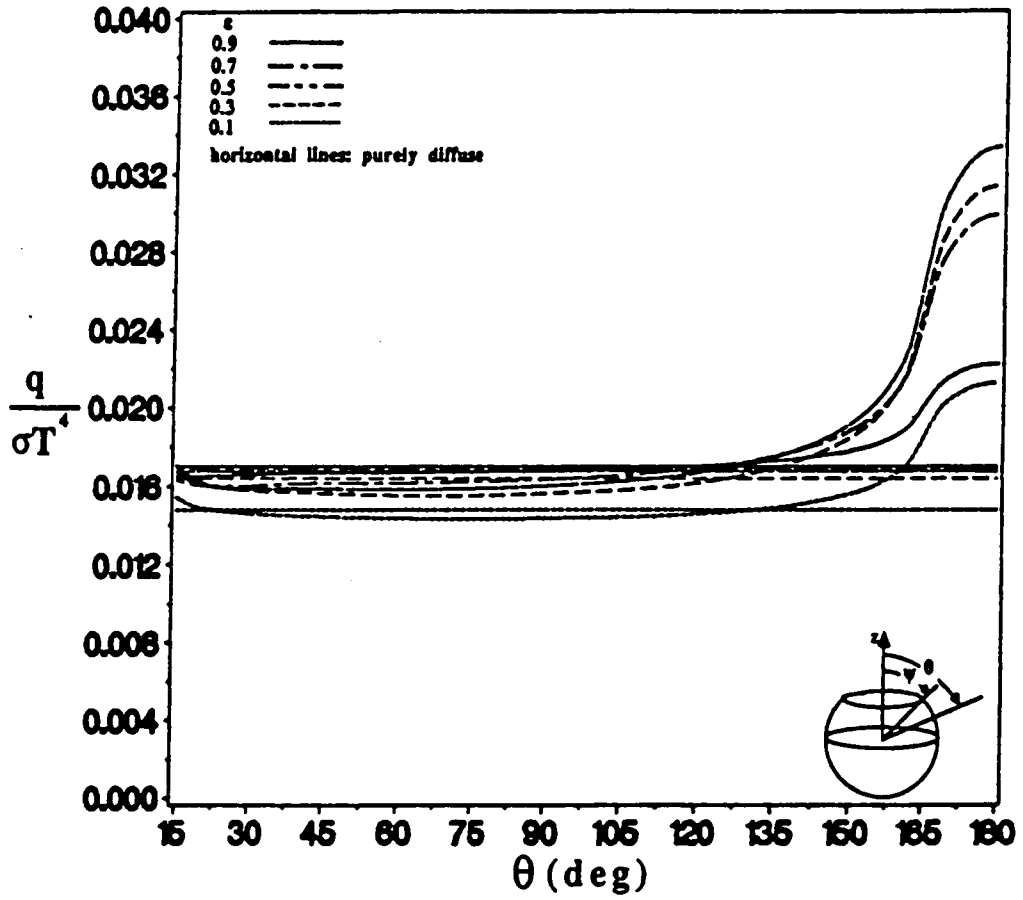

Fig. 43. Heat Transfer Distribution in a Spherical Cavity: Comparison of Diffuse-Specular and Purely Diffuse Wall Cases, Opening Angle ψ = 15 deg.

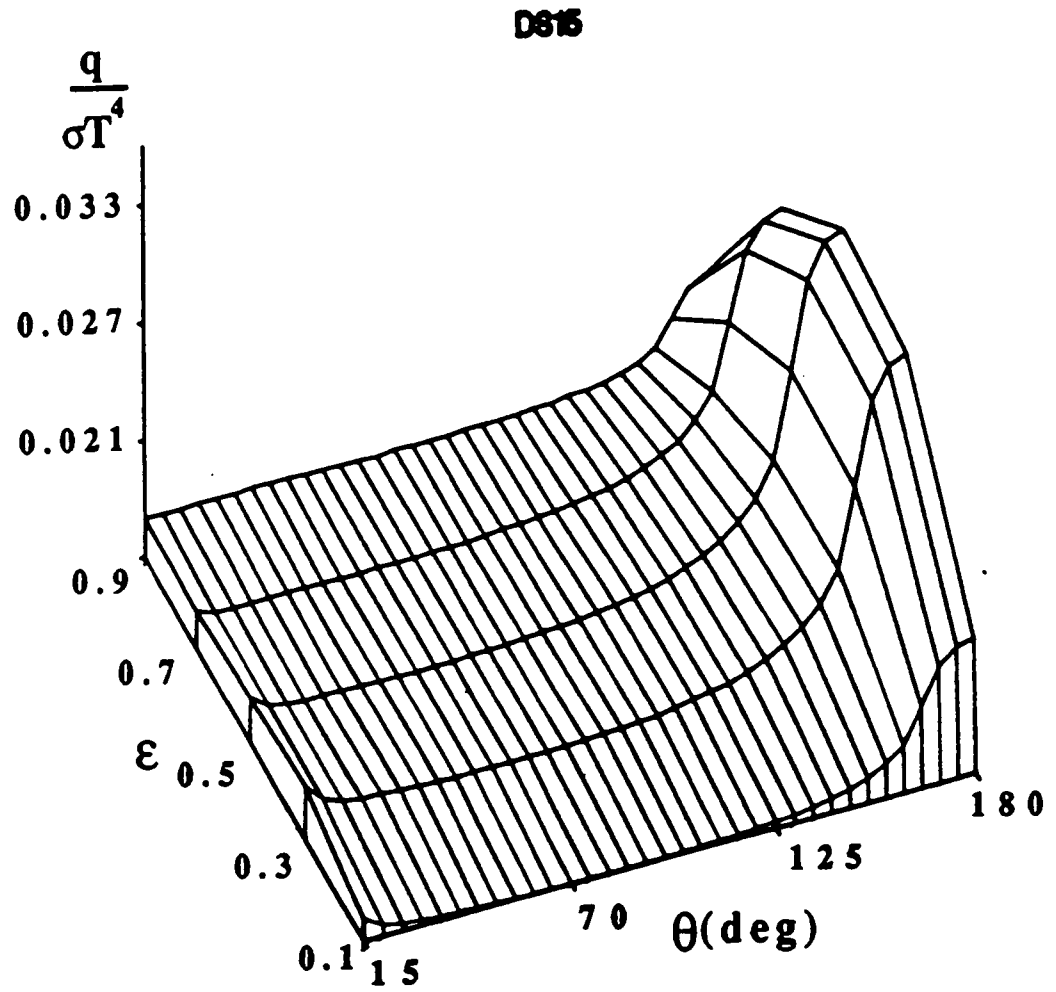

Fig. 44. Heat Transfer Distribution in a Spherical Cavity with Diffuse-Specular Walls as a Function of the Surface Emissivity; Opening Angle ψ = 15 deg.

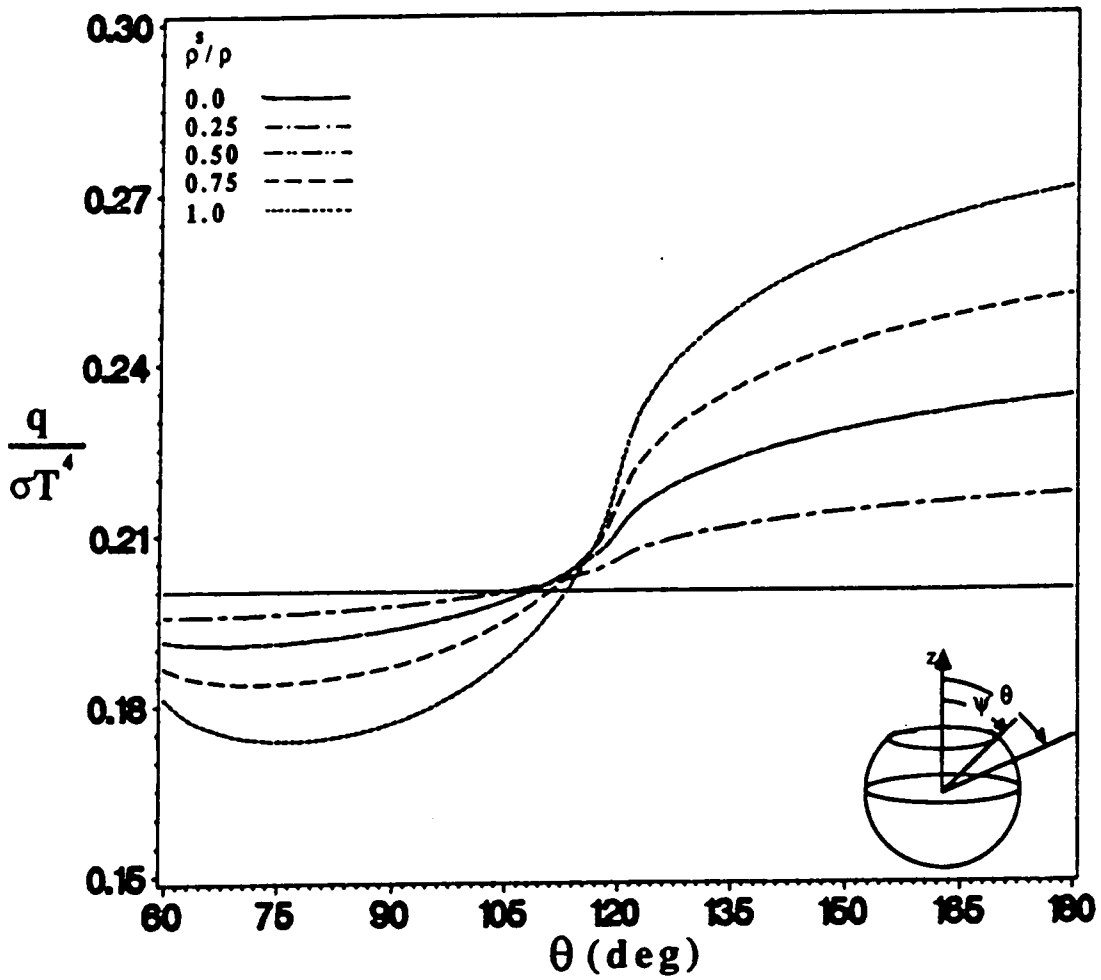

Fig. 45. Heat Transfer Distribution with Changing Reflectivity Ratio: Opening Angle ψ = 60 deg. and Emissivity ε = 0.5.

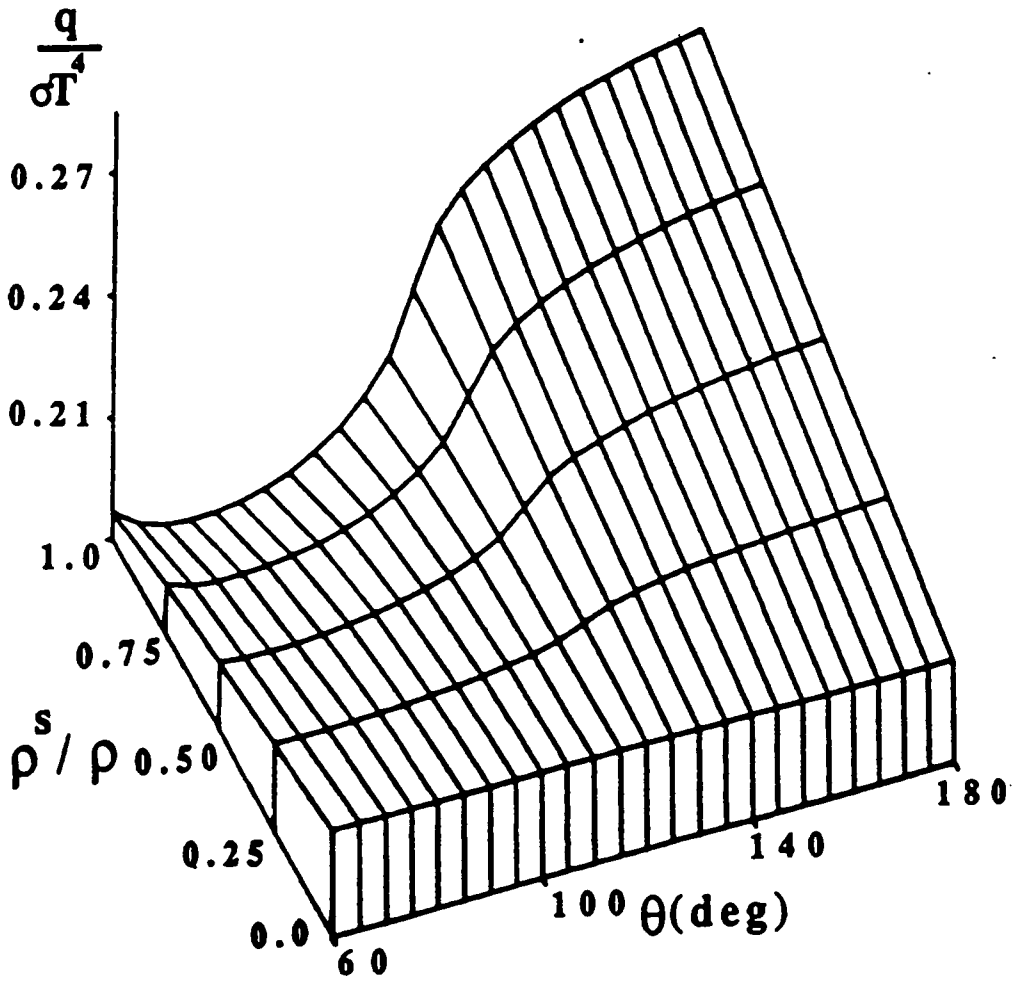

Fig. 46. Heat Transfer Distribution with Changing Reflectivity Ratio: Opening Angle ψ = 60 deg. and Emissivity ε = 0.5.

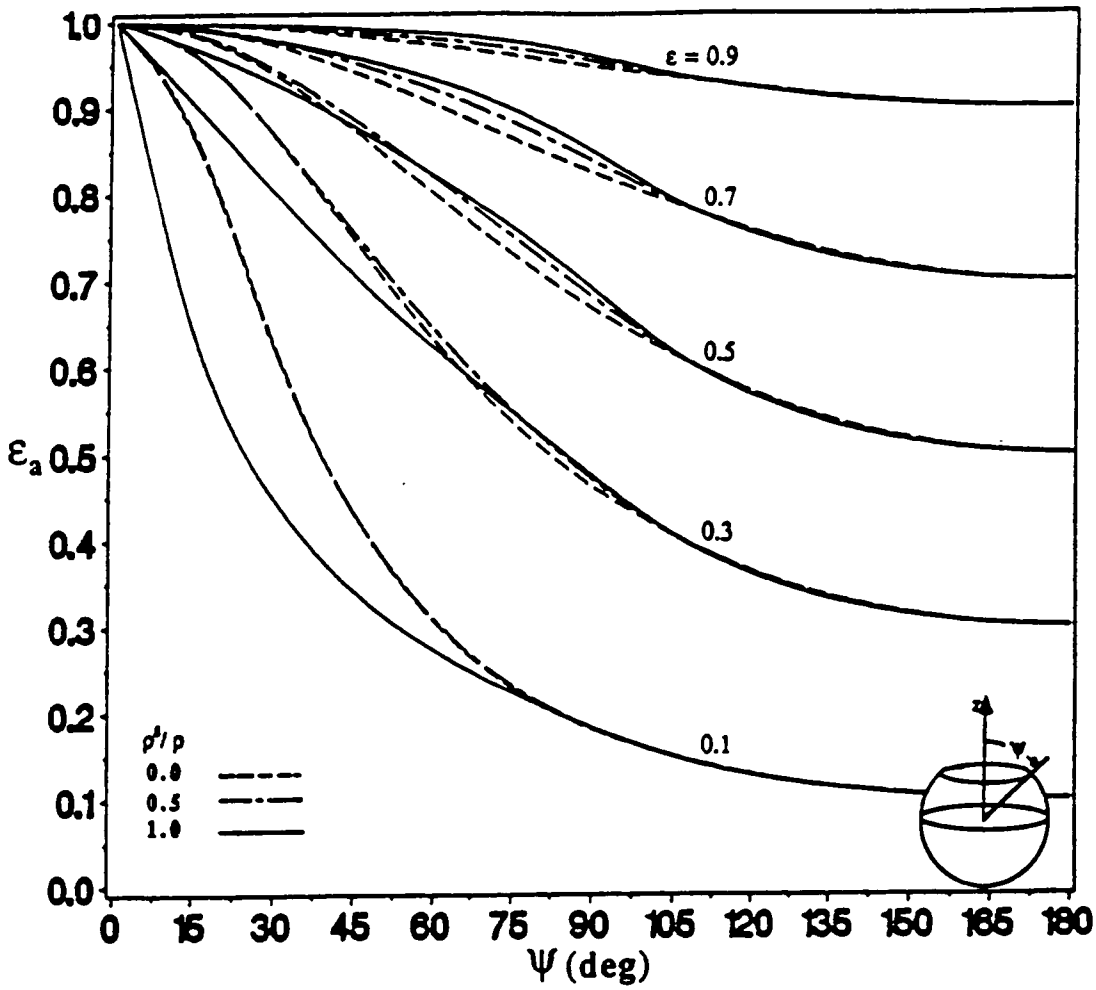

Fig. 47. Apparent Emissivity of Spherical Cavities for Various Surface Conditions and Cavity Opening Angles.

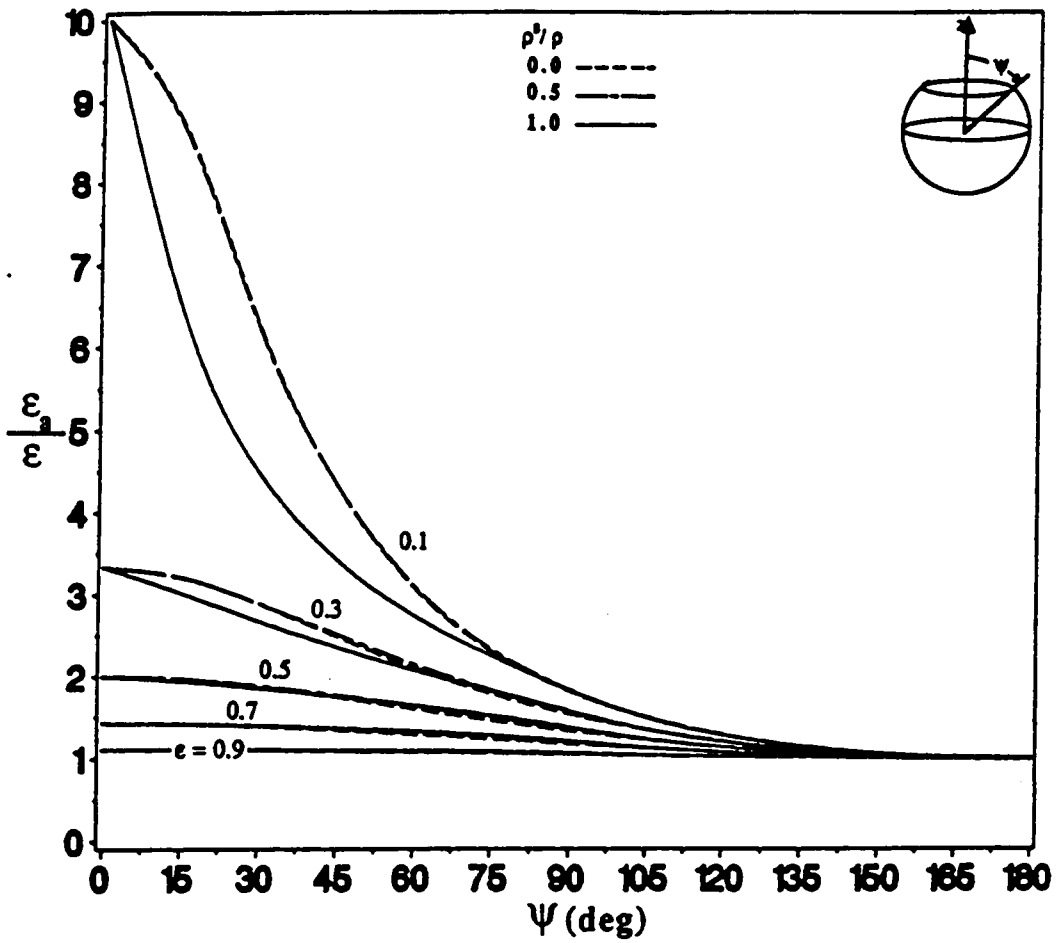

Fig. 48. Cavity Effect for Spherical Cavities.

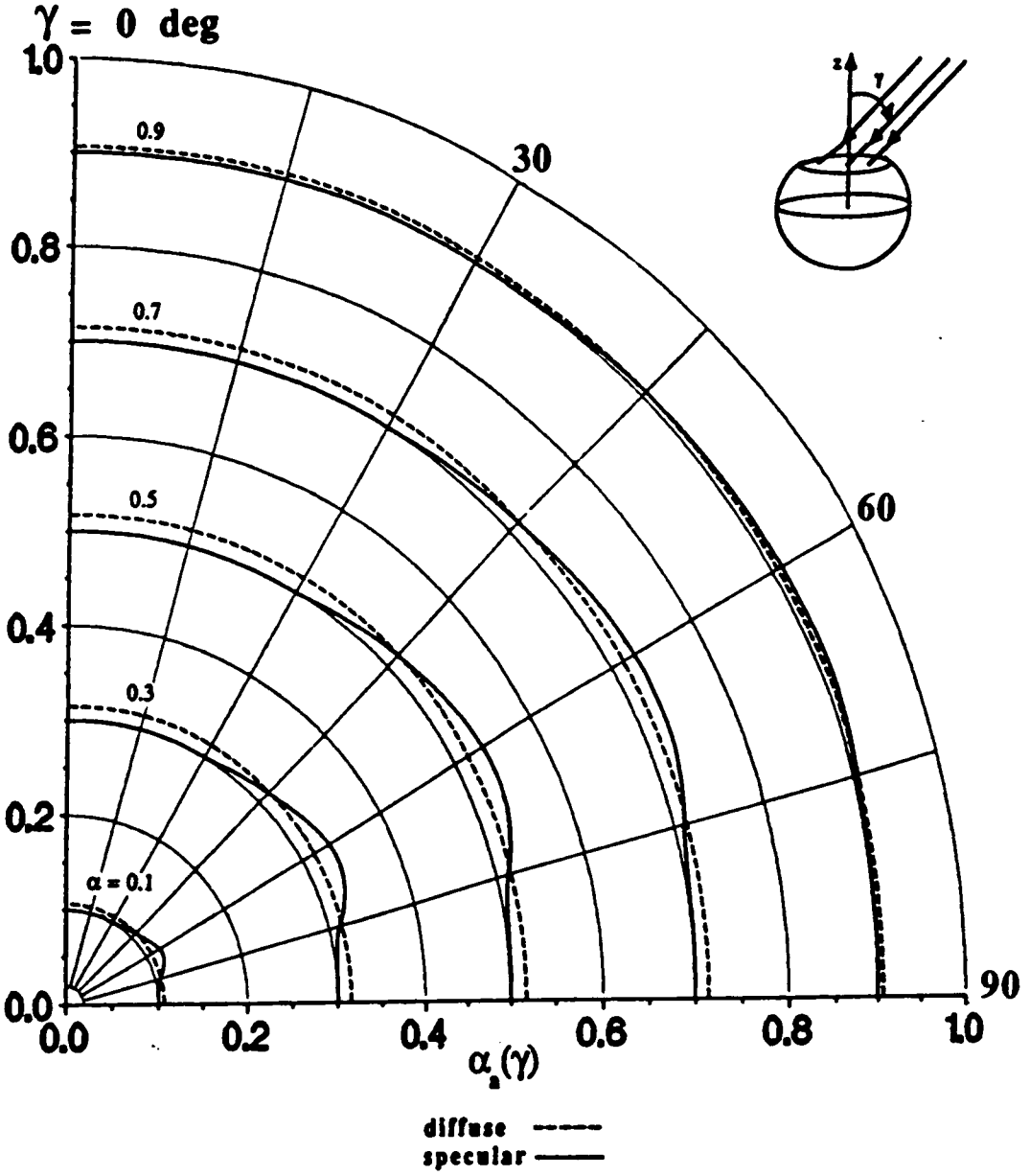

Fig. 49. Directional Apparent Absorptivity of Spherical Cavities; Opening Angle = 150 deg.

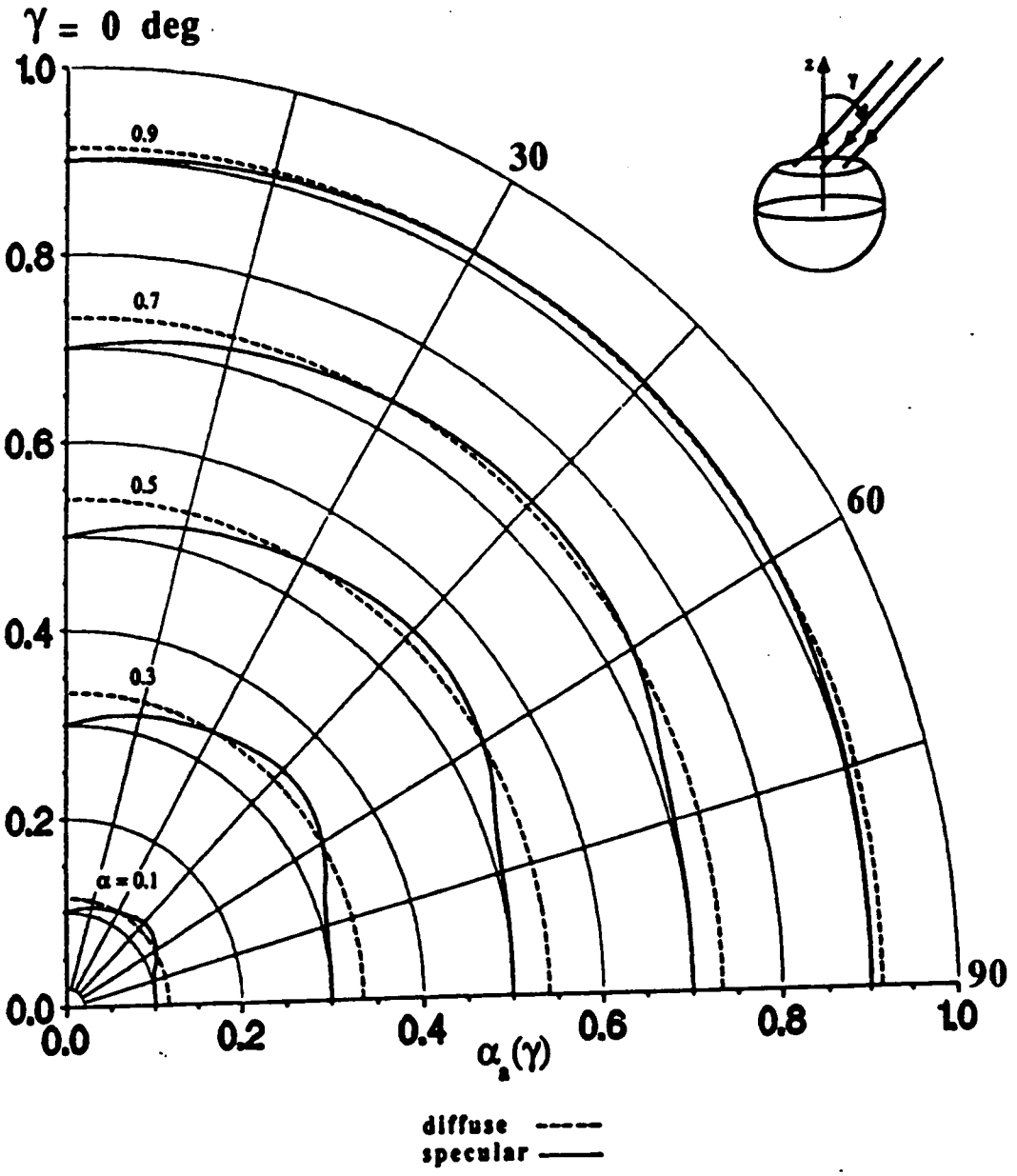

Fig. 50. Directional Apparent Absorptivity of Spherical Cavities; Opening Angle = 135 deg.

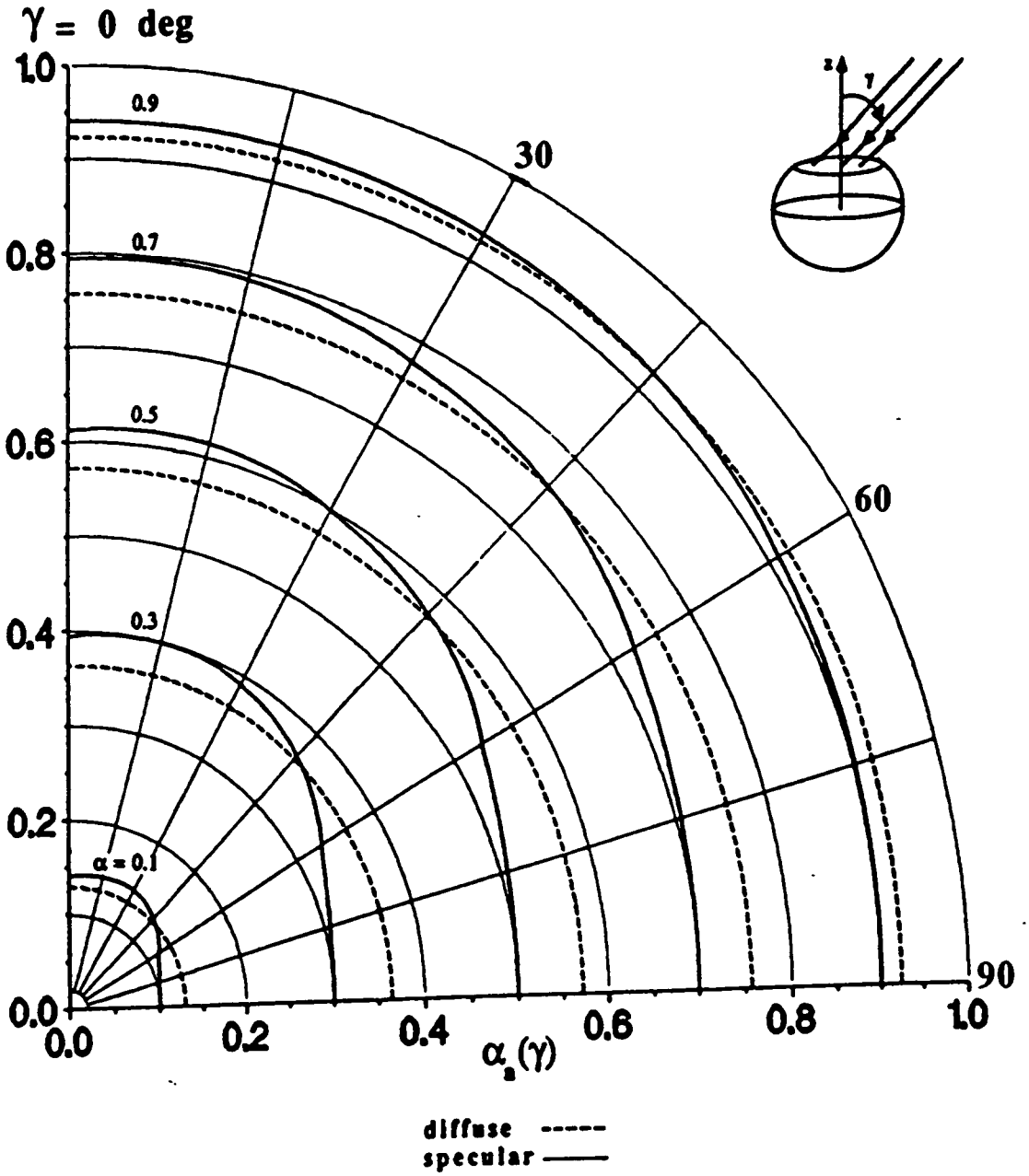

Fig. 51. Directional Apparent Absorptivity of Spherical Cavities; Opening Angle = 120 deg.

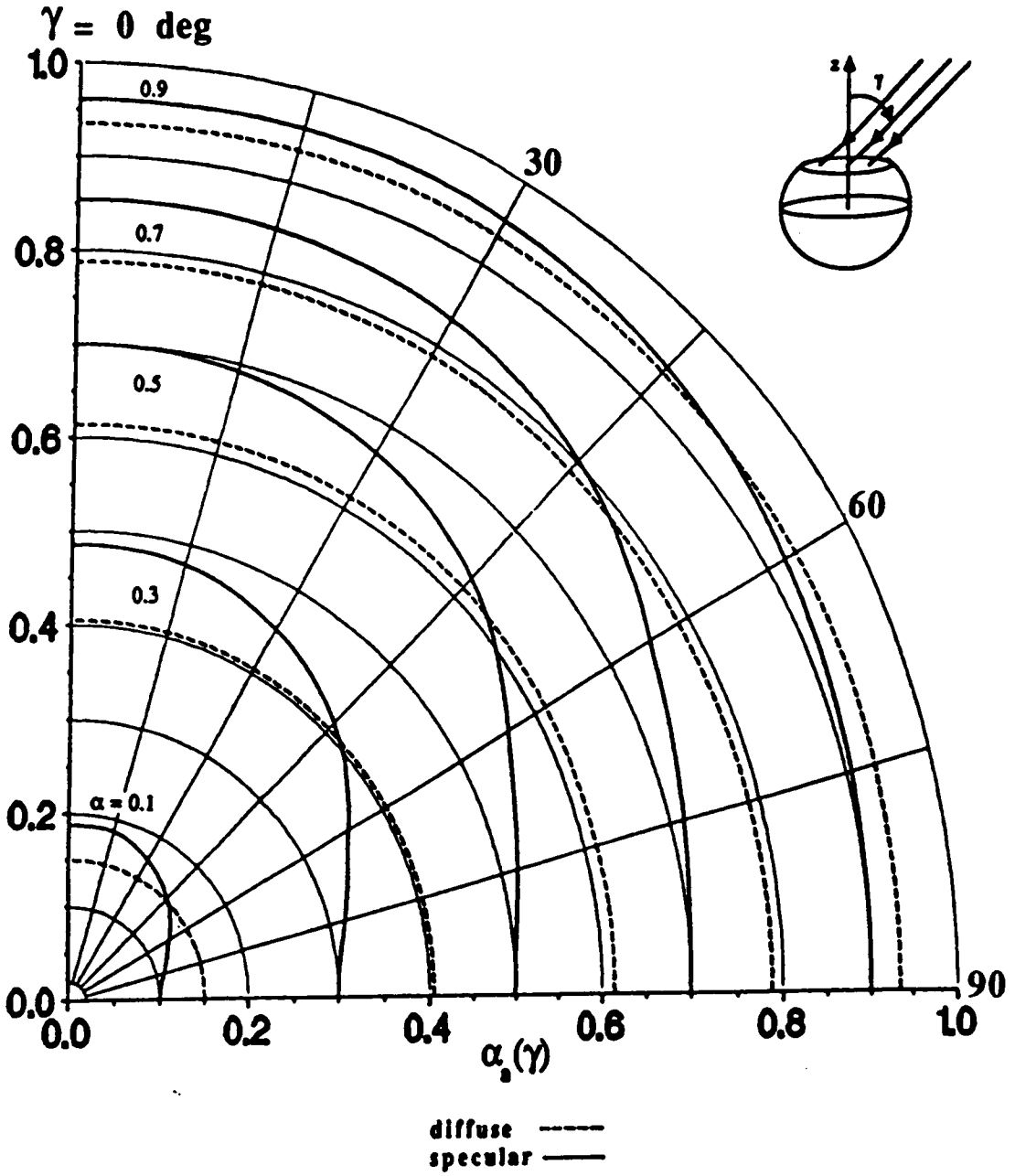

Fig. 52. Directional Apparent Absorptivity of Spherical Cavities; Opening Angle = 105 deg.

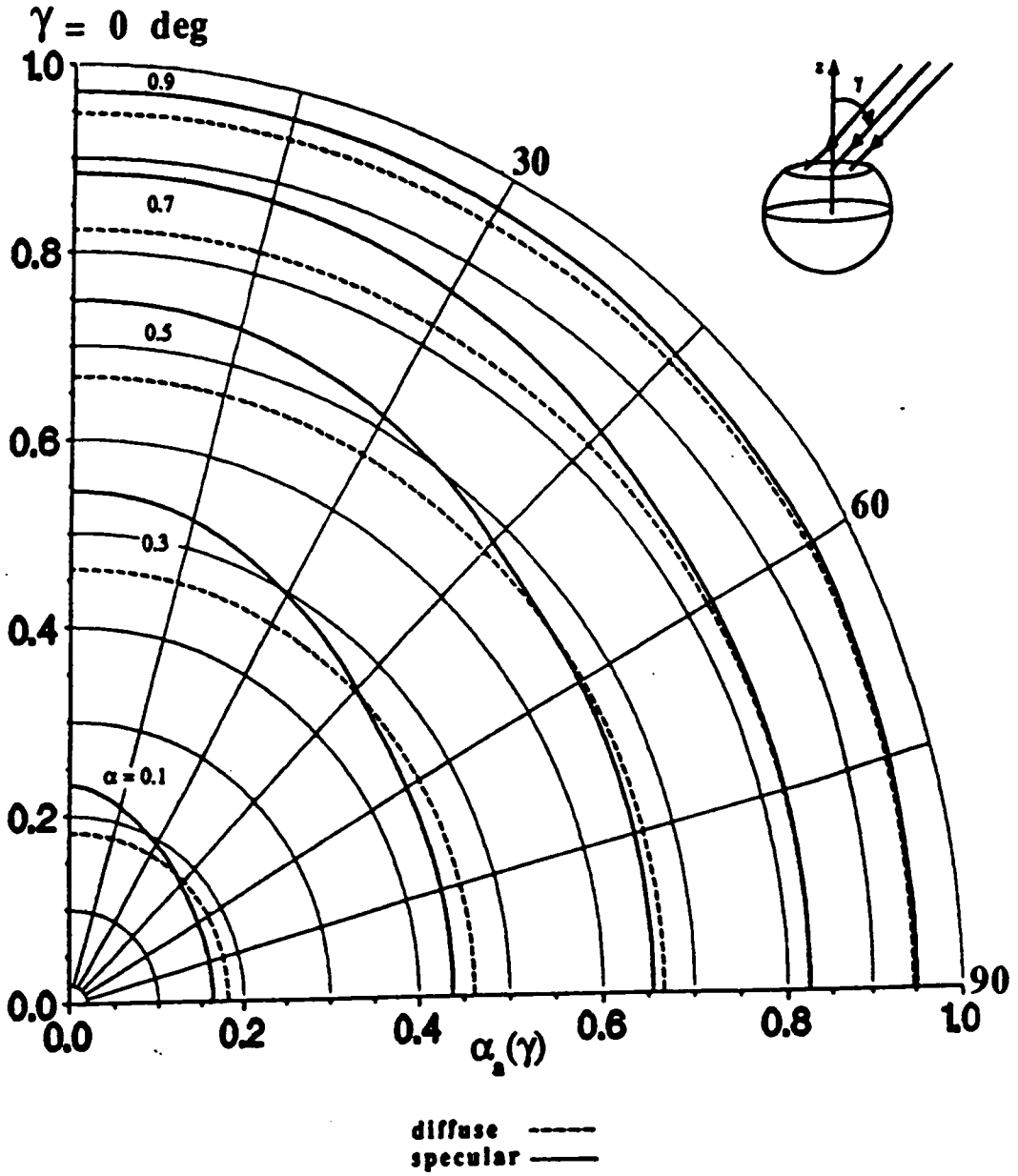

Fig. 53. Directional Apparent Absorptivity of Spherical Cavities; Opening Angle = 90 deg.

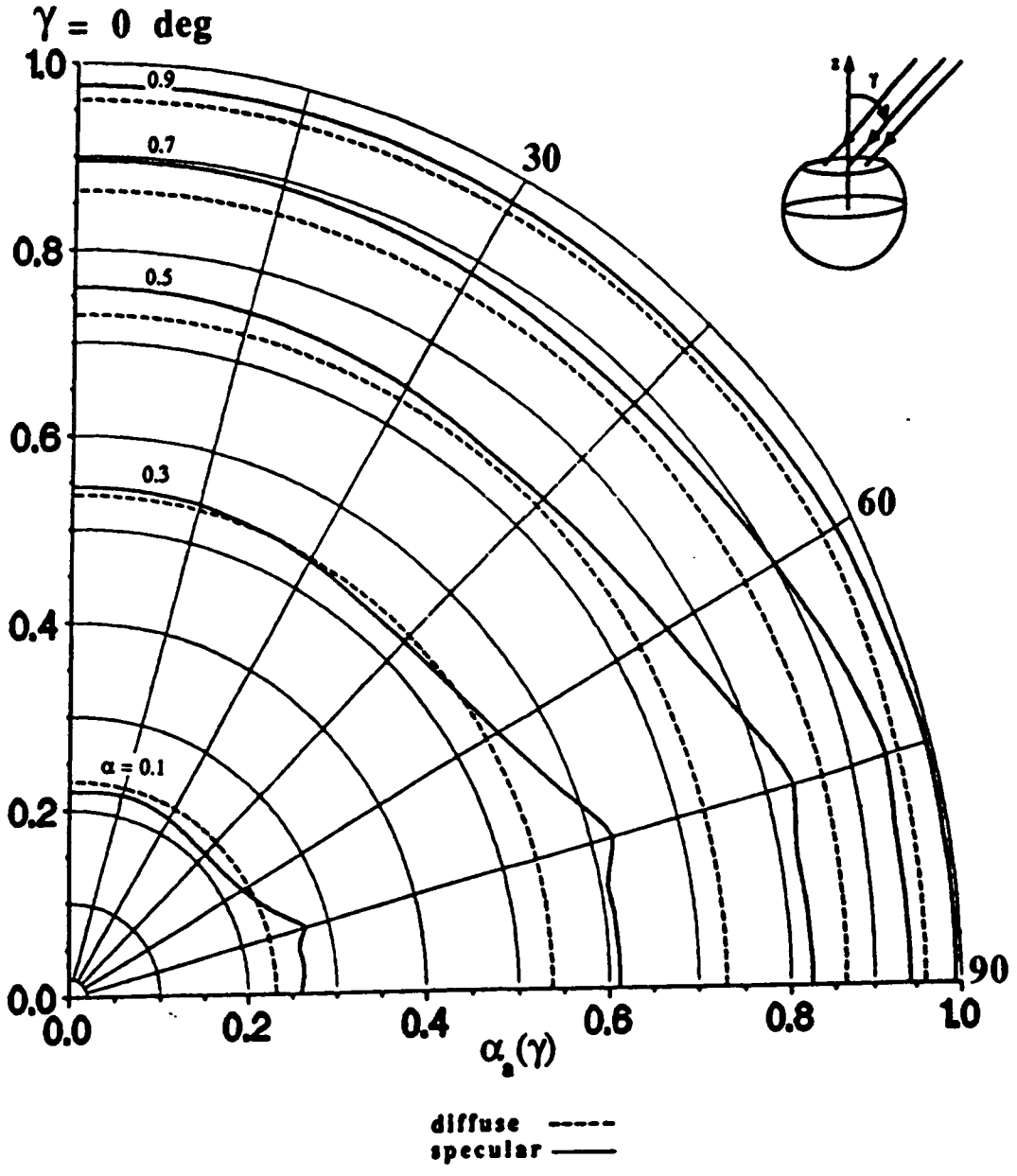

Fig. 54. Directional Apparent Absorptivity of Spherical Cavities; Opening Angle = 75 deg.

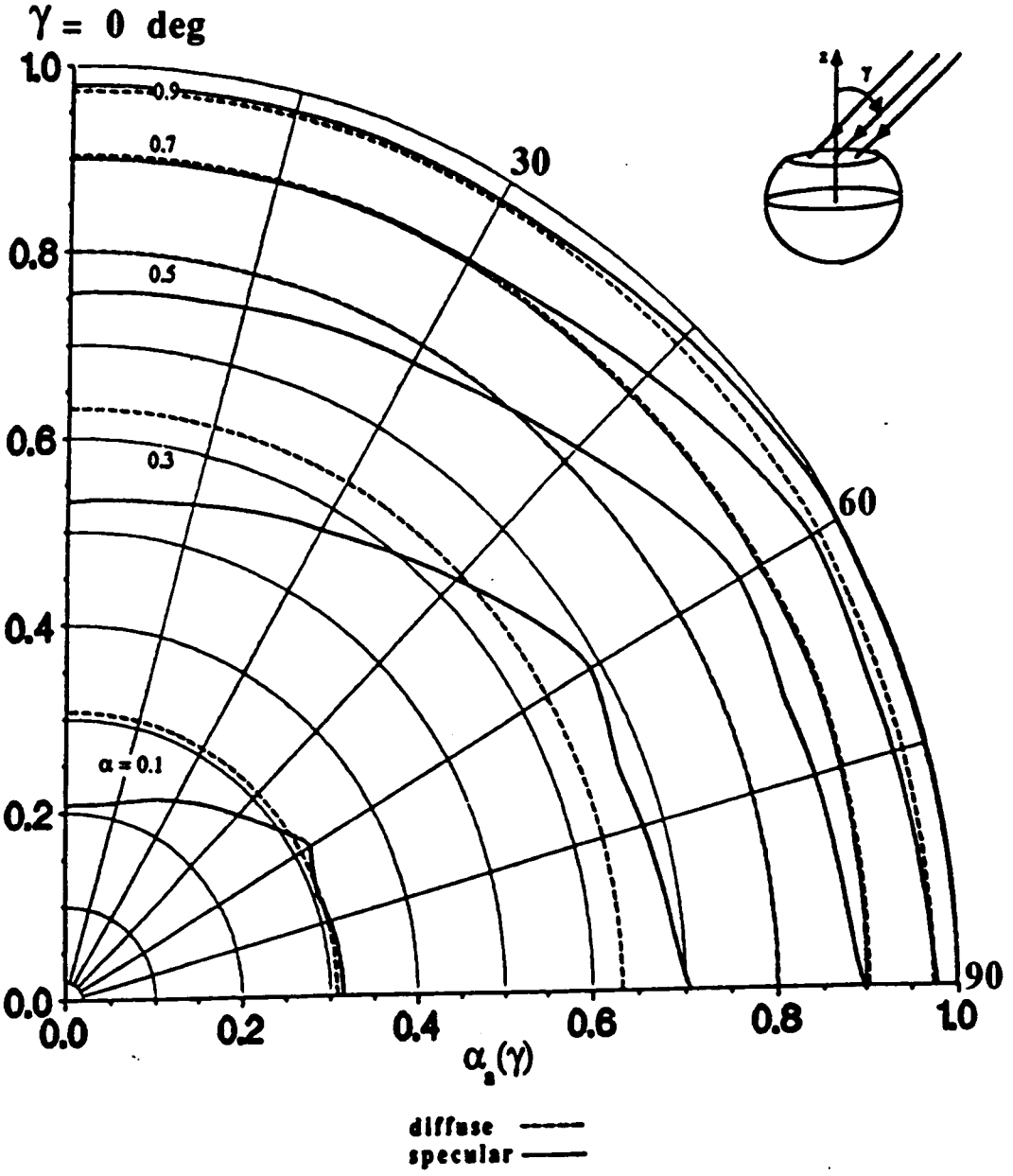

Fig. 55. Directional Apparent Absorptivity of Spherical Cavities; Opening Angle = 60 deg.

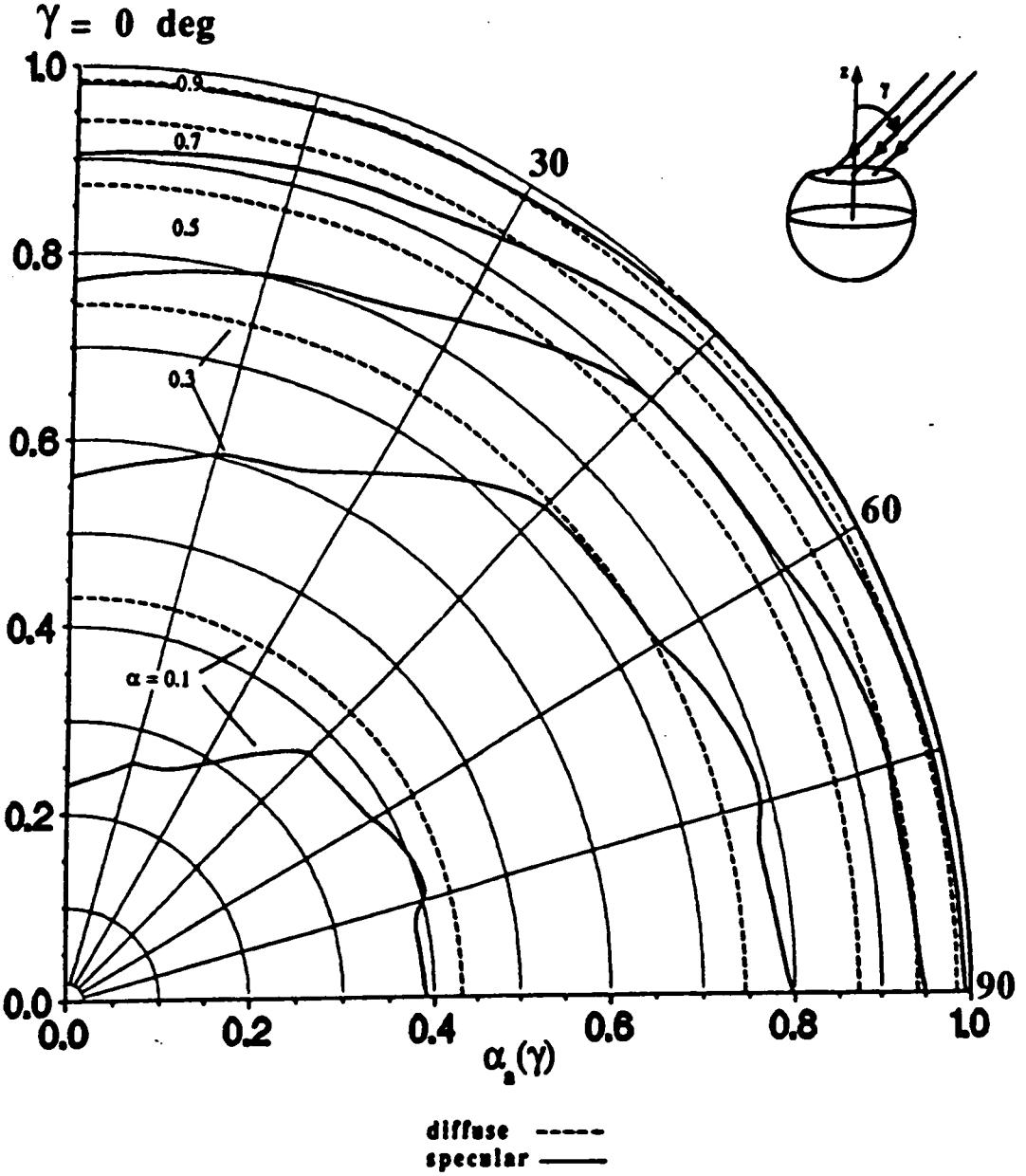

Fig. 56. Directional Apparent Absorptivity of Spherical Cavities; Opening Angle = 45 deg.

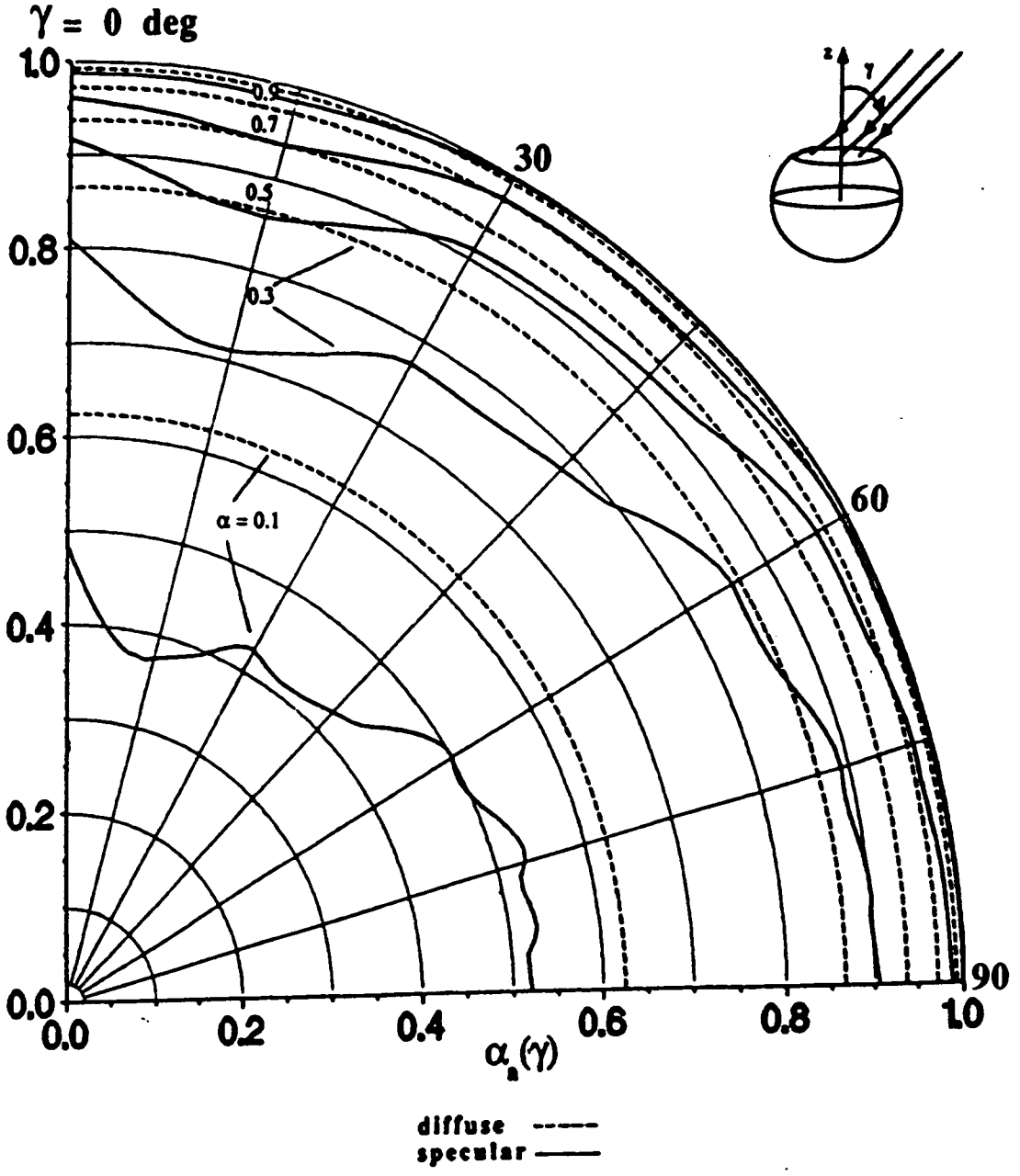

Fig. 57. Directional Apparent Absorptivity of Spherical Cavities; Opening Angle = 30 deg.

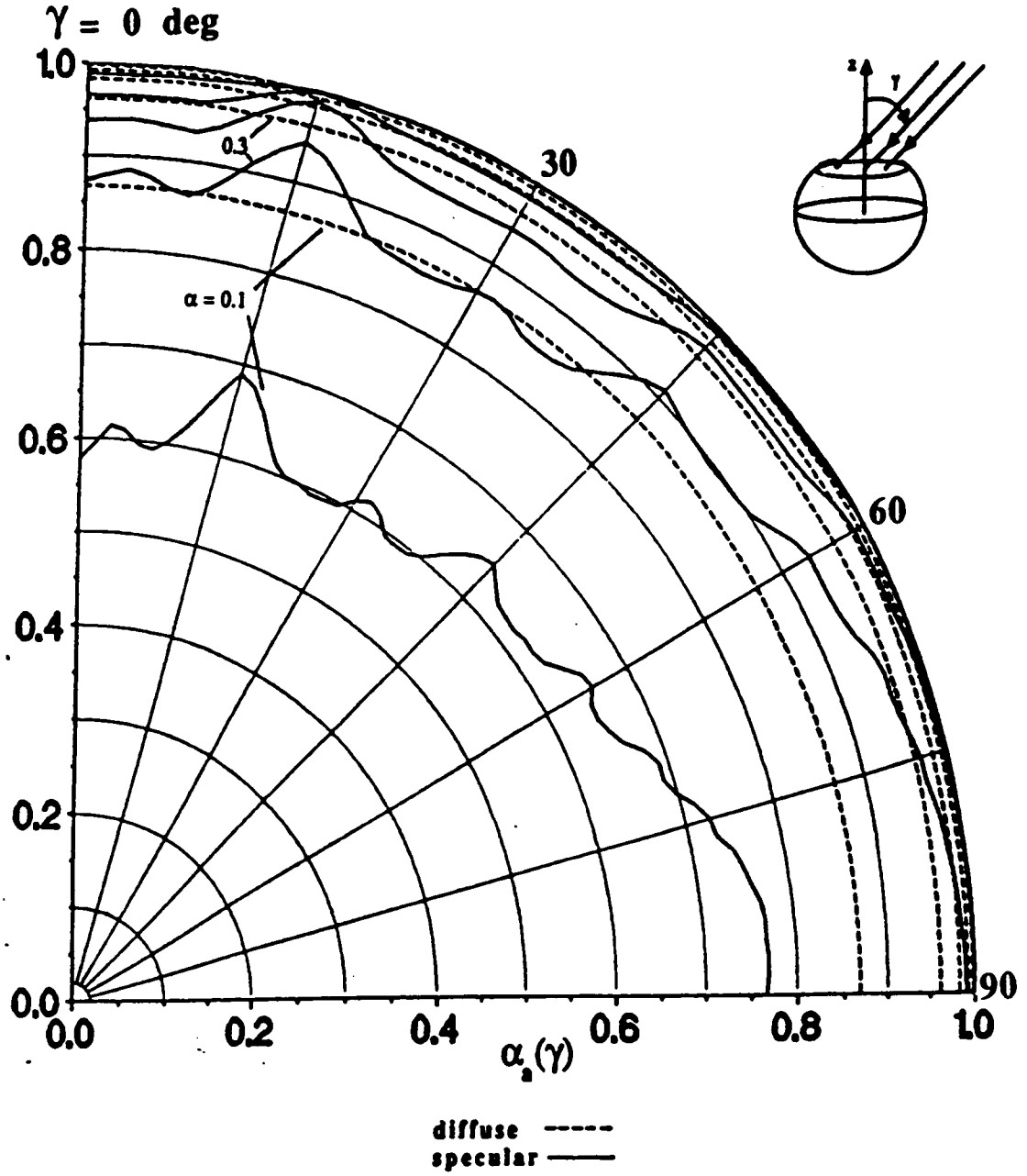

Fig. 58. Directional Apparent Absorptivity of Spherical Cavities; Opening Angle = 15 deg.

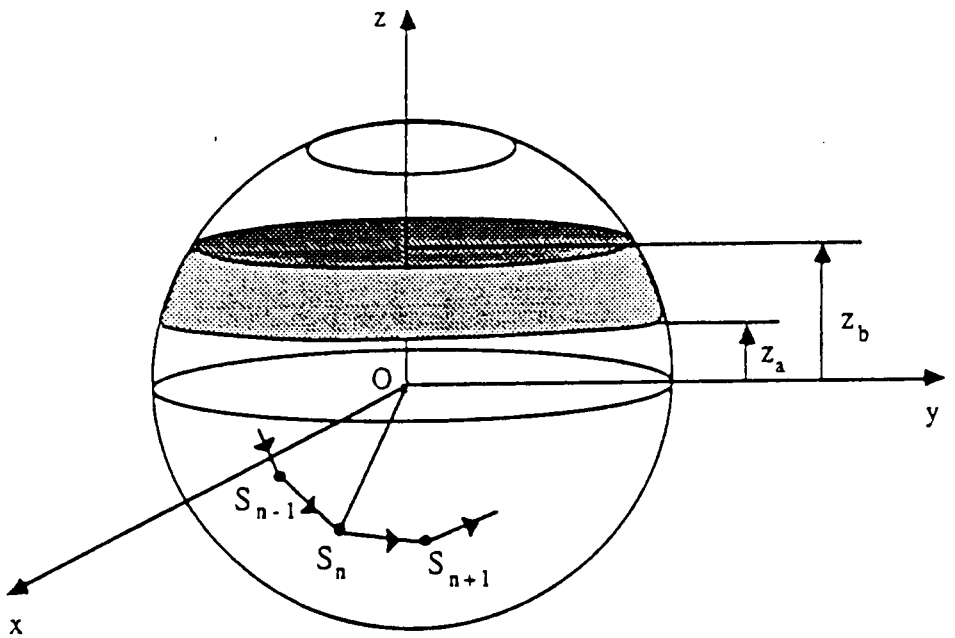

Fig. 59. Spherical Surface Element in Monte Carlo Calculations of the Distribution Factors.

References

1. Sparrow, E. M., and R. D. Cess, **Radiation Heat Transfer,** Augmented Edition, McGraw-Hill, New York, 1979.

2. Siegel, R., and J. R. Howell, **Thermal Radiation Heat Transfer,** 2nd Edition, McGraw-Hill, New York, 1981.

3. Eckert, E. R. G., and R. Drake, **Heat and Mass Transfer,** McGraw-Hill, New York, 1987.

4. Hottel, H. C., *Radiant Heat Transmission,* in Mc Adams, W. H. (ed.), **Heat Transmission,** 3rd Edition, Chapter 4, McGraw-Hill, New York, 1954.

5. Oppenheim, A. K., *Radiation Analysis by the Network Method* , **Transactions of ASME,** Vol. 78, 1956, pp. 725-735.

6. Gebhart, B., *A New Method for Calculating Radiant Exchange* , **Heating, Piping, and Air Conditioning,** Vol. 30, No. 7, 1958, pp. 131-135.

7. Jakob, M., **Heat Transfer,** Vol. II, John Wiley and Sons, New York, 1957.

8. Sparrow, E. M., J. L. Gregg, J. V. Szel, and P. Manos, *Analysis, Results, and Interpretation for Some Simply-Arranged Gray Surfaces,* **Journal of Heat Transfer,** Vol. C83, 1961, pp. 207-214.

9. Eckert, E. R. G., and E. M. Sparrow, *Radiative Heat Transfer Between Surfaces with Specular Reflection*, **International Journal of Heat and Mass Transfer**, Vol. 3, 1961, pp. 42-54.

10. Sparrow, E. M., E. R. G. Eckert, and V. K. Jonsson, *An Enclosure Theory for Radiative Exchange between Specularly and Diffusely Reflecting Surfaces*, **Journal of Heat Transfer**, Vol. C84, 1962, pp. 294-300.

11. Lin, S. H., *Radiant Interchange in Cavities and Passages with Specularly and Diffusely Reflecting Surfaces*, Ph.D Thesis, Department of Mechanical Engineering, University of Minnesota, Minneapolis, Minn., March, 1964.

12. Sarofim, A. F., and H. C. Hottel, *Radiative Exchange among Non-Lambert Surfaces*, **Journal of Heat Transfer**, Vol. C88, 1966, pp. 37-44.

13. Lin, S. H., and E. M. Sparrow, *Radiant Interchange Among Curved Specularly Reflecting Surfaces—Application to Cylindrical and Conical Cavities*, **Journal of Heat Transfer**, Vol. C87, 1965, pp. 299-307.

14. Plamondon, J. A., and T. E. Horton, *On the Determination of the View Function to the Images of a Surface in a Non Planar Specular Reflector*, **International Journal of Heat and Mass Transfer**, Vol. 10, 1967, pp. 665-679.

15. Rabl, A., *Radiation Transfer Through Specular Passages—A simple Approximation*, **International Journal of Heat and Mass Transfer**, Vol. 20, 1977, pp. 323-330.

16. Mahan, J. R., J. B. Kingsolver, and D. T. Mears, *Analysis of Diffuse-Specular Axisymmetric Surfaces With Application to Parabolic Reflectors*, **Journal of Heat Transfer**, Vol. C101, No. 4, November 1979, pp. 689-694.

17. Masuda, H., *Analysis of Radiation Heat Transmission on Specularly and Diffusely Reflecting Curved Surfaces*, **Reports of Institute of High Speed Mechanics**, Tohoku University, Vol. 42, 1980, pp. 59-78.

18. Bobco, R. P., *Radiation Heat Transfer in Semigray Enclosures with Specularly and Diffusely Reflecting Surfaces*, **Journal of Heat Transfer**, Vol. C86, 1964, pp. 123-130.

19. Bevans, T. J., and D. K. Edwards, *Radiation Exchange in an Enclosure with Directional Wall Properties*, **Journal of Heat Transfer**, Vol. C87, 1965, pp. 388-396.

20. Hammersley, J. M., and D. C. Handscomb, **Monte Carlo Methods**, Chapman and Hall, London England, 1979.

21. Howell, J. R., and M. Perlmutter, *Monte Carlo Solution of Thermal Transfer Through Radiant Media Between Gray Surfaces*, **Journal of Heat Transfer**, Vol. C86, 1964, pp. 116-122.

22. Corlett, R. C., *Direct Monte Carlo Calculation of Radiative Heat Transfer in Vacuum*, **Journal of Heat Transfer**, Vol. C88, 1966, pp. 376-382.

23. Mahan, J. R., F. Kowsary, N. Tira, and B. D. Gardiner, *Transient Conduction-Radiation Analysis of an Absolute Cavity Radiometer Using Finite Elements*, **International Symposium on Thermal Problems in Space-Based Systems**, ASME Winter Annual Meeting, Boston, Mass., December 1987, HTD-VOL83, PP. 39-48.

24. Mahan, J. R., and L. D. Eskin, *Application of the Monte Carlo Technique to Transient Thermal Modeling of Cavity Radiometers Having Diffuse-Specular Surfaces*, **Proceedings of the Fourth Conference on Atmospheric Radiation**, Toronto, Ontario, Canada, June 16-18, 1981.

25. Mahan, J. R., and L. D. Eskin, *The Radiation Distribution Factor—Its Calculation Using Monte Carlo Techniques and an Example of Its Application*, **Proceedings of First UK National Conference on Heat Transfer**, Leeds, England, July 3-5, 1984, pp. 1001-1012.

26. Toor, J. S., and R. Vistanka, *A Numerical Experiment of Radiant Heat Transfer by the Monte Carlo Method*, **International Journal of Heat and Mass Transfer**, Vol. 11, 1968, pp. 883-897.

27. Naraghi, M. H. N., and B. T. F. Chung, *A Stochastic Approach for Radiative Exchange in Enclosures with Nonparticipating Medium*, **Journal of Heat Transfer**, Vol. C106, November 1984, pp. 690-670.

28. Gouffé, A., *Aperture Correction for Artificial Blackbodies, Taking Account of Multiple Reflections*, **Revue d' Optique (Théorique et Instrumentale)**, Vol. 24, 1946, pp. 1-10, As Reviewed by Williams, C. S., *Discussion of the Theories of Cavity-Type Sources of Radiant Energy*, **Journal of the Optical Society of America**, Vol. 51, No. 5, 1961, pp. 564-571.

29. De Vos, J. C., *Evaluation of the Quality of a Blackbody*, **Physica**, Vol. 20, 1954, pp. 669-689.

30. Buckley, H., *Radiation From Interior of a Reflecting Cylinder*, **Philosophical Magazine**, Vol. 4, 1927, pp. 753-762.

31. Buckley, H., *Radiation From Inside a Circular Cylinder*, **Philosophical Magazine**, Vol. 6, 1928, pp. 447-457.

32. Buckley, H., *Radiation From the Inside of a Circular Cylinder*, **Philosophical Magazine**, Vol. 17, 1934, pp. 576-581.

33. Sparrow, E. M., and L. U. Albers, *Apparent Emissivity and Heat Transfer in a Long Cylindrical Hole*, **Journal of Heat Transfer**, Vol. C82, 1960, pp. 253-255.

34. Sparrow, E. M., L. U. Albers, and E. R. G. Eckert, *Thermal Radiation Characteristics of Cylindrical Enclosures* , **Journal of Heat Transfer**, Vol. C84, 1962, pp. 73-81.

35. Peavy, B. A., *A Note on the Numerical Evaluation of Thermal Radiation Characteristics of Diffuse Cylindrical and Conical Cavities*, **Journal of Research of the National Bureau of Standards**, Vol. 70c, No.2, 1966, pp.139-147.

36. Quinn, T. J., *The Calculation of the Emissivity of Cylindrical Cavities Giving Near Blackbody Radiation*, **British Journal of Applied Physics**, Vol. 18, 1967, pp. 1105-1113.

37. Vollmer, J., *Study of the Effective Thermal Emittance of Cylindrical Cavities*, **Journal of the Optical Society of America**, Vol. 47, No. 10, 1957, pp. 926-932.

38. Krishnan, K. S., *Effect of Specular Reflexions [sic] on the Radiation Flux from a Heated Tube*, **Nature**, Vol. 187, 1960, p. 135.

39. Berman, R., F. E. Simon, and J. M. Ziman, *The Thermal Conductivity of Diamond at Low Temperatures* , **Proceedings of Royal Society**, Vol. 220A, 1953, P. 176..

40. Krishnan, K. S., *Effect of Specular Reflexions [sic] on the Radiation Flux from a Heated Tube*, **Nature**, Vol. 188, 1960, p. 652.

41. Sparrow, E. M., and S. L. Lin, *Radiation Heat Transfer at a Surface Having Both Specular and Diffuse Reflective Components*, **International Journal of Heat and Mass Transfer**, Vol. 8, 1965, pp. 769-778.

42. Williams, C. S., *Specularly vs Diffusely Reflecting Walls for Cavity Type Sources of Radiant Energy*, **Journal of the Optical Society of America**, Vol. 59, No. 3, 1969, pp. 249-252.

43. Fussel, W. B., *Normal Emissivity of an Isothermal, Diffusely Reflecting Cavity (with Top) As a Function of Inside Radius*, **Journal of Research of the National Bureau of Standards**, Vol. A76, 1972, pp. 347-349.

44. Alfano, G. *Apparent Thermal Emittance of Cylindrical Enclosures With and Without Diaphragms*, **International Journal of Heat and Mass Transfer**, Vol. 15, 1972, pp. 2671-2674.

45. Sparrow, E. M., R. P. Heinisch, and N. Shamsundar, *Apparent Hemispherical Emittance of Baffled Cylindrical Cavities*, **Journal of Heat Transfer**, Vol. C96, 1974, pp. 112-114.

46. Sparrow, E. M., and R. P. Heinisch, *The Normal Emittance of Circular Cylindrical Cavities*, **Applied Optics**, Vol. 9, No. 11, 1970, pp. 2569-2572.

47. Alfano, G., and A. Sarno, *Normal and Hemispherical Thermal Emittance of Cylindrical Cavities*, **Journal of Heat Transfer**, Vol. C97, 1975, pp. 387-390.

48. Lin, S. H., and E. M. Sparrow, *Absorption Characteristics of a Specularly Reflecting Cylindrical Cavity Irradiated by an Obliquely Inclined Ray Bundle*, **Applied Optics**, Vol. 4, No. 3, 1965, pp. 277-283.

49. Sparrow, E. M., and V. K. Jonsson, *Radiant Emission Characteristics of Diffuse Conical Cavities*, **Journal of Optical Society of America**, Vol. 53, 1963, pp. 816-821.

50. Shirely, J. H., and J. H. Eberly, *Local Effective Emissivity of Conical Cavities*, **Applied Optics**, Vol. 18, No. 22, 1979, pp. 3810-3814.

51. Heinisch R. P., E. M. Sparrow, and M. Shamsundar, *Radiant Emission from Baffled Conical Cavities*, **Journal of Optical Society of America**, Vol. 63, No. 2, 1973, pp. 152-158.

52. Yoshika, O., *Numerical Calculation of Effective Emissivities of Diffuse Cones with a Series Technique*, **Applied Optics**, Vol. 20, No. 19, 1981, pp. 3332-3335.

53. Polgar, L. G., and J. R. Howell, **Directional Thermal-Radiative Properties of Conical Cavities**, NASA Technical Note D-2904, 1965.

54. Sparrow, E. M., and V. K. Jonsson, **Absorption and Emission Characteristics of Diffuse Spherical Enclosures**, NASA Technical Note D-1289, 1962.

55. Jenssen, H. H., *Some Notes on Heat Transfer by Radiation*, **Det Kgl. Danske Videnskalers Salskal Matematisk-fysike Meddelelser**, Vol. 24, No. 8, 1948, p. 16, as cited by Reference 1 page 271.

56. Fectau, M. L., *The Emissivity of Diffuse Spherical Cavities* , **Applied Optics**, Vol. 7, No. 7, 1968, pp. 1363-1364.

57. Edwards, D. E., University of Michigan Research Institute Report, No. 2144-105-T, 1956, as cited by Reference 58.

58. Campanaro, P., and T. J. Ricolfi, *Effective Emissivity of a Spherical Cavity*, **Applied Optics**, Vol. 5, No. 6, 1966, pp. 929-932.

59. Safwatt, H. H., *Absorption of Thermal Radiation in a Hemispherical Cavity*, **Journal of Heat Transfer**, Vol. C92, 1970, pp. 198-201.

60. Sparrow, E. M., and V. K. Jonsson, *Thermal Radiation Absorbtion in Rectangular-Groove Cavities*, **Journal of Applied Mechanics**, Vol. E30, 1963, PP. 237-244.

61. Sparrow, E. M., and V. K. Jonsson, *Absorption of Thermal Radiation in V-Groove Cavities*, **International Journal of Heat and Mass Transfer**, Vol. 5, 1962, pp. 1111-1115.

62. Sparrow, E. M., *Radiant Absorption Characteristics of Concave Cylindrical Cavities*, **Journal of Heat Transfer**, Vol. C84, 1962, pp. 283-293.

63. Howell, J. R., and M. Perlmutter, **Directional Behavior of Emitted and Reflected Radiant Energy From a Specular Gray, Asymmetric Groove**, NASA Technical Note D-1874, 1963.

64. Kanayama, K., *Apparent Directional Emittances of V-Groove and Circular-Groove Rough Surfaces*, **Heat Trsnsfer—Japanese Research**, Vol. 1, No. 1, 1972, pp. 11-21.

65. Perlmutter, M., and J. R. Howell, *A Strongly Directional Emitting and Absorbing Surface*, **Journal of Heat Transfer**, Vol. C85, 1963, pp. 282-283.

66. Black, W. Z., and R. J. Schoenhals, *A Study of Directional Radiation Properties of Specially Prepared V-Groove Cavities*, **Journal of Heat Transfer**, Vol. C90, 1968, pp. 420-428.

67. Black, W. Z., *Optimization of the Directional Emission from V-Groove and Rectangular Cavities*, **Journal of Heat Transfer**, Vol. C95, 1973, pp. 31-36.

68. Kholopov, G. K., *On the Emissivity of a Circular, Tubular Mirror Cavity with a Slit Aperture*, **Heat Transfer—Soviet Research**, Vol.5, No. 2, 1973, pp. 51-54.

69. Gerald, C. F., and P. O. Weatley, **Applied Numerical Analysis** , 3rd Edition, Addison Wesley, Reading Massachusetts, 1984.

70. Eskin, L. D., *Application of the Monte Carlo Method to the Transient Thermal Modeling of a Diffuse-Specular Radiometer Cavity*, M.S. Thesis, Department of Mechanical Engineering, Virginia Polytechnic Institute & State University, Blacksburg, Va, 1981.

Appendix A. Monte Carlo Implementation

In this Appendix the important steps implemented in the Monte Carlo programs which evaluate the apparent emissivity of a diffuse-specular, spherical cavity and the directional absorptivity of a purely specular, spherical cavity are discussed. The listing for these computer programs are shown in Appendix B (the program MCVTY for the apparent emissivity and the program MPRS for the directional apparent absorptivity calculations). The procedures for evaluating the distribution factors are similar to those used by Eskin [70].

A.1 Apparent Emissivity

The apparent emissivity of a cavity can be obtained by using *distribution factors.* In an enclosure whose surface has been divided into N elements, the distribution factor D_{ij} is defined as the fraction of the radiative energy emitted diffusely by the i^{th} element which is absorbed by the j^{th}, element due both to direct radiation and to all possible diffuse or

specular reflections. Based on this definition for the distribution factor, the radiative energy which escapes through the opening A_o of an isothermal cavity is simply given by

$$Q_{\text{escaped}} = \sum_{j=1}^{N} \varepsilon \, \sigma \, A_j \, T^4 \, D_{jo} \, , \tag{A.1}$$

where, ε is the surface emissivity , D_{jo} is the distribution factor from the j^{th} surface element to the cavity opening A_o, and A_j is the area of the element j. The apparent emissivity is, therefore, given by

$$\varepsilon_a = \frac{1}{A_o} \sum_{j=1}^{N} \varepsilon \, A_j \, D_{jo} \, . \tag{A.2}$$

For evaluation of the distribution factors D_{jo} the spherical cavity is first divided into N equal-area ring elements. In a spherical cavity this can be accomplished by dividing the z-axis into N equal-length divisions. The following steps may then be taken to determine the distribution factors D_{ij}.

Step 1. Selection of the point of emission

The point of emission for the *energy bundle* is selected randomly from the points within the j^{th} element. Because of symmetry, it is sufficient to make this selection only from the points of an arbitrary longitudinal line passing through the j^{th} element. The z-coordinate of the emission point can then be obtained from

$$z_e = z_a + R_e (z_b - z_a) \, . \tag{A.3}$$

In Eq. (A.3) z_a and z_b are, respectively, the z -coordinates corresponding to the lower and upper limits of the j^{th} element (see Fig. 59), and R_e is a random number, obtained from a random number generator. The x- and y-coordinates of the emission point are then

obtained easily by knowing the azimuthal angle ϕ (which, as mentioned previously, is selected arbitrarily).

Step 2. Selecting a direction for diffuse emission or reflection

In most situations the direction of emission (or diffuse reflection), indicated by an azimuthal angle ϕ and a zenith angle θ with respect to a local spherical coordinate system whose origin is at the point of emission (or reflection), is obtained by selecting two random numbers R_θ and R_ϕ and then using

$$\theta = \sin^{-1}\sqrt{R_\theta} \tag{A.4}$$

and

$$\phi = \frac{R_\phi}{2\pi} \ . \tag{A.5}$$

The justification for Eq. (A.4) is given in Reference 20. Of course, the direction thus obtained must then be converted into the global coordinates defined for the problem by following, normally, a complicated process. For the case of a sphere, however, there is no need for obtaining a direction for emission. This is because for diffuse emission, an emitted energy bundle can strike all points on the sphere with equal probability. Therefore, it is sufficient to select a point on the sphere randomly as the next point of incidence.

Step 3. Determination of the point of incidence

In cases of diffuse emission and diffuse reflection the point of incidence is already determined from Step 2. For the case of specular reflection the x,y,z- coordinates of the $n+1^{st}$ reflection point, S_{n+1} in Fig. 59, can be obtained by solving simultaneously the following three equations which are based on the laws of specular reflection:

1. the equation which is derived from the fact that the angle of incidence and the angle of reflection are equal;

$$\overline{S_n S_{n+1}} \cdot \overline{S_n O} = \overline{S_n S_{n-1}} \cdot \overline{S_n O} \ , \qquad (A.6)$$

where $\overline{S_n O}$ is the vector representing the surface normal at the n^{th} reflection point, S_n, and $\cdot$ indicates the dot product between two vectors.

2. the equation describing the plane in which the reflection occurs. This plane, as mentioned in Section 3.2.1, is identical for all reflections of a ray bundle in a spherical enclosure. Thus, it is easy to show that the equation for the plane of reflection (for all reflections of a given ray bundle) is given by

$$x - \frac{x_0 z_1 - x_1 z_0}{y_0 z_1 - y_1 z_0} y - \frac{x_1 y_0 - x_0 y_1}{y_0 z_1 - y_1 z_0} z = 0 , \qquad (A.7)$$

where (x_0 , y_0 , z_0) and (x_1 , y_1 , z_1) are coordinates of the point of emission and the first point of incidence, respectively.

3. the equation for the surface of a unit sphere;

$$x^2 + y^2 + z^2 = 1 \ . \qquad (A.8)$$

Once the coordinates of the $n+1^{st}$ point of incidence is determined, if it is within the range of the cavity opening, a variable n_{j_e}, which represents the number of energy bundles emitted from surface element j which escape from the sphere, is incremented and the next energy bundle is released by restarting the procedure from Step 1.

Step 4. Determining whether reflection occurs

A random number R_α is obtained at each incidence. If $R_\alpha \geq \alpha$, where α is the absorptivity of the surface, then the energy bundle is reflected from the surface, and the next step is followed. If the energy bundle is absorbed, then the next energy bundle is released by starting over from Step 1.

Step 5. Determining whether reflection is diffuse or specular

A random number, R_r is obtained. If $R_r > \frac{\rho^s}{\rho^s + \rho^d}$, then the reflection is diffuse; otherwise the reflection is specular. If the reflection is diffuse, the direction of reflection can be obtained by repeating Step 2. If the reflection is specular, the next incident point is obtained by repeating Step 3.

The above procedure is followed for a prescribed large number of energy bundles n_j. The distribution factor D_{j_o} is then given by the ratio $\frac{n_{j_o}}{n_j}$.

A.2. Directional Apparent Absorptivity

The apparent absorptivity is defined as the ratio of the energy absorbed by the cavity to that which enters the cavity through its opening. In this case the Monte Carlo method can be used to simulate parallel radiation entering the cavity from a given direction by a large number of energy bundles released from randomly selected positions within an imaginary surface stretched across the cavity opening. The initial direction of the energy bundles is the same as the direction of the incident parallel radiation. The subsequent history of each energy bundle can be determined by following Steps 3 through 5 in the previous section. The directional apparent absorptivity is then simply obtained by forming the ratio of the energy bundles that have been absorbed (total number of the energy bundles released minus energy bundles that escaped), to the total number of the energy bundles released.

Appendix B. Program Listings

```
**************************    CVTY    ***********************************
*                                                                        *
*  This program calculates the distribution of local irradiance in       *
*  an isothermal spherical cavity having completely or partially         *
*  specular walls.  For the case of partially specular walls the         *
*  problem is one of solving an integral equation ( Eq. (3.42)) by       *
*  iterations, while for the case of purely specular walls the           *
*  distribution is obtained by numerical integration.  For the case      *
*  of purely specular walls the flag IS must be given the value          *
*  1 while for the case of partially specular walls this flag            *
*  must be given the value 0.  In the latter case, however, the          *
*  program must initially be run with IS=1 to calculate the constant     *
*  term in the integral equation.                                        *
*                                                                        *
*  Variables:                                                            *
*              A           Lower limit of integration in PHI direction  *
*              B           Upper limit of integration in PHI direction  *
*              C(.)        Array of the constant terms in the integral  *
*                          equation                                     *
*              EM          Surface emissivity                           *
*              H(.)        Array of the irradiance at mesh points,      *
*                          dimensioned at least by NN+1                 *
*              HO(.)       Array of the irradiance at mesh points from  *
*                          previous iteration                           *
*              IS          A flag to indicate that cavity wall is       *
*                          perfectly specular (IS=1) or                 *
*                          diffuse-specular (IS=0).                     *
*              ITER        Iteration counter                            *
*              NFUNC       Gives the number of functional evaluation    *
*              NN          Number of mesh points minus 1                *
*              NTRM        Maximum number of reflections considered     *
*              PHIC1       The azimuthal angle above which circle of    *
*                          reflection does not intersect the opening    *
*              PHIC2       The azimuthal angle below which circle of    *
*                          reflection does not intersect the opening    *
*              RD          Approximate angular spacing                  *
*                          between the mesh points                      *
*              RFR         Reflectivity ratio                           *
*              RO          Surface reflectivity                         *
*              ROD         Diffuse component of the reflectivity        *
*              ROS         Specular component of the reflectivity       *
*              SID         Opening angle (deg)                          *
*              TETA(.)     Array of the zenith angle of mesh points,    *
*                          dimensioned at least by NN+1                 *
*              TOL1        Tolerance to terminate Romberg integration   *
*              TOL2        Tolerance to terminate the iterations        *
*                                                                       *
*************************************************************************
*
      IMPLICIT REAL*8 (A-H,O-Z)
      DIMENSION H(81),HO(81),C(81),TETA(81)
      COMMON/BLK1/ALF,SI,ROS
      COMMON/BLK2/NTRM,NFUNC,IS
      COMMON/BLK4/H,TETA
      EXTERNAL EF,EF2
*
      PI = DACOS(-1.0D0)
      PI32 = 3.0D0*PI/2.0D0
      PI12 = PI/2.0D0
      NFUNC = 0
      TOL1 = 1.0D-5
      TOL2 = 1.0D-3
      RD = 3.0D0
**                                                                      **
*  Input the opening angle and surface properies                        *
**                                                                      **
      WRITE(5,*) 'Enter 1 for purely specular calculations or'
```

```
      WRITE(5,*) '0 for diffuse-specular calculations:'
      READ(6,*) IS
      WRITE(5,*) 'Enter the opening angle (degrees):'
      READ(6,*) SID
      WRITE(5,*) 'Enter the reflectivity:'
      READ(6,*) RO
      WRITE(5,*) 'Enter the reflectivity ratio:'
      READ(6,*) RFR
*
      EM = 1.0D0-RO
      ROS = RFR*RO
      ROD = RO-ROS
      SI = SID*PI/180.0D0
      RDR = RD*PI/180.0D0
      NN = INT((PI-SI)/RDR)+1
      RDV = (PI-SI)/DFLOAT(NN)
      NTRM = INT(DLOG(0.001D0)/DLOG(ROS))+1
      ITER = 0
**                                                                    **
* Read the array of constants, C(.) for the diffuse-specular case.     *
* Also for initial guess let H(.) and HO(.)=C(.).  The array C(.)      *
* can be evaluated by running this program with IS=1                   *
* with the same surface parameters.                                    *
**                                                                    **
      IF(IS.NE.1) THEN
      open (82)
      DO 100 I=1,NN+1
      READ(82,*) TETAD,C(I)
      TETA(I) = TETAD*PI/180.0D0
      H(I) = C(I)
 100  HO(I) =  C(I)
      END IF
**                                                                    **
* Begin Iterations                                                     *
**                                                                    **
 2000 ITER = ITER+1
      IF(IS.NE.1) WRITE(6,*) 'ITER=',ITER
**                                                                    **
* Do-loop over all the mesh points                                     *
**                                                                    **
      DO 1000 J=1,NN+1
      TETA(J) = SI+DFLOAT(J-1)*RDV+0.000001D0
      ALF = TETA(J)
      ALFD = ALF*180.0D0/PI
*
      CPHID=ALFD+SID
      IF(CPHID.LT.180.0D0) THEN
**                                                                    **
* In this case the domain of integration is divided into three regions*
* within each of which the integrand is a smooth function.             *
**                                                                    **
      RAD = DCOS(SI)**2-DCOS(ALF)**2
      OOO = DSQRT(RAD)/DSIN(ALF)
      PHIC1 = PI-DASIN(OOO)
      PHIC2 = 2.0D0*PI-PHIC1
      A = PI12
      B = PHIC1-.000000001D0
      CALL ROMB(EF,A,B,TOL1,RESULT)
      IF(IS.EQ.1) THEN
      RESULT = RESULT+(PHIC2-PHIC1)/((1.0d0-ROS)*2.0D0*PI)
      GOTO 19
      END IF
      A = PHIC1+0.000000001D0
      B = PHIC2-0.000000001D0
      CALL ROMB(EF2,A,B,TOL1,RESULTP)
      RESULT = RESULT+RESULTP
 19   A = PHIC2+0.000000001D0
```

```
      B = PI32
      CALL ROMB(EF,A,B,TOL1,RESULTP)
      RESULT = RESULT+RESULTP
      ELSE
C**                                                                  **C
C* In this case there is no need in dividing the domain of integration *C
C* into regions since the integrand is a smooth function throughout    *C
C* the region of interest.                                            *C
C**                                                                  **C
      A = PI12
      B = PI32
      CALL ROMB(EF,A,B,TOL1,RESULT)
      END IF
      RESULT = 2.0D0*RESULT
C
      IF(IS.EQ.1) THEN
      H(J) = EM*RESULT
      Else
      H(J) = C(J)+ROD*RESULT
      end if
      TETAD = TETA(J)*180.0D0/PI
 1000 CONTINUE
      IF (IS.EQ.1) GOTO 1550
C**                                                                  **C
C*  Check for convergence                                           *  C
C**                                                                  **C
      SUME = 0.0D0
      DO 1500 I=1,NN+1
      SUME = SUME+(H(I)-HO(I))**2
 1500 HO(I) = H(I)
      SUME = DSQRT(SUME)
C**                                                                  **C
C*  If convergence has not occurred continue iterations            *  C
C**                                                                  **C
      IF(SUME.GT.TOL2) GOTO 2000
 1550 CONTINUE
      close (82)
      open (82)
C**                                                                  **C
C* Write out the results                                           *  C
C**                                                                  **C
      DO 1600 I = 1,NN+1
      TETAD = TETA(I)*180.0D0/PI
 1600 WRITE(82,*) TETAD,H(I)
C
      WRITE(6,*) NFUNC
C
      STOP
      END
C                                                                    *C
C*************************    EF    ***********************************C
C                                                                     *C
C This function subroutine performs the inside integration either    *C
C numerically (diffuse-specular case) or in closed form              *C
C (purely specular).  All calculations are performed within the      *C
C domain of the circle of reflection.                                *C
C                                                                    *C
C Variables:                                                         *C
C          A(.)      Array of the lower limit polar angles of       *C
C                    subareas making up the fictitious area         *C
C                    (collection 'w' in Section 3.2.3.), dimensioned*C
C                    at least by NTRM*(NTRM+1)/2.                   *C
C          B(.)      Array of the upper limit polar angles of       *C
C                    subareas making up the fictitious area         *C
C                    (collection 'w' in Section 3.2.3.), dimensioned*C
C                    at least by NTRM*(NTRM+1)/2.                   *C
C          HL(.)     Array of the lower limit polar angles of       *C
```

```
C                    subareas within the collection 'u' defined in    C
C                    section 3.2.3., dimensioned at least by          C
C                    NTRM*(NTRM+1)/2.                                 C
C          HU(.)     Array of the upper limit polar angles of         C
C                    subareas within the collection 'u' defined in    C
C                    section 3.2.3., dimensioned at least by          C
C                    NTRM*(NTRM+1)/2.                                 C
C          IMAX      Number of subareas in collection 'w'.            C
C          JMAX      Number of subareas in collection 'u'.            C
C          IR        Gives the nubmer of disjointed circular arcs     C
C                    obtained by intersecting a longitudinal line     C
C                    with the cavity area.  It has either the value   C
C                    of 1 or 2.                                       C
C          N         Number of reflections                            C
C          K         Represents a sequence of reflections             C
C          SI1       The lower limit polar angle of the circular arc  C
C                    which represents the opening.                    C
C          SI2       The upper limit polar angle of the circular arc  C
C                    which represents the opening.                    C
C          TA1       Lower limit of the receiving element             C
C          TA2       Upper limit of the receiving element             C
C          T1K       Lower limit of the fictitious area assuming thereC
C                    is no opening                                    C
C          T2K       Upper limit of the fictitious area assuming thereC
C                    is no opening                                    C
C                                                                     C
CCCCCCCCCCCCCCCCCCCCCCCCCCCCCCCCCCCCCCCCCCCCCCCCCCCCCCCCCCCCCCCCCCCCCC
C

      FUNCTION EF(PHI)
C
      IMPLICIT REAL*8 (A-H,O-Z)
      DIMENSION HL(5000),HU(5000),S1(0:90),S2(0:90),A(5000),B(5000)
      COMMON/BLK1/ALF,SI,ROS
      COMMON/BLK2/NTRM,NFUNC,IS
      COMMON/BLK3/XPHI,N,K
      EXTERNAL F
C
      TOL = 1.0D-3
C
      XPHI = PHI
      PI =DACOS(-1.0D0)
CC                                                                    CC
C* Find the polar angles for the limits of the opening.               *C
CC                                                                    CC
      CALL TETLMT(SI,ALF,PHI,SI1,SI2)
C
      IR = 1
      IF(SI2.LT.PI) IR=2
      EF = 0.0D0
CC                                                                    CC
C* Do-loop over the number of regions IR.                             *C
CC                                                                    CC
      DO 200 IJ = 1,IR
CC                                                                    CC
C* Assign the correct values for TA1 and TA2.                         *C
CC                                                                    CC
      TA1 = 0.0D0
      TA2 = PI
      IF(IJ.EQ.1.AND.SI1.LT.PI) TA2 = SI1
      IF(IJ.EQ.2) TA1 = SI2
C
      EFCT = 0.0D0
CC                                                                    CC
C* For the zeroth reflection the collection 'u' consists only of the  *C
C* circular arc defined by SI1 and SI2.                               *C
CC                                                                    CC
```

```
      HU(1) = SI2
      HL(1) = SI1
      JMAX = 1
**                                                                    **
* Do-loop over all reflections                                       *
**                                                                    **
      DO 100 N=0,NTRM
      J = 1
      SBSUM = 0.0D0
**                                                                    **
* Do-loop over all sequence of reflections                           *
**                                                                    **
      DO 10 K=0,N
**                                                                    **
* Start the logical operations to obtain the collection 'w' (Eq. 3.35)*
**                                                                    **
       T1K = (TA1+PI*DFLOAT(2*K))/DFLOAT(N+1)
       T2K = (TA2+PI*DFLOAT(2*K))/DFLOAT(N+1)
       A(1) = T1K
       B(1) = T2K
       IMAX =1
       IF(N.EQ.0) GOTO 31
 15    IF(HU(J).LE.T1K) THEN
       J = J+1
       IF(J.GT.JMAX) GOTO 31
       GOTO 15
       ELSEIF(HL(J).LE.T1K) THEN
       IF(HU(J).GE.T2K) GOTO 9
       I=1
       A(I) = HU(J)
       J=J+1
       IF(J.GT.JMAX) GOTO 30
       GOTO 20
       ELSEIF(HL(J).GT.T1K) THEN
       IF(HL(J).GE.T2K) GOTO 31
       I=1
       A(I) = T1K
       GOTO 21
       END IF
 20    IF(HL(J).GE.T2K) GOTO 30
 21    B(I) = HL(J)
       IF(HU(J).LT.T2K) THEN
        I = I+1
        A(I) = HU(J)
        J = J+1
        IMAX = I
        IF(J.GT.JMAX) GOTO 30
        GOTO 20
       ELSE
        IMAX = I
        GOTO 31
       END IF
 30    B(I) = T2K
 31    CONTINUE
**                                                                    **
* Integrate over all subareas of collection 'w'                      *
**                                                                    **
       IF(IS.EQ.1) THEN
       DO 41 I=1,IMAX
       SBSUM = SBSUM+DABS(DCOS(B(I))-DCOS(A(I)))
 41    CONTINUE
       ELSE
       DO 42 I=1,IMAX
       AA = A(I)*DFLOAT(N+1)-DFLOAT(2*K)*PI
       BB = B(I)*DFLOAT(N+1)-DFLOAT(2*K)*PI
       CALL ROMBP(F,AA,BB,TOL,RESULT)
       SBSUM = SBSUM+RESULT
```

```
 42     CONTINUE
        END IF
*
 9      S2(K) = (PI*DFLOAT(2*K)+SI2)/DFLOAT(N+1)
 10     S1(K) = (PI*DFLOAT(2*K)+SI1)/DFLOAT(N+1)
*
        IF(IS.NE.1) SBSUM=SBSUM*ROS**N/DFLOAT(N+1)
        IF(IS.EQ.1) SBSUM=SBSUM*ROS**N
        EFCT= EFCT+SBSUM
**                                                                    **
* Start the logical operations to determine the collection 'u'.       *
* (See Eq. 3.36)                                                     *
**                                                                    **
        IF(N.EQ.0) GOTO 100
        J = 1
        IF(S2(0).LT.HL(1)) THEN
        DO 50 I=2,JMAX+1
        II = JMAX+3-I
        HU(II) = HU(II-1)
 50     HL(II) = HL(II-1)
        HU(1) = S2(0)
        HL(1) = S1(0)
        JMAX = JMAX+1
        J = J+1
        ELSE
        HL(1) = S1(0)
        END IF
        K = 1
 60     IF(K.EQ.N) GOTO 104
 101    IF(S2(K).LT.HU(J)) GOTO 102
        J = J+1
        GOTO 101
 102    IF(S1(K).GT.HL(J)) THEN
        K=K+1
        GOTO 60
        END IF
        IF(S2(K).GT.HL(J).AND.S1(K).GT.HU(J-1)) THEN
        HL(J) = S1(K)
        K = K+1
        GOTO 60
        END IF
        IF(S2(K).GT.HL(J).AND.S1(K).LT.HU(J-1)) THEN
        HU(J-1) = HU(J)
        DO 105 I=J,JMAX-1
        HU(I) = HU(I+1)
 105    HL(I) = HL(I+1)
        JMAX = JMAX-1
        J = J-1
        K = K+1
        GOTO 60
        END IF
        IF(S1(K).GT.HU(J-1)) THEN
        DO 106 I=J+1,JMAX+1
        II = JMAX+J+2-I
        HU(II) = HU(II-1)
 106    HL(II) = HL(II-1)
        HU(J) = S2(K)
        HL(J) = S1(K)
        JMAX = JMAX+1
        J = J+1
        K = K+1
        GOTO 60
        ELSE
        HU(J-1) = S2(K)
        K = K+1
        GOTO 60
        END IF
```

```
 104     IF(S1(N).GT.HU(JMAX)) THEN
         HU(JMAX+1) = S2(N)
         HL(JMAX+1) = S1(N)
         JMAX = JMAX+1
         ELSE
         HU(JMAX) = S2(N)
         END IF
 100     CONTINUE
*
        EF = EF+EFCT
 200    CONTINUE
 210    EF = EF/(4.0D0*PI)
        NFUNC=NFUNC+1
        RETURN
        END
*                                                                      *
*************************    EF2    ***********************************
*                                                                      *
* This function subroutine evaluates the inside integration when the   *
* circle of reflection does not intersect the opening.                 *
*                                                                      *
************************************************************************
*                                                                      *
        FUNCTION EF2(PHI)
*
        IMPLICIT REAL*8 (A-H,O-Z)
        COMMON/BLK1/ALF,SI,ROS
        COMMON/BLK2/NTRM,NFUNC,IS
        COMMON/BLK3/XPHI,N,K
        EXTERNAL F
*
        TOL = 1.0D-3
*
        XPHI = PHI
        PI =DACOS(-1.0D0)
*
        EF2 = 0.0D0
        TA1 = 0.0D0
        TA2 = PI
        DO 100 N=0,NTRM
        DO 100 K=0,N
         CALL ROMBP(F,TA1,TA2,TOL,RESULT)
         EF2 = EF2+ROS**N/DFLOAT(N+1)*RESULT
 100     CONTINUE
        EF2 = EF2/(4.0D0*PI)
        NFUNC=NFUNC+1
        RETURN
        END
*                                                                      *
*************************    F    ************************************
*                                                                      *
* This function subroutine evaluates the local irradiance at a         *
* desired location by interpolating irradiances of the two nearest     *
* mesh points.                                                         *
*                                                                      *
************************************************************************
*                                                                      *
        FUNCTION F(TET)
        IMPLICIT REAL*8 (A-H,O-Z)
        DIMENSION H(81),TETA(81)
        COMMON/BLK1/ALF,SI,ROS
        COMMON/BLK3/XPHI,N,K
        COMMON/BLK4/H,TETA
*
        PI = DACOS(-1.0D0)
        PHI = XPHI
**                                                                    **
```

```
*  Obtain the zenith angle of the global coordinate system from the    *
*  coordinates of the source-oriented coordinate system.               *
**                                                                     **
      TETAA = DACOS(DCOS(ALF)*DCOS(TET)+DSIN(ALF)*DSIN(TET)*DSIN(PHI))
*
      I = 2
 1000 IF(TETAA.LT.TETA(I)) THEN
      HR = H(I)+(H(I-1)-H(I))*((TETA(I)-TETAA)/(TETA(I)-TETA(I-1)))
      F = HR*DABS(DSIN((DFLOAT(2*K)*PI+TET)/DFLOAT(N+1)))
      ELSE
      I = I+1
      GOTO 1000
      END IF
      RETURN
      END
*                                                                      *
*************************  TETLMT  ************************************
*                                                                      *
*  This subroutine evaluates polar angles of the intersection of a     *
*  given circle of refelection with the cavity opening.  Calculations  *
*  are based on Eq. (3.41).                                            *
*                                                                      *
************************************************************************
*                                                                      *
      SUBROUTINE TETLMT(SI,ALF,PHI,TA1,TA2)
      IMPLICIT REAL*8 (A-H,O-Z)
*
      PI = DACOS(-1.0D0)
      PIT2 = 2.0D0*PI
*
      A = 1.0D0
      IF(PHI.LT.1.0D-6) PHI = 0.0D0
      B = DTAN(ALF)*DSIN(PHI)
      C = DCOS(SI)/DCOS(ALF)
      DD = DSQRT(A*A+B*B)
      IF(B.EQ.0.0D0) THEN
      GAM = DACOS(A/DD)
      GOTO 10
      END IF
      GAM = PI+(DABS(B)/B)*(DACOS(A/DD)-PI)
 10   AA = C/DD
      IF(AA.GT.1.0D0.OR.AA.LT.-1.0D0) WRITE(6,*) 'SMTG WRONG IN TETLMT'
      TTA1 = (GAM+DACOS(AA))
      TTA2 = (GAM - DACOS(AA))
      IF(TTA1.GE.PIT2) TTA1=TTA1-PIT2
      IF(TTA1.LT.0.0D0) TTA1=TTA1+PIT2
      IF(TTA2.GE.PIT2) TTA2=TTA2-PIT2
      IF(TTA2.LT.0.0D0) TTA2=TTA2+PIT2
      TA1 = DMIN1(TTA1,TTA2)
      TA2 = DMAX1(TTA1,TTA2)
      RETURN
      END
```

```
C*********************************** PRS ***********************************
C                                                                           *
C This program evaluates the directional apparent absorptivity of a         *
C spherical cavity having purely specular walls for a given                 *
C cavity opening angle, wall reflectivity, and several directions of        *
C incidence ranging from 0 to 90 deg.                                       *
C                                                                           *
C Variables:                                                                *
C           A           Lower limit of integration in PHI direction       *
C           B           Upper limit of integration in PHI direction       *
C           RO          Wall reflectivity                                 *
C           SID         Cavity opening angle (deg)                        *
C           EAR         Dimensionless radiative energy incident on the    *
C                       cavity opening                                    *
C           ALF         Angle of incidence                                *
C           AAB         Directional apparent absorptivity                 *
C           AABD        Directional apparent absorptivity for the         *
C                       Corresponding diffuse case                        *
C           DALFD       Increment for the angle of incidence              *
C           TOL         Tolerence for terminating Romberg integration     *
C           NTRM        Maximum number of reflections considered          *
C           NNN         Total number of incident angles considered        *
C                                                                           *
C***************************************************************************

      IMPLICIT REAL*8 (A-H,O-Z)
      COMMON/BLK1/ALF,SI,RO,NTRM
      EXTERNAL FPR
C
      PI = DACOS(-1.0D0)
      PI12=PI/2.0D0
      PI32=3.0D0*PI/2.0D0
      TOL = 1.0D-7
      NN = 60
C*                                                                        **
C* Input the cavity opening angle and the wall reflectivity                *
C**                                                                       **
      WRITE(6,*) 'Enter the opening angle:'
      READ(5,*)  SID
      WRITE(6,*) 'Enter the reflectivity:'
      READ(5,*)  RO
C
      WRITE(75,*)  SID,RO
C
      SI = SID*PI/180.0D0
      SIC = PI-SI
      DALFD = 90.0D0/DFLOAT(NN)
      NNN = NN+1
      NTRM = INT(DLOG(0.0001D0)/DLOG(RO))+1
C*                                                                        **
C* calculate the direcional apparent absorptivity for the                 *
C* diffuse cavity                                                         **
C**
      AABD = (1.0D0-RO)/(1.0D0-0.5D0*RO*(1.0D0+DCOS(SI)))
C
      ALFD = 0.0D0
C*                                                                        **
C* Do-loop over all angles of incidence                                   *
C**                                                                       **
      DO 100 J=1,NNN
       ALFD=DFLOAT(J-1)*DALFD
       IF(ALFD.EQ.SID) ALFD = SID+0.0000001D0
       IF(J.EQ.NNN) ALFD = 89.99
       ALF = ALFD*PI/180.0D0
       EAR = PI*(DSIN(SI)**2)*DCOS(ALF)
C**                                                                       **
```

```
C Find limits of integration over PHI direction                    C
CC                                                                 CC
        IF(SI.LT.PI12) THEN
         IF(ALF.LT.SI) THEN
          A = PI12
          B = PI32
         ELSE
          RAD = DCOS(SI)**2-DCOS(ALF)**2
          OOO = DSQRT(RAD)/DSIN(ALF)
          PHIC1 = PI-DASIN(OOO)
          A = PI12
          B = PHIC1-.000000000001D0
         END IF
        ELSE
         IF(ALF.LT.SIC) THEN
          A = PI12
          B = PI32
         ELSE
          RAD = DCOS(SI)**2-DCOS(ALF)**2
          OOO = DSQRT(RAD)/DSIN(ALF)
          PHIC2 = PI+DASIN(OOO)
          A = PHIC2+.000000000001D0
          B = PI32
         END IF
        END IF
CC                                                                 CC
C Call ROMB to integrate over the PHI direction                    C
CC                                                                 CC
        CALL ROMB(FPR,A,B,TOL,RESULT)
        IF(ALF.GT.SI.OR.ALF.GT.SIC) RESULT=2.0D0*RESULT
        AAB = RESULT/EAR
CC                                                                 CC
C Write out the result                                             C
CC                                                                 CC
        WRITE(75,31) ALFD,AAB,AABD
        ALFD = ALFD + DALFD
 100   CONTINUE
C
 31    FORMAT(1X,3F9.4)
       STOP
       END
C                                                                  C
C                                                                  C
CCCCCCCCCCCCCCCCCCCCCCCCCCCCCCCCCCCCCCCCCCCCCCCCCCCCCCCCCCCCCCCCCCCCC
C                                                                  C
C This function subroutine calculates the energy absorbed within a C
C longitudinal band at a given azimuthal angle PHI.  Depending on  C
C values of PHI and ALF this function subroutine calls subroutines C
C REG1 or REG2 to calculate the absorbed energy.                   C
C                                                                  C
CCCCCCCCCCCCCCCCCCCCCCCCCCCCCCCCCCCCCCCCCCCCCCCCCCCCCCCCCCCCCCCCCCCCC
C
       FUNCTION FPR(PHI)
       IMPLICIT REAL*8 (A-H,O-Z)
       COMMON/BLK1/ALF,SI,RO,NTRM
C
       PI = DACOS(-1.0D0)
       PI12 = PI/2.0D0
       PI32 = 3.0D0*PI/2.0D0
       PIT2 = PI*2.0D0
       SIC = PI-SI
CC                                                                 CC
C Call TLMT to get the polar angles that define the opening.       C
CC                                                                 CC
       CALL TLMT(SI,ALF,PHI,BA1,BA2)
C
       IF(SI.LT.PI12) THEN
```

```
        IF(ALF.LT.SI) THEN
         FPR = 0.0D0
         CALL REG2(BA1,BA2,RO,NTRM,EABS)
         FPR = FPR+EABS
         BA2I = 2.0D0*PI-BA1
         BA1I = 2.0D0*PI-BA2
         CALL REG2(BA1I,BA2I,RO,NTRM,EABS)
         FPR = FPR+EABS
        ELSE
         CALL REG1(BA1,BA2,RO,NTRM,EABS)
         FPR = EABS
        END IF
       ELSE
        IF(ALF.LT.SIC) THEN
         FPR = 0.0D0
         CALL REG2(BA1,BA2,RO,NTRM,EABS)
         FPR = FPR+EABS
         BA2I = 2.0D0*PI-BA1
         BA1I = 2.0D0*PI-BA2
         CALL REG2(BA1I,BA2I,RO,NTRM,EABS)
         FPR = FPR+EABS
        ELSE
         CALL REG2(BA1,BA2,RO,NTRM,EABS)
         FPR = EABS
        END IF
       END IF
*
       RETURN
       END
*                                                                      *
*********************************** REG1 ***********************************
*                                                                      *
* This subroutine, which is called by the function subroutine FPR,     *
* calculates the energy absorbed within a circle of reflection when    *
* the opening angle is less than 90 deg and the angle of incidence is  *
* greater than the opening angle.                                      *
*                                                                      *
* Variables:                                                           *
*           ALL         Lower limit polar angle for rays entering      *
*                       the circle of reflection                       *
*           ALU         Upper limit polar angle for rays entering      *
*                       the circle of reflection                       *
*           ALB         Absorptivity                                   *
*           A(.)        Lower limits of the circular arcs which        *
*                       represent the rays that survive through the    *
*                       N'th reflection                                *
*           BLL         Lower limit for the opening                    *
*           BLU         Upper limit for the opening                    *
*           B(.)        Upper limits of the circular arcs which        *
*                       represent the rays that survive through the    *
*                       N'th reflection                                *
*           CK1         Lower limit of the point of incidence during   *
*                       a given reflection N                           *
*           CK2         Upper limit of the point of incidence during   *
*                       a given reflection N                           *
*           EABS        Energy absorbed by all reflections considered  *
*           EARR        Energy entering the circle of reflection       *
*           J           Indicates the circular arc whose limits are    *
*                       defined by A(J) and B(J)                       *
*           JMAX        Maximum number of circular arcs defined by     *
*                       A(J) and B(J) during a given reflection N      *
*           N           Indicates the N'th reflection                  *
*           NP          The number of cycles travelled by a ray        *
*           SI1         Upper limit polar angle of the opening in the  *
*                       NP-1'th  cycle                                 *
*           SI2         Lower limit polar angle of the opening in the  *
*                       NP'th cycle                                    *
```

```
*           SI3         Upper limit polar angle of the opening in the  *
*                       NP'th cycle                                    *
*                                                                      *
************************************************************************
*
      SUBROUTINE REG1(BAL,BAU,RO,NTRM,EABS)
      IMPLICIT REAL*8 (A-H,O-Z)
      DOUBLE PRECISION  A(2400),B(2400)
*
      PI = DACOS(-1.0D0)
      PIO2 = PI/2.0D0
      PIT2 = PI*2.0D0
*
      ALL = BAL
      ALU = BAU
      IF(BAU.GE.PIO2) ALU=PI-BAU
*
      EARR = 0.5D0*(DSIN(ALU)**2-DSIN(ALL)**2)
      ALB = 1.0D0 - RO
      EABS = ALB*EARR
      EABM = EABS
**                                                                    **
* Initialize A(1) and B(1) based on first reflection points            *
**                                                                    **
      A(1) = PI - ALU
      B(1) = PI - ALL
      JMAX = 1
**                                                                    **
* Do-loop over maximum number of reflections.                          *
**                                                                    **
      DO 100 N=2,NTRM
      J = 0
 200  J = J+1
      IF(J.GT.JMAX) GOTO 150
**                                                                    **
* Find the locations of the rays represented by A(J) and B(J) during   *
* the N'th reflection (Eq. 3.45)                                       *
**                                                                    **
      CK1 = DFLOAT(1-N)*PI+DFLOAT(2*N-1)*A(J)
      CK2 = DFLOAT(1-N)*PI+DFLOAT(2*N-1)*B(J)
**                                                                    **
* Find the number of cycles that the upper limit ray has travelled     *
**                                                                    **
      NP = INT(CK2/(2.0D0*PI))
**                                                                    **
* Find the corresponding polar angles of the opening in this cycle     *
**                                                                    **
      SI1 = 2.0D0*PI*DFLOAT(NP-1)+BAU
      SI2 = 2.0D0*PI*DFLOAT(NP)+BAL
      SI3 = 2.0D0*PI*DFLOAT(NP)+BAU
**                                                                    **
* Find what portion of the rays represented by CK1 and CK2 remain      *
* in the circle of reflection after the N'th reflection.               *
**                                                                    **
      IF(CK2.GE.SI3) THEN
*
      IF(CK1.GE.SI3) GOTO 200
      IF(CK1.GE.SI2) THEN
      A(J) = (SI3 - DFLOAT(1-N)*PI)/DFLOAT(2*N-1)
      GOTO 200
      ELSE
      JJ =J+1
      DO 101 I=JJ,JMAX+1
      II = JMAX+J+2-I
      A(II) = A(II-1)
      B(II) = B(II-1)
 101  CONTINUE
```

```
      A(JJ) = (SI3 - DFLOAT(1-N)*PI)/DFLOAT(2*N-1)
      B(J) = (SI2 - DFLOAT(1-N)*PI)/DFLOAT(2*N-1)
      J = J+1
      JMAX = JMAX+1
      GOTO 200
      END IF
*
      ELSE IF(CK2.GE.SI2) THEN
*
      IF(CK1.GE.SI2) THEN
       IF(J.EQ.JMAX) THEN
        JMAX = JMAX-1
        GOTO 150
       END IF
      DO 102 I=J,JMAX-1
      A(I) = A(I+1)
      B(I) = B(I+1)
 102  CONTINUE
      JMAX = JMAX-1
      J = J-1
      GOTO 200
      ELSE IF(CK1.GE.SI1) THEN
      B(J) = (SI2 - DFLOAT(1-N)*PI)/DFLOAT(2*N-1)
      GOTO 200
      ELSE
      A(J) = (SI1 - DFLOAT(1-N)*PI)/DFLOAT(2*N-1)
      B(J) = (SI2 - DFLOAT(1-N)*PI)/DFLOAT(2*N-1)
      GOTO 200
      END IF
C
*
      ELSE
*
      IF(CK1.GE.SI1) GOTO 200
      A(J) = (SI1 - DFLOAT(1-N)*PI)/DFLOAT(2*N-1)
      GOTO 200
*
      END IF                                                          **
**                                                                    *
* Calculate the energy absorbed during the N'th reflection by summing *
* over all the circular arcs which represent the rays that have       *
* survived the N'th reflection.                                       **
**
 150  EABP = 0.0D0
      DO 160 I=1,JMAX
      TERM =  0.5D0*ALB*(RO**(N-1)*(DSIN(A(I))**2-DSIN(B(I))**2))
 160  EABP = EABP+TERM
      EABS = EABS+EABP
 100  CONTINUE
*
      RETURN
      END                                                             *
*
********************************* REG2 ********************************
*                                                                     *
* This subroutine, which is called by the function subroutine FPR,    *
* calculates the energy absorbed within a circle of reflection when   *
* the angle of incidence is less than the opening angle for the case  *
* of the opening angle less than 90 deg, or when the opening angle    *
* is greater than 90 deg.                                             *
*                                                                     *
* Variables:     same as those in REG1                                *
*                                                                     *
***********************************************************************
*
      SUBROUTINE REG2(BAU,BAL,RO,NTRM,EABS)
      IMPLICIT REAL*8 (A-H,O-Z)
```

```
      DOUBLE PRECISION  A(2400),B(2400)
*
      PI = DACOS(-1.0D0)
      PIO2 = PI/2.0D0
      PIT2 = PI*2.0D0
*
      ALU = BAU
      IF(BAU.GT.PIO2) ALU = PI-BAU
      ALL=0.00000001D0
      IF(BAL.LT.PI) ALL = PI-BAL
*
      EARR = 0.5D0*(DSIN(ALU)**2-DSIN(ALL)**2)
      ALB = 1.0D0 - RO
      EABS = ALB*EARR
      EABM = EABS
**                                                                    **
* Initialize A(1) and B(1) based on first reflection points            *
**                                                                    **
      A(1) = PI - ALU
      B(1) = PI - ALL
      JMAX = 1
**                                                                    **
* Do-loop over maximum number of reflections.                          *
**                                                                    **
      DO 100 N=2,NTRM
      J = 0
 200  J = J+1
      IF(J.GT.JMAX) GOTO 150
**                                                                    **
* Find the locations of the rays represented by A(J) and B(J) during   *
* the N'th reflection (Eq. 3.45)                                       *
**                                                                    **
      CK1 = DFLOAT(1-N)*PI+DFLOAT(2*N-1)*A(J)
      CK2 = DFLOAT(1-N)*PI+DFLOAT(2*N-1)*B(J)
**                                                                    **
* Find the number of cycles that the upper limit ray has travelled     *
**                                                                    **
      NP = INT(CK2/(2.0D0*PI))
**                                                                    **
* Find the corresponding polar angles of the opening in this cycle.    *
**                                                                    **
      SI1 = 2.0D0*PI*DFLOAT(NP-1)+BAL
      SI2 = 2.0D0*PI*DFLOAT(NP)+BAU
      SI3 = 2.0D0*PI*DFLOAT(NP)+BAL
**                                                                    **
* Find what portion of the rays represented by CK1 and CK2 remain      *
* in the circle of reflection after the N'th reflection.               *
**                                                                    **
      IF(CK2.GE.SI3) THEN
*
      IF(CK1.GE.SI3) THEN
      IF(J.EQ.JMAX) THEN
      JMAX = JMAX-1
      GOTO 150
      END IF
      DO 101 I=J,JMAX-1
      A(I) = A(I+1)
      B(I) = B(I+1)
 101  CONTINUE
      JMAX = JMAX-1
      J = J-1
      GOTO 200
      ELSE IF(CK1.GE.SI2) THEN
      B(J) = (SI3 - DFLOAT(1-N)*PI)/DFLOAT(2*N-1)
      GOTO 200
      ELSE
      A(J) = (SI2 - DFLOAT(1-N)*PI)/DFLOAT(2*N-1)
```

```
      B(J) = (SI3 - DFLOAT(1-N)*PI)/DFLOAT(2*N-1)
      GOTO 200
      END IF
*
      ELSE IF(CK2.GE.SI2) THEN
*
      IF(CK1.GE.SI2) GOTO 200
      IF(CK1.GE.SI1) THEN
      A(J) = (SI2 - DFLOAT(1-N)*PI)/DFLOAT(2*N-1)
      GOTO 200
      ELSE
      JJ =J+1
      DO 102 I=JJ,JMAX+1
      II = JMAX+J+2-I
      A(II) = A(II-1)
      B(II) = B(II-1)
 102  CONTINUE
      A(JJ) = (SI2 - DFLOAT(1-N)*PI)/DFLOAT(2*N-1)
      B(J) = (SI1 - DFLOAT(1-N)*PI)/DFLOAT(2*N-1)
      J = J+1
      JMAX = JMAX+1
      GOTO 200
      END IF
*
      ELSE
*
      IF(CK1.GE.SI1) THEN
      IF(J.EQ.JMAX) THEN
      JMAX = JMAX-1
      GOTO 150
      END IF
      DO 103 I=J,JMAX-1
      A(I) = A(I+1)
      B(I) = B(I+1)
 103  CONTINUE
      JMAX = JMAX-1
      J = J-1
      GOTO 200
      ELSE
      B(J) = (SI1 - DFLOAT(1-N)*PI)/DFLOAT(2*N-1)
      GOTO 200
      END IF
      END IF
*
 150  EABP = 0.0D0
**                                                                    **
* Calculate the energy absorbed during the N'th reflection by summing *
* over all the circular arcs which represent the rays that have       *
* survived the N'th reflection.                                       *
**                                                                    **
      DO 160 I=1,JMAX
      TERM =  0.5D0*ALB*(RO**(N-1)*(DSIN(A(I))**2-DSIN(B(I))**2))
 160  EABP = EABP+TERM
      EABS = EABS+EABP
 100  CONTINUE
*
      RETURN
      END                                                            *
*
********************************* TLMT ***********************************
*                                                                       *
* This subroutine calculates the polar angles that define the opening   *
* in the circle of reflection for a given opening angle SI, an angle    *
* of incidence ALF, and azimuthal angle PHI.                            *
* Calculations are based on Eq. (3.41).                                 *
*
```

```
*****************************************************************************
*                                                                           *
      SUBROUTINE TLMT(SI,ALF,PHI,TA1,TA2)
      IMPLICIT REAL*8 (A-H,O-Z)
*
      PI = DACOS(-1.0D0)
      PIT2 = 2.0D0*PI
*
      A = 1.0D0
      IF(PHI.LT.1.0D-6) PHI = 0.0D0
      B = DTAN(ALF)*DSIN(PHI)
      C = DCOS(SI)/DCOS(ALF)
      DD = DSQRT(A*A+B*B)
      IF(B.EQ.0.0D0) THEN
      GAM = DACOS(A/DD)
      GOTO 10
      END IF
      GAM = PI+(DABS(B)/B)*(DACOS(A/DD)-PI)
 10   AA = C/DD
      IF(AA.GT.1.0D0.AND.AA.LT.1.000001D0) AA=0.99999999D0
      IF(AA.LT.-1.0D0.AND.AA.GT.-1.000001D0) AA=-0.99999999D0
      IF(AA.GT.1.0D0.OR.AA.LT.-1.0D0) WRITE(6,*) 'SMTG WRONG IN TLMT'
      TTA1 = (GAM+DACOS(AA))
      TTA2 = (GAM - DACOS(AA))
      IF(TTA1.GE.PIT2) TTA1=TTA1-PIT2
      IF(TTA1.LT.0.0D0) TTA1=TTA1+PIT2
      IF(TTA2.GE.PIT2) TTA2=TTA2-PIT2
      IF(TTA2.LT.0.0D0) TTA2=TTA2+PIT2
      TA1 = DMIN1(TTA1,TTA2)
      TA2 = DMAX1(TTA1,TTA2)
      RETURN
      END
```

```
*********************************** ROMB ************************************
*
*
*
*     Subroutine ROMB:
*                        Subroutine for Romberg integration. Program
*     begins with trapezoidal integration with 10 subintervals.
*     Intervals are then halved and results are extrapolated up to
*     eight order.  Maximum number of subintervals used in program is
*     2560.  The source for this subroutine is Applied Numerical
*     Analysis, 3rd Edition, by Gerald, C. F. and Wheatly, P. O.
*
*     Variables:
*     FCN    - Function that computes F(x), declared EXTERNAL in main
*     A,B    - Integration limits
*     TOL    - Tolerence value used to terminate the iteration
*     RESULT - Returns value to the integral caller
*     TRAP   - Doubly subscripted array that holds intermediate values
*              for comparison and extrapolation
*     KFLAG  - Flag used internally to signal non-convergence. When
*              KFLAG = 0, means non-convergent, =1 means all ok.
*
*
*
      SUBROUTINE ROMB(FCN,A,B,TOL,RESULT)
      IMPLICIT REAL*8 (A-H,O-Z)
      DIMENSION TRAP(9,9)
      INTEGER I,L,K,KFLAG
*
*
*
*  Set flag at 1 initially
*
      KFLAG = 1
      IPRINT = 0
*
*  Compute first integral with 10 subintervals and using trap rule
*
      H = (B-A)/10.0D0
      SUM = FCN(A)+FCN(B)
      X = A
      DO 10 I = 2,10
        X = X+H
        SUM = SUM+FCN(X)*2.0D0
 10   CONTINUE
      TRAP(1,1) = H/2.0D0*SUM
*
*
*
*   Recompute integral with H halved, extrapolate and test. Repeat
*   up to eight times.
*
      DO 20 I=1,8
       H = H/2.0D0
       X = A+H
       K = 10*2**I
       DO 30 J=2,K,2
         SUM = SUM + FCN(X)*2.0D0
         X = X+H+H
 30    CONTINUE
       TRAP(1,I+1) = H/2.0D0*SUM
       DO 40 L = 1,I
        TRAP(L+1,I+1) = TRAP(L,I+1)+1.0D0/(4.0D0**L-1.0D0)*
     *                  (TRAP(L,I+1)-TRAP(L,I))
 40    CONTINUE
       IF(DABS(TRAP(I+1,I+1)-TRAP(I,I+1))-TOL) 50,50,20
```

```
 20     CONTINUE
*
*
*
*  If tolerance not met after 8 extrapolations, print note and set
*  KFLAG = 0.
*
       KFLAG = 0
       PRINT 200
*
*
*
*  Print imediate results
*
 50    I = I+1
       IF(IPRINT.EQ.0) GOTO 80
       DO 70 L = 1,I
        PRINT 203, (TRAP(J,L),J=1,L)
 70     CONTINUE
 80     IF(KFLAG.EQ.0) STOP
        RESULT = TRAP(I,I)
 200    FORMAT(/' TOLERANCE NOT MET. CALCULATED VALUES WERE ')
 203    FORMAT(1X,8F12.6)
        RETURN
        END
```

```
**************************** MCVTY ************************************
*                                                                      *
* This program uses the Monte Carlo technique to calculate the         *
* apparent emissivity of an isothermal cavity as a function of the     *
* cavity opening angle, wall reflectivity, and the reflectivity        *
* ratio.  Cavity surface is divided into a given number of equal       *
* area ring elements, and the distribution factor between all such     *
* ring elements and the cavity opening is calculated.  These           *
* distribution factors are then used to calculate the                  *
* apparent emissivity according to the procedure given in Appendix     *
* A.  Even though not used in the apparent emissivity calculations,    *
* the program also calculates the distribution factors between all     *
* spherical ring elements                                              *
*                                                                      *
* Variables:                                                           *
*           AREA        Area of each ring element                      *
*           ARAP        Area of the flat surface stretched across the  *
*                       opening                                        *
*           ATA(.)      The lower limit zenith angles of rings         *
*           DAZ         Increment size in the z-axis, for dividing     *
*                       the cavity surface into equal area rings       *
*           DF(.,.)     Matrix of the distribution factors between     *
*                       the spherical ring elements                    *
*           DFA(.)      Array of the distribution factors between the  *
*                       ring elements and the cavity opening           *
*           EM          Emissivity                                     *
*           IAZ         Indicates the element number at the point of   *
*                       reflection                                     *
*           IRUN        A flag giving the user the option for further  *
*                       runs                                           *
*           ISHTS       A counter that keeps track of shots            *
*           NAZ         Number of rings in the cavity                  *
*           NDV         Number of equal area ring elements for         *
*                       a complete sphere, input by the user           *
*           NSHTS       Total number of shots                          *
*           PHI(.)      An array giving the azimuthal angles of the    *
*                       N-1'st, N'th, and N+1'st reflection points     *
*                       (is dimensioned by three)                      *
*           RN          Random number                                  *
*           RO          Reflectivity                                   *
*           RFR         Reflectivity ratio                             *
*           SID         Cavity opening angle (must be given in deg)    *
*           TTA(.)      An array giving the zenith angles of the       *
*                       N-1'st, N'th, and N+1'st reflection points     *
*                       (is dimensioned by three)                      *
*           X(.)      An array giving the x-coordinates of the         *
*                       N-1'st, N'th, and N+1'st reflection points     *
*                       (is dimensioned by three)                      *
*           Y(.)      An array giving the y-coordinates of the         *
*                       N-1'st, N'th, and N+1'st reflection points     *
*                       (is dimensioned by three)                      *
*           Z(.)      An array giving the y-coordinates of the         *
*                       N-1'st, N'th, and N+1'st reflection points     *
*                       (is dimensioned by three)                      *
*                                                                      *
************************************************************************

      IMPLICIT REAL*8 (A-H,O-Z)
      DIMENSION Z(3),Y(3),X(3),TTA(3),PHI(3),ATA(30),
     *          DF(30,30),DFA(30)
*
      PI = DACOS(-1.0D0)
      PIO2 = PI/2.0D0
      NDV = 4
*
 9000 WRITE(6,*) 'Enter 1 for further runs:'
```

```
      READ(5,*) IRUN
      WRITE(6,*) 'Enter the number of shots:'
      READ(5,*) NSHTS
      WRITE(6,*)'Enter the opening angle in degrees:'
      READ(5,*) SID
      WRITE(6,*)'Enter the reflectivity:'
      READ(5,*) RO
      WRITE(6,*)'Enter the reflectivity ratio:'
      READ(5,*) RFR
*
      EM = 1.0D0-RO
*
      WRITE(75,*)
      WRITE(75,31) EM,RFR
 31   FORMAT(1X,'Emissivity =',F6.3,10x,'Reflectivity Ratio =',F6.3)
      WRITE(75,*)
*
      SEED = 7654321.0D0
      DAZ = 2.0D0/DFLOAT(NDV)
*
      SI = SID*PI/180.0D0
      NAZ = INT((1.0D0+DCOS(SI))/DAZ)+1
      DAZ = (1.0D0+DCOS(SI))/DFLOAT(NAZ)
*
      DO 1 I=1,NAZ
      ATA(NAZ-I+1) = DACOS(DFLOAT((I-1)+1)*DAZ-1.0D0)
  1    CONTINUE
*
      ARAP = PI*DSIN(SI)**2
      AREA = DAZ*2.0D0*PI
**                                                              **
* Do-loop over all elements                                     *
**                                                              **
      DO 7000 KM=1,NAZ
**                                                              **
* Initialize the distribution factor matrix                     *
**                                                              **
      DO 700 JM=1,NAZ
      DF(KM,JM) = 0.0D0
 700  CONTINUE
      DFA(KM) = 0.0D0
**                                                              **
* Obtain the zenith angles that define element KM               *
**                                                              **
      TTAL0 = ATA(KM)
      IF(KM.EQ.NAZ) THEN
      TTAU0 = PI
      GOTO 111
      END IF
      TTAU0 = ATA(KM+1)
*
 111  TTAL0D = TTAL0*180.0D0/PI
      TTAU0D = TTAU0*180.0D0/PI
*
      RN = -1.0D0
      IN = 0
      ISHTS = 0
      C1 =  DSIN(TTAL0)
      C2 =  DSIN(TTAU0)
**                                                              **
* Determine the emission sight                                  *
**                                                              **
 1000 CALL RAND(SEED,IN,RN)
      PHI(1) = 0.0D0
      CALL RAND(SEED,IN,RN)
      CC = C1*C1+RN*(C2*C2-C1*C1)
      TTA(1) = DASIN(DSQRT(CC))
```

```
        IF(TTAL0.GE.PI02) TTA(1)=PI-TTA(1)
        X(1) = DSIN(TTA(1))*DCOS(PHI(1))
        Y(1) = DSIN(TTA(1))*DSIN(PHI(1))
        Z(1) = DCOS(TTA(1))
**                                                                    **
* Determine the first point of incidence                              *
**                                                                    **
        CALL RAND(SEED,IN,RN)
        TTA(2) = 2.0D0*DASIN(DSQRT(RN))
        CALL RAND(SEED,IN,RN)
        PHI(2) =2.0D0*PI*RN
        X(2) = DSIN(TTA(2))*DCOS(PHI(2))
        Y(2) = DSIN(TTA(2))*DSIN(PHI(2))
        Z(2) = DCOS(TTA(2))
 100    CONTINUE
**                                                                    **
* Check to see if the ray has escaped                                 *
**                                                                    **
        IF(TTA(2).LE.SI) THEN
        DFA(KM) =  DFA(KM)+1.0D0
        GOTO 999
        END IF
**                                                                    **
* Draw a random number to check for absorption                        *
**                                                                    **
        CALL RAND(SEED,IN,RN)
        IF(RN.LT.RO) THEN
**                                                                    **
* Draw a random number to check for the type of reflection            *
**                                                                    **
         CALL RAND(SEED,IN,RN)
         IF(RN.LT.RFR) THEN
**                                                                    **
* If reflection is specular, call SRCH to obtain the next reflection  *
* point                                                               **
**
          CALL SRCH(X,Y,Z)
*
          CALL CNVRT(X(3),Y(3),Z(3),TTA(3),PHI(3))
          DO 110 J=1,2
          X(J) = X(J+1)
          Y(J) = Y(J+1)
          Z(J) = Z(J+1)
          TTA(J) = TTA(J+1)
          PHI(J) = PHI(J+1)
 110      CONTINUE
          GOTO 100
         ELSE
**                                                                    **
* If reflection is diffuse, draw two random numbers to find the       *
* next reflection point                                               **
**
          CALL RAND(SEED,IN,RN)
          TTA(3) = 2.0D0*DASIN(DSQRT(RN))
          CALL RAND(SEED,IN,RN)
          PHI(3) =2.0D0*PI*RN
          X(3) = DSIN(TTA(3))*DCOS(PHI(3))
          Y(3) = DSIN(TTA(3))*DSIN(PHI(3))
          Z(3) = DCOS(TTA(3))
          DO 120 J=1,2
          X(J) = X(J+1)
          Y(J) = Y(J+1)
          Z(J) = Z(J+1)
          TTA(J) = TTA(J+1)
          PHI(J) = PHI(J+1)
 120      CONTINUE
          GOTO 100
```

```
         END IF
        ELSE
C*                                                                    **
C* If absorption occurs, increment the distribution factor             *
C*                                                                    **
         IAZ = INT((DCOS(SI)-DCOS(TTA(2)))/DAZ)
         DF(KM,IAZ) = DF(KM,IAZ)+1.0D0
        END IF
C
 999    ISHTS = ISHTS+1
C*                                                                    **
C* Check for the number of shots, and start over if all shots have not *
C* been fired.                                                         *
C*                                                                    **
        IF(ISHTS.LT.NSHTS) GOTO 1000
C*                                                                    **
C* Calculate the distribution factor from element KM to all other      *
C* elements.                                                          **
C*
        DFA(KM) = DFA(KM)/DFLOAT(NSHTS)
        DO 5 I=1,NAZ
        DF(KM,I) = DF(KM,I)/DFLOAT(NSHTS)
 5      CONTINUE
 7000   CONTINUE
C*                                                                    **
C* Calculate the apparent emissivity                                   *
C*                                                                    **
        APEM = 0.0D0
        DO 200 I=1,NAZ
        APEM = APEM+DFA(I)
 200    CONTINUE
        APEM = APEM*EM*(AREA/ARAP)
C*                                                                    **
C* Write out the result                                                *
C*                                                                    **
        WRITE(75,32) APEM
        WRITE(75,*) '**************************************************'
        WRITE(75,*)
 32     FORMAT(1X,'Apparent Emissivity =',F6.3)
        IF(IRUN.EQ.1) GOTO 9000
C
        WRITE(6,*) EM , APEM
C
        STOP
        END
C*                                                                    *
C************************** SRCH ***************************************
C*                                                                    *
C*  This subroutine, by applying the laws of specular reflection,     *
C*  determines the next point of incidence given the two previous     *
C*  points of incidence in a spherical enclosure.                     *
C*                                                                    *
C**********************************************************************
C*
        SUBROUTINE SRCH(X,Y,Z)
        IMPLICIT REAL*8 (A-H,O-Z)
        DIMENSION X(3),Y(3),Z(3)
C
        DEN = Y(1)*Z(2)-Y(2)*Z(1)
        APR = (-Z(2)*X(1)+Z(1)*X(2))/DEN
        BPR = (-X(2)*Y(1)+X(1)*Y(2))/DEN
        N = 2
        CNST = X(N)*X(N-1)+Y(N)*Y(N-1)+Z(N)*Z(N-1)
        DEN = Y(N)/X(N)-APR
        A1 = CNST/(X(N)*DEN)
        A2 = (BPR-Z(N)/X(N))/DEN
        B1 = (CNST-A1*Y(N))/X(N)
```

```
        B2 = -(A2*Y(N)+Z(N))/X(N)
        DEN = B2*B2+A2*A2+1.0D0
        D1 = 2.0D0*(B1*B2+A1*A2)/DEN
        D2 = (B1*B1+A1*A1-1.0D0)/DEN
        Z1 = 0.5D0*(-D1+DSQRT(D1*D1-4.0D0*D2))
        Z2 = 0.5D0*(-D1-DSQRT(D1*D1-4.0D0*D2))
        X1 = B1+B2*Z1
        X2 = B1+B2*Z2
        Y1 = A1+A2*Z1
        Y2 = A1+A2*Z2
        E1 = (X(N-1)-X1)**2+(Y(N-1)-Y1)**2+(Z(N-1)-Z1)**2
        E2 = (X(N-1)-X2)**2+(Y(N-1)-Y2)**2+(Z(N-1)-Z2)**2
        N = N+1
        IF(E1.LT.1.0D-10) THEN
        X(N) = X2
        Y(N) = Y2
        Z(N) = Z2
        END IF
        IF(E2.LT.1.0D-10) THEN
        X(N) = X1
        Y(N) = Y1
        Z(N) = Z1
        END IF
        RETURN
        END
*                                                                      *
*********************** CNVRT ***********************************
*                                                                      *
*  This subroutine converts the Cartesian coordinates into spherical  *
*  coordinates.                                                        *
*                                                                      *
************************************************************************
*
        SUBROUTINE CNVRT(XX,YY,ZZ,TA,PH)
        IMPLICIT REAL*8 (A-H,O-Z)
        PI = DACOS(-1.0D0)
        TA = DACOS(ZZ)
        SNPH = YY/DSIN(TA)
        CSPH = XX/DSIN(TA)
        PH = PI+(DABS(SNPH)/SNPH)*(DACOS(CSPH)-PI)
        RETURN
        END
```

```
C*********************************  MPRS  ***********************************
C                                                                            *
C This program uses the Monte Carlo technique to calculate the               *
C directional apparent absorptivity of a spherical cavity having             *
C specular walls as a function of the cavity opening angle, wall             *
C absorptivity, and the direction of incidence.  Collimated radiation        *
C is simulated by emitting an energy bundle from a randomly chosen           *
C location on the plane of the cavity opening in the same direction          *
C as that of the collimated radiation.  The path of this energy bundle       *
C is then followed until it either escapes from the opening or loses         *
C a significant portion of its energy because of multiple reflections.       *
C                                                                            *
C Variables:                                                                 *
C           AABS        Directional apparent absorptivity                    *
C           APR         A coefficient in the equation for the plane          *
C                       of reflection                                        *
C           BPR         A coefficient in the equation for the plane          *
C                       of reflection                                        *
C           EABS        Number of energy bundles absorbed                    *
C           GAMA        Direction of the collimated radiation                *
C           ISHTS       A counter to keep track of number of shots           *
C           NREF        Maximum number of reflections considered             *
C           NSHTS       Total number of shots                                *
C           RF          Random number used to determine the angular          *
C                       position of the emission sight                       *
C           RO          Reflectivity                                         *
C           RR          Random number used to determine the radial           *
C                       position of the emission sight                       *
C           X(.)        Array of the x-coordinates of all reflection         *
C                       points                                               *
C           Y(.)        Array of the y-coordinates of all reflection         *
C                       points                                               *
C           Z(.)        Array of the z-coordinates of all reflection         *
C                       points                                               *
C                                                                            *
C*****************************************************************************
C
      IMPLICIT REAL*8 (A-H,O-Z)
      DIMENSION Z(500),Y(500),X(500)
      PI = DACOS(-1.0D0)
      SEED = 7654321.0D0
C
      WRITE(6,*) 'Enter the number of shots:'
      READ(5,*) NSHTS
      WRITE(6,*) 'Enter the opening angle in degrees:'
      READ(5,*) SID
      WRITE(6,*) 'Enter the wall reflectivity:'
      READ(5,*) RO
      WRITE(6,*) 'Enter the direction of incidence in degrees:'
      READ(5,*) GAMD
C
      GAM = GAMD*PI/180.0D0
      SI = SID*PI/180.0D0
      NREF = INT(DLOG(.0005D0)/DLOG(RO))+1
      EABS = 0.0D0
C
      RR = -1.0D0
      IN = 0
      ISHTS = 1
C**                                                                          **
C* Draw two random number to determine the emission sight.                    *
C**                                                                          **
 1000  CALL RAND(SEED,IN,RR)
      CALL RAND(SEED,IN,RF)
      R = DSIN(SI)*DSQRT(RR)
      FI = RF*(2.0D0*PI)
      XO = R*DCOS(FI)
```

```
        Y0 = R*DSIN(FI)
        Z0 = DCOS(SI)
C**                                                                    **
C* Determine the next two points of reflection.                        *
C**                                                                    **
        BP = Y0*DSIN(GAM)-Z0*DCOS(GAM)
        CP = X0*X0+Y0*Y0+Z0*Z0-1.0D0
        DP = DSQRT(BP*BP-CP)
        T1 = -BP-DP
        T2 = -BP+DP
        Z(1) = Z0-T1*DCOS(GAM)
        Z(2) = Z0-T2*DCOS(GAM)
        Y(1) = Y0+T1*DSIN(GAM)
        Y(2) = Y0+T2*DSIN(GAM)
        X(1) = X0
        X(2) = X0
C
        EABS = EABS+(1.0D0-R0)
C**                                                                    **
C* Determine the constants for the reflection plane                     *
C**                                                                    **
        DEN = Y(1)*Z(2)-Y(2)*Z(1)
        APR = (-Z(2)*X(1)+Z(1)*X(2))/DEN
        BPR = (-X(2)*Y(1)+X(1)*Y(2))/DEN
C**                                                                    **
C* Do-loop over the maximum number of reflections                       *
C**                                                                    **
        DO 200 I=3,NREF
C**                                                                    **
C* Call SRCH to determine the next reflection point                     *
C**                                                                    **
        CALL SRCH(X,Y,Z,APR,BPR,I)
        IF(Z(I).GE.Z0) THEN
C**                                                                    **
C* Energy bundle has escaped, start over with a new one.                *
C**                                                                    **
         ISHTS = ISHTS+1
         GOTO 2000
        END IF
C**                                                                    **
C* Energy bundle has hit the cavity wall, add on to the total amount    *
C* absorbed                                                           **
C**
        EABS = EABS+(1.0D0-R0)*(R0**(I-2))
 200    CONTINUE
C**                                                                    **
C* Increment the counter and start over if all shots are not fired.     *
C**                                                                    **
        ISHTS = ISHTS+1
 2000   IF(ISHTS.LE.NSHTS) GOTO 1000
C**                                                                    **
C* Calculate the directional apparent absorptivity.                     *
C**                                                                    **
        AABS = EABS/DFLOAT(NSHTS)
        WRITE(6,*) AABS
C
        STOP
        END
C                                                                      *
C************************** SRCH ***************************************
C                                                                      *
C  This subroutine, by applying the laws of specular reflection,       *
C  determines the next point of incidence given the two previous       *
C  points of incidence in a spherical enclosure.                       *
C                                                                      *
C**********************************************************************
C                                                                      *
```

```
      SUBROUTINE SRCH(X,Y,Z,APR,BPR,N)
      IMPLICIT REAL*8 (A-H,O-Z)
      DIMENSION X(500),Y(500),Z(500)
      N = N-1
      CNST = X(N)*X(N-1)+Y(N)*Y(N-1)+Z(N)*Z(N-1)
      DEN = Y(N)/X(N)-APR
      A1 = CNST/(X(N)*DEN)
      A2 = (BPR-Z(N)/X(N))/DEN
      B1 = (CNST-A1*Y(N))/X(N)
      B2 = -(A2*Y(N)+Z(N))/X(N)
      DEN = B2*B2+A2*A2+1.0D0
      D1 = 2.0D0*(B1*B2+A1*A2)/DEN
      D2 = (B1*B1+A1*A1-1.0D0)/DEN
      Z1 = 0.5D0*(-D1+DSQRT(D1*D1-4.0D0*D2))
      Z2 = 0.5D0*(-D1-DSQRT(D1*D1-4.0D0*D2))
      X1 = B1+B2*Z1
      X2 = B1+B2*Z2
      Y1 = A1+A2*Z1
      Y2 = A1+A2*Z2
      E1 = (X(N-1)-X1)**2+(Y(N-1)-Y1)**2+(Z(N-1)-Z1)**2
      E2 = (X(N-1)-X2)**2+(Y(N-1)-Y2)**2+(Z(N-1)-Z2)**2
      N = N+1
      IF(E1.LT.1.0D-8) THEN
      X(N) = X2
      Y(N) = Y2
      Z(N) = Z2
      END IF
      IF(E2.LT.1.0D-8) THEN
      X(N) = X1
      Y(N) = Y1
      Z(N) = Z1
      END IF
      RETURN
      END
*                                                                      *
*************************** CNVRT ***********************************
*                                                                      *
*  This subroutine converts the Cartesian coordinates into spherical  *
*  coordinates.                                                        *
*                                                                      *
************************************************************************
*
      SUBROUTINE CNVRT(XX,YY,ZZ,TA,PH)
      IMPLICIT REAL*8 (A-H,O-Z)
      PI = DACOS(-1.0D0)
      TA = DACOS(ZZ)
      SNPH = YY/DSIN(TA)
      CSPH = XX/DSIN(TA)
      PH = PI+(DABS(SNPH)/SNPH)*(DACOS(CSPH)-PI)
      RETURN
      END
```

The vita has been removed from the scanned document